UNIHI-SEAGRANT-TR-80-01

University of Hawaii Sea Grant College Program

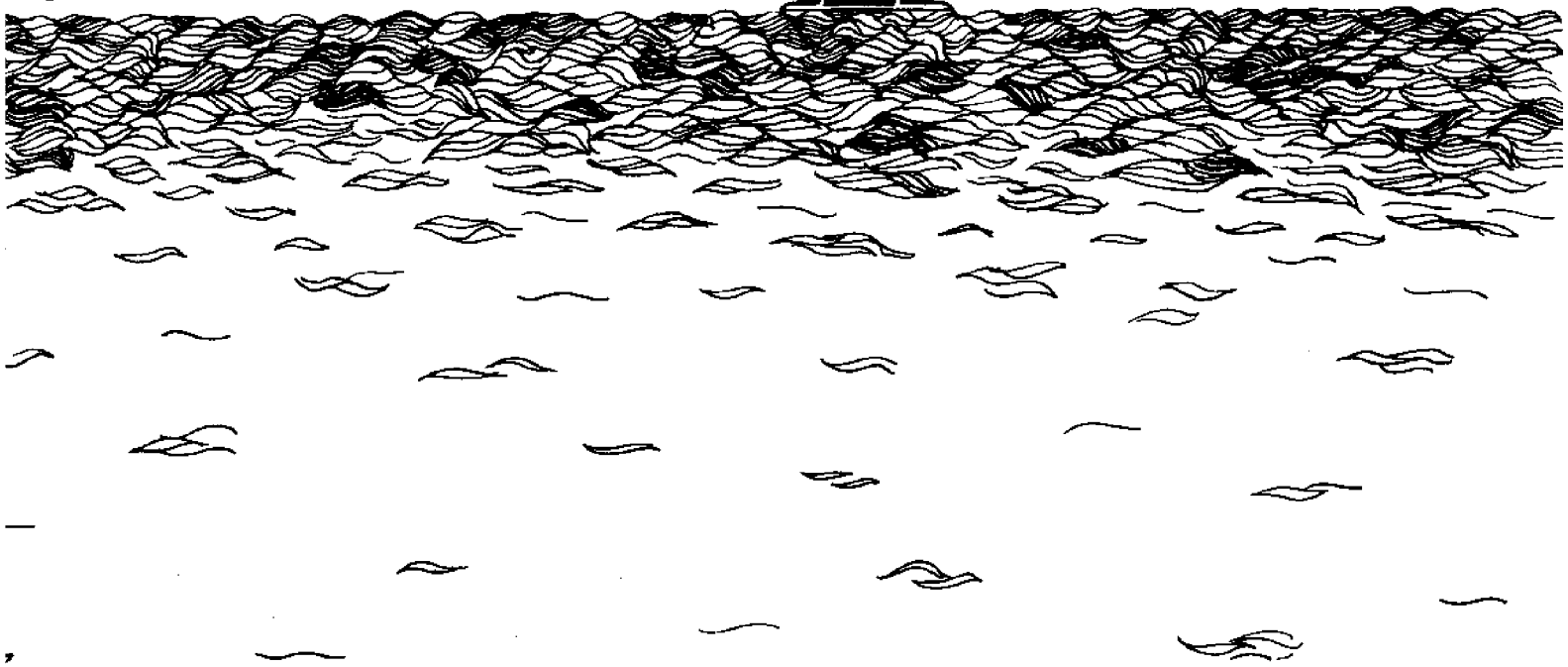

Bubble Nucleation in Supersaturated Fluids

Thomas D. Kunkle

BUBBLE NUCLEATION IN SUPERSATURATED FLUIDS

by

Thomas D. Kunkle

Report on the Sea Grant projects, Human Performance in the Sea (R/DP-01) and Exogenous Gas Bubble Disease: Its Detection, Prevention, and Treatment (R/DP-02); Sea Grant Years 06-11.

Sea Grant Technical Report
UNIHI-SEAGRANT-TR-80-01

December 1979

This work is the result of research sponsored by the University of Hawaii Sea Grant College Program under Institutional Grant Nos. 04-3-158-29, 04-5-158-17, 04-6-158-44026, 04-6-158-44114, and 04-7-158-44129 from NOAA Office of Sea Grant, Department of Commerce. The US Government is authorized to produce and distribute reprints for governmental purposes notwithstanding any copyright notations that may appear hereon.

The statements contained herein are not those of the University of Hawaii Sea Grant College Program, but those of the author.

ABSTRACT

An understanding of the physics of bubble formation is of importance in such diversified endeavors as propeller design, fluid flow, undersea medicine, and the brewing of beer. While the properties of preformed bubbles are well understood, relatively little is known about the physical mechanisms responsible for their creation. This publication reports on the principal results of a program designed to elucidate the nature of the bubble nucleation process, and it briefly explores the applicability of the findings to decompression sickness.

The first chapter contains an introduction to the physics of bubbles, followed by an outline of the theory of homogeneous nucleation. Sample calculations using this theory lead to the conclusion that bubbles within common liquids ordinarily do not form de novo, *but instead arise at certain "weak points" in the fluid that are associated with physical structures known as cavitation nuclei. The problem of understanding bubble formation is thereby transformed into the task of determining the physical nature of cavitation nuclei.*

In Chapter 2 the results of an experimental program in which transparent gelatin was used to stabilize bubbles against floatation are reported. This technique for trapping bubbles at their point of origin has allowed detailed studies of the nucleation process to be made. The results indicate that the cavitation nuclei in gelatin are stable, gas-filled structures which are normally permeable to gas. The initial distribution of nuclear sizes is shown to be exponential, with the largest nuclei having diameters of less than 3 μm.

In Chapter 3 the existing models of cavitation nuclei are classified into four major groups, and each group is briefly discussed. Most of the models are in conflict with observations and thus can be dismissed. The most viable model, and the main subject of this report, is the surfactant-stabilized model. The history of this model is examined, and the differences between the two mathematical formulations that have been introduced so far are discussed.

In Chapter 4 the principal thesis of this work is advanced: that the cavitation nuclei present in common fluids consist of spherical gas phases encased in monomolecular skins of surface-active molecules. A set of second-order, nonlinear, coupled, partial differential equations describing such a nucleus is developed in the first section of this chapter. The second section outlines a computational algorithm which allows these equations to be solved numerically. Finally, the results of the gelatin experiments are analyzed in terms of the computational model. The model is found to be in good agreement with these data and to be capable of giving meaningful explanations of the observed behavior.

In Chapter 5 the surface-active material forming the skin of the nuclei observed in gelatin is shown to be similar to several commonly occurring surfactants, namely the saturated lecithins and phosphatidylethanolamines. The gaseous permeability of the nuclear skin is investigated through a thermodynamic argument. This chapter also examines mechanisms which could result in the observed exponential size distribution and investigates the rate at which a nucleus will isobarically change size in response to its chemical environment.

The final chapter explores the application of the results of this research to the study of decompression sickness. In the first section the connection among the number, the size, and the placement of bubbles within the body and the probability of the occurrence of signs or symptoms of decompression sickness is examined. The next section summarizes the experimental data concerning pressure reduction limits in rats and humans and shows the similarity between animals and the gelatin model. The nature of the cavitation nuclei in animals is further considered in the third section, where it is argued that the stabilization mechanism is the same as that found in gelatin. The final section deals with the calculation of decompression schedules based on this hypothesis. Quantitative decompression profiles are calculated for saturation exposures, and the extension of this work to non-saturation diving is discussed.

ACKNOWLEDGMENTS

Many people have provided encouragement and assistance during the course of this five-year interdisciplinary project. I would particularly like to thank Dr. Richard Strauss for introducing me to this field of research, and Dr. Edward Beckman, whose numerous conversations were instrumental in extending this research to the study of decompression sickness.

Most of the physics presented in this report were developed in close collaboration with Dr. David Yount, whose extensive contributions, useful discussions, and constructive comments on the manuscript are gratefully acknowledged.

Special thanks is given to the University of Hawaii Institute for Astronomy, Dr. J.T. Jefferies, director, for supplying the computer time required to develop and run the codes used in this report and for providing me with the freedom and moral support necessary to undertake this outside research project.

TABLE OF CONTENTS

TABLE OF CONTENTS (continued)

LIST OF FIGURES

Figure

LIST OF FIGURES (continued)

LIST OF FIGURES (continued)

LIST OF TABLES

LIST OF ACRONYMS AND SYMBOLS

Acronyms

ESP	Equilibrium Spreading Pressure
SS model	Surfactant Stabilized model
STP	Standard Temperature and Pressure
VP model	Varying Permeability model
msw	meters sea water
fsw	feet sea water

Symbol	Definition	Defining Equation	Units
A	Area per surfactant molecule	(4.18)	cm^2
A_{diff}	Area for diffusion per surfactant molecule	(4.52)	cm^2
A_{min}	Minimum value of A	(4.25)	cm^2
A_o	Cross-sectional area of a surfactant molecule	(4.19)	cm^2
A_1	Surfactant area parameter	(4.22)	cm^2
A_γ	Molecular area at which Π is equal to γ	(4.88)	cm^2
B_p	First-order virial coefficient	(4.1)	$cm^2\ dyne^{-1}$
B_1	Surfactant dynamic parameter	(4.27)	$dyne\ sec^{1/2}\ cm^{-2}$
C_p	Second-order virial coefficient	(4.1)	$cm^4\ dyne^{-2}$
C_1	Surfactant compression parameter	(4.22)	$dyne\ cm^{-1}$
C_j^I	Inert gas uptake parameter of the j^{th} body structure	(6.18)	$mole\ erg^{-1}\ sec^{-1}$
D	Diffusion coefficient		$cm^2\ sec^{-1}$
DZ	Thickness of the layers dividing the gelatin slab	(4.31)	cm
$D\rho$	Thickness of the shells dividing the nuclear domain	(4.44)	cm
D_1	Gas uptake constant	(4.37)	cm^{-1}
E_{sol}	Molecular desorption energy		erg
$f(r)$	Rate of nuclear destruction	(5.20)	sec^{-1}
F	Gas flux		$mole\ cm^{-2}\ sec^{-1}$

Symbol	Definition	Defining Equation	Units
$g(r)$	Initial distribution of gas in the nuclear domain; or	(1.8)	mole cm^{-3}
	Rate of nuclear creation	(5.20)	sec^{-1} cm^{-4}
H	Fraction of the nuclear surface available for gas diffusion	(4.52)	
k	Boltzmann constant		erg $°K^{-1}$
n	Number of shells dividing the nuclear domain	(4.44)	
$n(r)$	Distribution of nuclear radii	(2.3)	cm^{-4}
N	Amount of gas; or	(1.2)	moles
	Number of bubbles per ml		cm^{-3}
$N(r)$	Integral distribution of nuclear radii	(2.3)	cm^{-3}
N_{mol}	Number of surfactant molecules	(4.62)	
N_{tau}	Number of layers dividing the gelatin slab	(4.31)	
p	Gas pressure	(1.1)	dyne cm^{-2}
p_{amb}	Ambient pressure	(1.1)	dyne cm^{-2}
p^{j}_{amb}	Absolute pressure at the j^{th} point in the ambient pressure profile	(4.29)	dyne cm^{-2}
p_{crush}	Crushing pressure	(2.2)	dyne cm^{-2}
p_f	Final pressure		dyne cm^{-2}
p_m	Maximum pressure		dyne cm^{-2}
p_s	Saturation pressure		dyne cm^{-2}
p_{ss}	Supersaturation pressure	(1.18)	dyne cm^{-2}
p_o	Initial pressure		dyne cm^{-2}
p_j^*	Minimum supersaturation pressure required for bubble formation in the j^{th} body structure	(6.21)	dyne cm^{-2}
p^{ℓ}	Probability of contacting the ℓ^{th} type of decompression sickness syndrome	(6.3)	
q_j	Dummy variables defined for notation purposes: $q_1 \equiv r$, $q_2 \equiv p$, $q_3 \equiv N$, $q_4 \equiv \Pi$	(4.72)	

Symbol	Definition	Defining Equation	Units
r	Radius, measured to liquid-gas interface, of a bubble or nucleus	(1.1)	cm
r_c	Critical radius for bubble growth	(1.20)	cm
r_o	Initial radius of a bubble or nucleus	(1.16)	cm
R	Gas constant		erg $mole^{-1}$ $°K^{-1}$
$\overline{R}$	Gas constant corrected for non-ideal gas behavior	(4.10)	erg $mole^{-1}$ $°K^{-1}$
s	Steepness parameter	(4.89)	
S	Solubility	(1.5)	mole cm^{-1} $dyne^{-1}$
S_j^I	Inert gas solubility of the j^{th} body structure	(6.19)	mole cm^{-1} $dyne^{-1}$
t	Time		sec
t_j	Elapsed time to the j^{th} point of the ambient pressure profile	(4.29)	sec
T	Temperature	(1.2)	°K
U	Gas concentration	(1.5a)	mole cm^{-3}
U_o	Equilibrium gas concentration	(1.5)	mole cm^{-3}
U_j	Gas concentration in the j^{th} shell of the nuclear domain; or	(4.43)	mole cm^{-3}
	Gas concentration in the j^{th} body structure	(6.17)	mole cm^{-3}
U_j^I	Inert gas concentration in the j^{th} body structure	(6.18)	mole cm^{-3}
V	Volume	(1.2)	cm^3
$\overline{V}$	Volume corrected for non-ideal gas behavior	(4.10)	cm^{-3}
V_j	Volume of the j^{th} shell in the nuclear domain; or	(4.47)	cm^3
	Volume of evolved gas in the j^{th} body structure	(6.2)	cm^3
W_j	Gas concentration in the j^{th} layer of the gelatin slab	(4.32)	mole cm^{-3}
α	Gas-permeability coefficient	(1.4)	cm sec^{-1}
γ	Surface tension	(1.1)	dyne cm^{-1}
δ	Accuracy parameter	(4.72)	
Δp	Pressure reduction		dyne cm^{-2}
Δr	Increment in radius	(4.71)	cm

Symbol	Definition	Defining Equation	Units
Δt	Length of time step	(4.71)	sec
Δt_j	Set of maximum time steps	(4.73)	sec
κ	Nuclear growth rate constant	(5.15)	sec^{-1}
ξ	Slope constant	(4.86)	dyne cm^{-1}
Π	Surface pressure of the surfactant	(4.6)	dyne cm^{-1}
Π_{max}	Maximum value of Π	(4.27)	dyne cm^{-1}
ρ	Radial variable		cm
ρ_{max}	Radius of the nuclear domain	(4.41)	cm
σ	Thermodynamic fluctuation in area	(5.1)	cm^2
τ	Gas tension	(1.5)	dyne cm^{-2}
τ_j	Gas tension in the j^{th} body structure	(6.17)	dyne cm^{-2}
ϕ	Fraction of fluctuations that uniformly increase the area of a diffusion-window	(5.2)	
F	Fraction of surfactant molecules available for diffusion	(5.11)	

CHAPTER 1. INTRODUCTION

Nucleation in supersaturated fluids is the process which permits some or all of the excess gas present to evolve into bubbles. It is usually illustrated by the familiar example of bubble formation in carbonated beverages such as champagne or tonic water. When such a beverage is uncorked, bubbles form both on the walls of the container and within the liquid itself. They quickly grow in size as gas diffuses into them from the surrounding fluid, and as they grow, they float rapidly to the surface where they dissipate. Eventually, all of the excess gas is released, either into bubbles or by diffusion through the surface, at which time bubble formation and growth cease and the beverage becomes "flat."

This example illustrates two fundamental characteristics of the nucleation process: that critical supersaturation is required to form bubbles and that this critical pressure is surprisingly small. The second point is of particular significance because, as will be discussed later in this chapter, the supersaturation pressure required for bubble nucleation in a pure fluid is expected to be greater than 1,000 bar. Evidently, the bubbles observed to form in common fluids at modest supersaturation pressures do not form *de novo*, but instead arise at "weak points" in the fluid that serve as cavitation nuclei.

In this chapter the relationship between bubble formation and cavitation nuclei will be systematically explored. The first section introduces definitions and physical concepts concerning the physics of gas bubbles that will be used throughout the remainder of the text. The second section outlines the theory of homogeneous nucleation, which describes the process by which bubbles are formed within pure fluids by thermodynamic fluctuations. The final section establishes the existence of cavitation nuclei by showing that real fluids do not behave as ideal pure fluids should and must therefore contain impurities responsible for the precocious bubble formation.

1.1. Bubble definitions and concepts

The analysis of experimental and theoretical work concerning gas phase nucleation in fluids often requires precise knowledge of the nature of bubbles. In this section an introduction to the physics of gas bubbles is presented and definitions, concepts, and equations that will be used for future work are developed.

A "bubble" in a fluid is defined to be a spherical gas cavity characterized by the mechanical equilibrium of the internal gas pressure and the sum of the ambient pressure and the fluid surface pressure,

$$p = p_{amb} + 2\gamma/r \ , \tag{1.1}$$

where p is the internal gas pressure, p_{amb} is the ambient pressure, γ is the liquid-gas surface tension, and r is the bubble radius. This equation by itself does not provide sufficient information to calculate the size of the bubble. An equation of state for the internal gas is needed to establish a relationship between the internal pressure, the bubble radius, and the amount of gas. A particularly simple equation of state is the ideal gas law

$$pV = NRT \ , \tag{1.2}$$

where V is the volume of the bubble, N is the amount of gas contained in the bubble, R is the universal gas constant, and T is the absolute temperature. Combining equations (1.1) and (1.2) yields the cubic equation

$$4\pi(p_{amb}r^3 + 2\gamma r^2) = 3NRT \ , \tag{1.3}$$

which may be solved for r if the values of N, p_{amb}, and γ are known.

The amount of gas contained in a bubble is not necessarily constant; it can vary due to gas diffusion. Thus, mechanical equilibrium does not imply diffusion equilibrium. The rate of gas transport is determined by the difference equation

$$\frac{dN}{dt} = 4\pi r^2 \alpha[U(r) - U_O] \ , \tag{1.4}$$

where $U(r)$ is the concentration of gas in the fluid just beyond the liquid-gas dividing surface, U_O is the concentration necessary to establish equilibrium with the gas in the bubble, and α is a constant of proportionality. The function $U(\rho)$ is defined to be the gas concentration in the fluid at a radial distance ρ from the center of the bubble, which is assumed to be spherically symmetric. The value of $U(\rho)$ is related to the solubility of the gas, S, through Henry's law

$$U(\rho) = S\tau(\rho) \ , \tag{1.5a}$$

where τ is "gas tension." In a "diffusion-equilibrated" fluid the gas tension is equal to the gas pressure, $\tau = p$, while in a "saturated" fluid the gas tension is equal to the ambient pressure, $\tau = p_{amb}$. The value of U_O is therefore determined by the equation

$$U_O = Sp \ . \tag{1.5b}$$

Equation (1.3) may be differentiated to yield the relationship between differential changes in r, p_{amb}, and N, namely

$$dr = \left[\frac{3RT}{4\pi r^2}\, dN - r dp_{amb}\right] \Big/ \left[3p_{amb} + 4\gamma/r\right] , \tag{1.6}$$

where it is assumed that the temperature is constant. Dividing by dt and substituting from equations (1.4) and (1.5b) yields

$$\frac{dr}{dt} = \left\{3RT\alpha[U(r,t) - Sp] - r\,\frac{dp_{amb}}{dt}\right\} \Big/ \left(3p_{amb} + 4\gamma/r\right) . \tag{1.7}$$

This equation allows the bubble radius to be calculated at any time, given an initial size and the values of $U(r,t)$ and $p_{amb}(t)$.

The value of $U(r,t)$ must be known before equation (1.7) can be solved. The concentration $U(\rho,t)$ is determined by the Fickian diffusion equation

$$\frac{\partial U}{\partial t} = D\nabla^2 U + \vec{v} \cdot \nabla U \ , \tag{1.8a}$$

where D is the diffusion constant and $\vec{v}$ is the velocity of the fluid. Solutions of equation (1.8a) must also satisfy the boundary conditions

$$\lim_{\rho \to \infty} U(\rho,t) = S\tau(t) \ , \tag{1.8b}$$

where $\tau(t)$ is the ambient gas tension, where $U(\rho,t)$ satisfies the equation

$$D \left.\frac{\partial U(\rho,t)}{\partial \rho}\right|_r = \alpha[U(r,t) - Sp(t)] \ , \tag{1.8c}$$

and where the initial concentration is

$$U(\rho,0) = g(\rho) \ . \tag{1.8d}$$

Because the variables $p(t)$ and $r(t)$ occur in equation (1.8), while $U(\rho,t)$ occurs in equation (1.7), these equations are mathematically coupled and must be solved simultaneously. Exact solutions to this system, if they exist at all, are probably too formidable for practical use. Hence, numerical methods must be employed or simplifying assumptions made.

One set of simplifying assumptions, first applied to bubbles by Epstein and Plesset (1950), is that the transport term $\vec{v} \cdot \nabla U$ in equation (1.8a) may be neglected, and that the exchange of gas across the liquid-gas dividing surface is sufficiently fast that the fluid just outside the dividing surface is nearly in equilibrium with the internal gas,

$$U(r,t) \simeq Sp(t) \ . \tag{1.9}$$

Epstein and Plesset (1950) found that the initial concentration gradient at the interface is then given by the equation

$$\left.\frac{\partial U(\rho,t)}{\partial \rho}\right|_r = S(p_{amb} - p)/r \ . \tag{1.10}$$

Comparison of this equation with equation (1.8c) shows that this result will be correct only if the inequality

$$S\frac{2\gamma}{r^2} < \frac{\alpha}{D}[U(r) - Sp(0)] \tag{1.11}$$

is satisfied. Because the left-hand side of equation (1.11) diverges as r goes to zero, the assumption in equation (1.9) must fail for small bubbles. By assuming that equation (1.9) is valid to 10 percent, the radius of the smallest bubble to which this approximation may be accurately applied can be computed. The result is

$$r_{min} = 10\frac{D}{\alpha} \ , \tag{1.12a}$$

where p_{amb} is taken to be zero. Substituting the values for D and α from Table 4.2 for nitrogen in water, the following numerical value is obtained:

$$r_{min} = 5.3 \times 10^{-2} \text{ cm} . \tag{1.12b}$$

For bubbles larger than this radius, the gas flux is limited by the rate at which gas diffuses through the liquid and is said to be "diffusion-limited." For bubbles smaller than this size, the flux is limited by the rate of gas transport across the liquid-gas interface, and the flux is said to be "perfusion-limited." Evidently, the approximation in equation (1.9) is correct in the diffusion-limited case.

A useful approximation for perfusion-limited bubbles is that the diffusion of gas in the liquid is much faster than the transport across the interface. In this case $U(r,t)$ is nearly equal to the gas concentration at a large distance from the bubble,

$$U(r\ t) = \lim_{\rho \to \infty} U(\rho,t) = S\tau(t) . \tag{1.13}$$

This approximation is also valid for a bubble in a stirred fluid or for a rapidly moving bubble. Substitution of equation (1.13) into equation (1.7) yields

$$\frac{dr}{dt} = \left[3RT\alpha S \left(\tau - p_{amb} - \frac{2\gamma}{r} \right) - r \frac{dp_{amb}}{dt} \right] \Bigg/ \left(3p_{amb} + 4\gamma/r \right) . \tag{1.14}$$

This equation approximates the dynamic evolution of a perfusion-limited bubble. It should be noted from equation (1.8a) that the rate of gas transport in a spherical coordinate system depends on the term $(\partial^2 U/\partial\rho^2) + (2/\rho)(\partial U/\partial\rho)$, and that the ratio of the perfusion rate to the diffusion rate for a fixed concentration gradient is thus proportional to r. This indicates that the approximation in equation (1.13) is better for smaller bubbles, and that equation (1.14) becomes increasingly more accurate as the bubble size decreases.

1.1.1. Bubbles in saturated fluids

A particularly instructive application of equation (1.7) is to a bubble in a saturated fluid held at a constant ambient pressure. In this case the derivative dp_{amb}/dt is zero, $\tau(t)$ is equal to p_{amb}, and $g(\rho)$ is taken to be equal to Sp_{amb}. The diffusion-limited case of this problem has been considered by Epstein and Plesset (1950), Fox and Herzfeld (1954), Bernd (1963), and Yang and Liang (1972). The calculations of Epstein and Plesset indicate that a bubble having an initial radius of 100 μm will completely dissolve in water at STP in 5.88 x 10^3 sec, or about 100 minutes, while a 10 μm bubble will dissipate in just 6.63 seconds.

For perfusion-limited bubbles, equation (1.14) may be employed in the form

$$\frac{dr}{dt} = -[6RT\alpha S\gamma/r]/[3p_{amb} + 4\gamma/r] . \tag{1.15}$$

This equation can be immediately integrated to yield

$$(\alpha SRT)t = \frac{p_{amb}}{4\gamma}(r_o^2 - r^2) + \frac{2}{3}(r_o - r) \ , \tag{1.16}$$

where r_o is the initial radius of the bubble. As can be seen from equation (1.15), if γ is not equal to zero, then the bubble is unstable and will contract until it is extinguished. The physical cause of this contraction is the diffusion of the internal gas into the surrounding fluid, a process driven by the inequality between the internal gas pressure p and the ambient gas tension τ. A necessary requirement for the stability of a bubble in a saturated fluid is that the surface pressure vanishes. This can occur only if the surface tension is zero or the radius is infinite. Since both of these possibilities must be ruled out for real bubbles, it is concluded that *all bubbles that exist in saturated fluids are unstable and will eventually collapse.* The lifetime of a small bubble can be calculated from equation (1.16) by setting r to zero and solving for t:

$$t = \left(\frac{p_{amb}}{4\gamma} r_o^2 + \frac{2}{3} r_o\right) \Big/ \alpha SRT \ . \tag{1.17}$$

1.1.2. Growth of bubbles in supersaturated fluids

When the concentration of gas dissolved in a fluid is larger than the equilibrium value, the fluid is said to be "supersaturated." Mathematically, this means that τ is greater than p_{amb}. The difference between the gas tension and the ambient pressure is defined as the supersaturation pressure

$$p_{ss} \equiv \tau - p_{amb} \ . \tag{1.18}$$

The growth rate of a small bubble in a supersaturated fluid held at constant ambient pressure may be found by substituting equation (1.18) into equation (1.14) to yield

$$\frac{dr}{dt} = \alpha SRT(p_{ss} - 2\gamma/r)/(p_{amb} + 4\gamma/3r) \ . \tag{1.19}$$

This equation demonstrates the existence of a "critical radius for bubble growth" defined by

$$r_c = 2\gamma/p_{ss} \ . \tag{1.20}$$

A bubble larger than this critical radius will grow, while one smaller than this size will contract until it vanishes. If the gas tension is assumed to be constant, then equation (1.19) can be integrated to yield

$$r_c\left(\frac{2}{3} + \frac{p_{amb}}{p_{ss}}\right) ln\left(1 - \frac{r}{r_c}\right) + \frac{p_{amb}}{p_{ss}} r = (\alpha SRT)t + K \ ; \ r < r_c \tag{1.21a}$$

or

$$r_c\left(\frac{2}{3}+\frac{p_{amb}}{p_{ss}}\right)\ln\left(\frac{r}{r_c}-1\right)+\frac{p_{amb}}{p_{ss}}\,r=(\alpha SRT)t+K\;;\;r>r_c \qquad (1.21b)$$

where the constant of integration must be chosen to satisfy the initial condition that $r(0)$ is equal to r_o.

1.2. The nucleation of bubbles in pure fluids

The minimum supersaturation pressure required to induce bubble formation within a pure fluid can be calculated using the theory of homogeneous nucleation. This theory estimates the probability of creating a bubble of a particular radius via random molecular motion; the corresponding supersaturation pressure is determined from equation (1.20). The problem of computing the minimum supersaturation pressure is therefore converted into the task of estimating the size of the largest bubble that can be formed by thermodynamic fluctuations. This theory was first proposed by Becker and Döring (1935) and is described in detail in standard texts such as Frenkel (1946) and Landau and Lifshitz (1938).

The cornerstone of the theory of homogeneous nucleation is the use of the Boltzmann equation to determine the relative probability of the spontaneous creation of a bubble due to random molecular motion. If the formation energy of a bubble is E, then the relative probability of its *de novo* occurrence at any particular point in the liquid is given by the equation

$$p \propto e^{-E/kT}\;. \qquad (1.22)$$

The formation energy is the difference in energy between a spherical volume of fluid and a bubble of equal size. Two terms contribute to this energy differential. The first is the free surface energy of the newly formed liquid-gas interface, given by Landau and Lifshitz (1938) as

$$E_1 = 4\pi r^2\gamma\;. \qquad (1.23)$$

The second is the difference in internal energy between the gas in the bubble and that dissolved in an equal volume of fluid. Assuming an ideal gas, this energy is

$$E_2 = -\,(N - N_{fluid})RT \qquad (1.24)$$

where N_{fluid} is the number of moles of gas dissolved in the fluid. Using equations (1.2) and (1.5), equation (1.24) becomes

$$E_2 = -\,\frac{4}{3}\,\pi r^3(p_{amb} + 2\gamma/r - \tau SRT)\;. \qquad (1.25)$$

For the case of nitrogen in water at room temperature, the product SRT is 1.64×10^{-2}. As can be seen from the final results of this calculation, the $2\gamma/r$ term normally dominates in this expression. Therefore, the total formation

energy is given approximately by

$$E = \frac{4}{3}\pi r^2\gamma \ . \tag{1.26}$$

It should be noted that this energy is not equal to the work done in the expansion of a pre-existing bubble through a continuum of equilibrium states.

The constant of proportionality occurring in equation (1.22) may be estimated by assuming that bubbles are the only permissible energy fluctuations, and that the integral sum of all such fluctuations is unity. This yields

$$C = 1/\int_0^\infty e^{-\frac{4}{3}\pi r^2\gamma/kT}\, dr = 4\sqrt{\gamma/3kT} \ . \tag{1.27}$$

The absolute probability of creating a bubble larger than radius r can now be found by integrating equation (1.22) over all radial values larger than r,

$$P(r) = 4\sqrt{\gamma/3kT}\int_r^\infty e^{-\frac{4}{3}\pi\xi^2\gamma/kT}\, d\xi \simeq \frac{1}{2\pi r\sqrt{\gamma/3kT}}\, e^{-\frac{4}{3}\pi r^2\gamma/kT} \tag{1.28}$$

This last equation gives the absolute probability of finding a bubble larger than a certain radius at a particular location in the fluid. The number of independent points in a unit volume of fluid in which a bubble of radius r may form is given roughly by

$$n = 1/\frac{4}{3}\pi r^3 \ . \tag{1.29}$$

The formation time of a bubble is determined approximately by the time interval required for a molecule moving at the velocity of sound to cross the bubble,

$$t_{cross} \simeq 2r/v_{sonic} \ . \tag{1.30}$$

The total rate of formation of bubbles larger than radius r is therefore given by

$$N(r) \simeq nP/t_{cross} \simeq \frac{3v_{sonic}}{16\pi\sqrt{\gamma/3kT}}\,\frac{1}{r^5}\, e^{-\frac{4}{3}\pi r^2\gamma/kT} \tag{1.31}$$

The critical radius corresponding to a formation rate of one bubble per ml per second in water ($\gamma = 72$ dyne/cm, $v_{sonic} \simeq 10^5$ cm/sec) is about 1.0 nm. This radius corresponds to a threshold supersaturation pressure of over 1,400 bar. It should be noted that raising r to 1.1 nm lowers the formation rate by nine orders of magnitude, and that the threshold pressure is therefore very sharply defined.

The threshold supersaturation pressure for pure water determined using equation (1.31) is much larger than the tensile strength, which has been computed by Apfel (1970) to be about 1,400 bar. This difference arises because the E_2 energy term was included in the bubble formation energy while Apfel used only the E_1 term. The physical difference between the two treatments is that Apfel computed the probability of the occurrence of a vapor cavity while equation (1.31) gives the probability of the occurrence of a true bubble. Because equation (1.20) has been used to convert from a radius to a critical supersaturation pressure, and because this equation is based on the validity of the defining equation (1.1), it is clearly necessary that the energy E_2 be included in the formation energy. Since the threshold supersaturation pressure of the gas-liquid system is larger than the tensile strength of the pure liquid, saturating a fluid with an inert gas evidently does not alter its tensile strength.

1.3. The existence of cavitation nuclei

The theory of homogeneous nucleation outlined in the previous section works well for certain very pure liquids. Apfel (1971) showed, for example, that the measured tensile strengths of ether and n-hexane are close to the theoretical levels. In most fluids, however, the critical supersaturation pressure for bubble formation is well below the expected value. In water at room temperature the predicted cavitation threshold is found from equation (1.31) to be about 2,100 bar. The highest threshold actually observed in water of extreme purity was found by Hemmingsen (1970) to be 270 bar. Samples of common tap water cavitate at ultrasonic and supersaturation pressures of less than one bar, a result which is more than three orders of magnitude below the theoretical prediction. Yount and Strauss (1976) reported that weak gelatin mixtures will cavitate when decompressed by 0.83 bar, while the onset of decompression sickness in humans was found by Gray (1944) to occur at 0.6 bar. It is evident that the bubbles formed in common fluids at modest supersaturation pressures do not originate *de novo* from thermodynamic fluctuations within the liquids. Therefore, the bubbles must arise from weak spots in the fluids that are associated with the impurities known as "cavitation nuclei."

This argument for the existence of cavitation nuclei has been known since the time of Becker and Döring (1935). Its relevance to decompression sickness in humans was first pointed out by Harvey et al. (1944). In the remainder of this publication are reported the results of experimental and theoretical studies designed to elucidate the physical properties of the cavitation nuclei that occur in common fluids, including animal tissue.

CHAPTER 2. THE GELATIN EXPERIMENTS

A possible method of studying bubble formation in fluids is to saturate a sample with gas by exposing it to elevated pressure for a sufficient amount of time and to then decompress until the desired supersaturation is achieved. In liquid samples, however, the resulting bubbles float rapidly to the surface, making exact observation of their numbers and sizes difficult. Several workers have made the suggestion that this problem could be avoided by employing, instead of a liquid, a viscous medium in which bubbles would be stabilized where they were formed. The first application of this technique was accomplished by Le Messurier (1972) and Le Messurier et al. (1979), who used weak gelatin mixtures to trap bubbles resulting from various pressure schedules.

In the period from 1972 to 1973 an experimental protocol for cavitation experiments was independently developed by Strauss (1974). In his experiments samples of transparent gelatin were exposed by saturation pressure schedules and then decompressed to produce bubbles. The most important difference between the gelatin model as developed by Le Messurier (1972) and Strauss (1974) is the adherence to saturation dives by Strauss; saturation insures that diffusion equilibrium has been reached within the gelatin, and this greatly simplifies the analysis of the resulting data.

In the following sections the protocol of the gelatin model experiments as developed by Strauss is outlined, and the principal results of several experimental programs are compiled.

2.1. Experimental protocol

The basic apparatus involved in these experiments consists of a small pressure vessel, four glass counting chambers in which the gelatin is held during the course of the experiment, and a large stock of frozen gelatin samples. The general layout of the experimental apparatus is shown in Figure 2.1.

The pressure vessel was constructed from a 27 cm length of seamless welding pipe having an internal diameter of 15 cm. Machined collars were welded to the ends of the pipe, and faceplates were bolted through these collars. The front plate contains a circular plexiglass window surrounded with lights by means of which the interior of the chamber may be illuminated for viewing. The pressure vessel was fitted with inlet and outlet valves and with an accurately calibrated pressure gauge.

Inside the chamber rests a small platform which supports a glass dish of rectangular shape having an optically polished front window. Within this dish are suspended the four cells containing the gelatin samples. The dish is filled with water to buffer the samples from the fluctuations in the ambient gas temperature which occur during compression and decompression. A mercury thermometer, visible through the front window, is suspended in the water to allow the temperature of the gelatin to be monitored.

The four counting chambers which contain the gelatin are identified as CS1, CS2, CS3, and CS4. They were constructed by sealing one end of sections of optically polished pyrex glass tubing, and forming lips around the open end. The counting chambers have rectangular cross-sections of 3.00 x 0.84 cm and have lengths of 50, 44, 38, and 32 mm, respectively. These staggered lengths

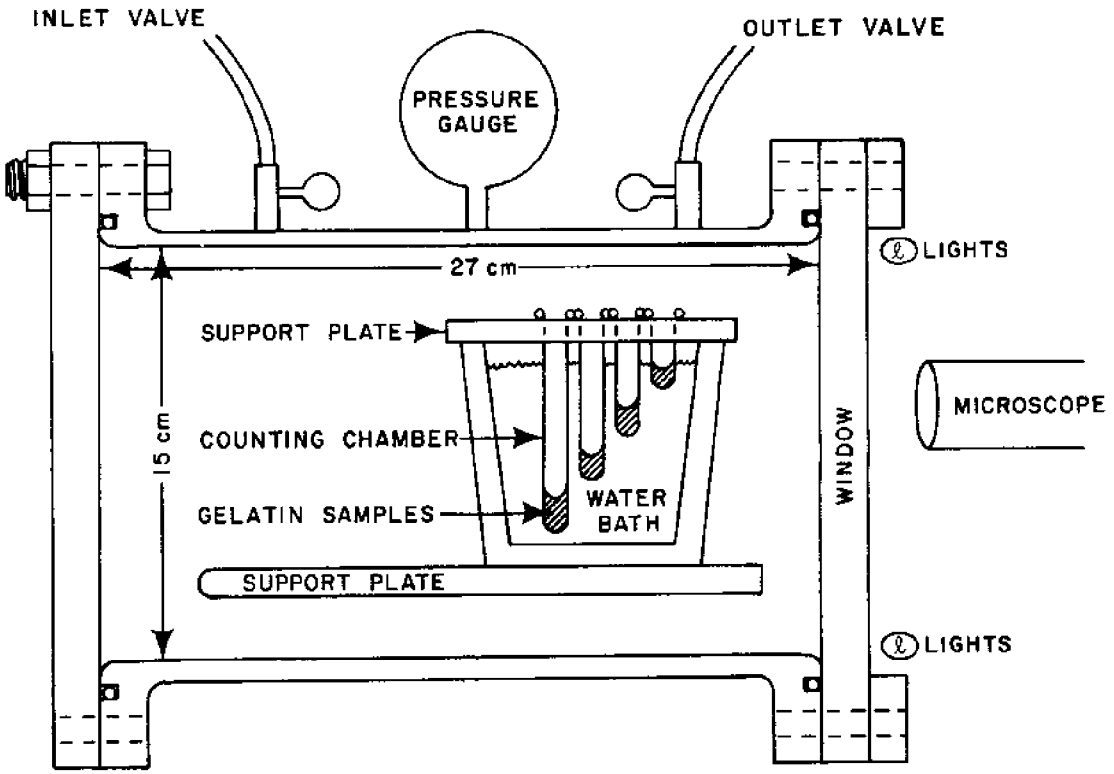

Figure 2.1. Apparatus used for the gelatin experiments

allow the lowest 6 mm of each cell to be seen when the chambers are suspended from their lips in sequential order. When the chambers are in position within the pressure vessel, all four may be simultaneously examined through the window of the vessel. A set of grid lines etched into the lower 6 mm of each cell provides fiducial reference marks for filling of the chambers and for counting of bubbles. A photograph of CS4 is shown in Figure 2.2.

To insure uniformity of behavior, the gelatin used in these experiments was produced in large batches and frozen in individual aliquots for subsequent use. The gelatin was mixed with distilled water that had stood overnight to allow time for gross bubbles to float to the surface and for small bubbles to diffuse away. To prepare a batch, 27 g of unflavored Knox gelatin powder were first mixed into 800 ml of water at room temperature. The resulting gelatin sludge was diluted with an additional 2,000 ml of water which had been warmed to 37°C and was poured through a funnel into a large plastic bottle which was then placed in a 40°C waterbath. An additional 2,200 ml of water were added to bring the total volume of gelatin to 5,000 ml. The solution was left in the bottle for 50 minutes to dissolve thoroughly, during which time it was stirred occasionally. After 50 minutes a small volume of the gelatin was siphoned through a rubber tube into a beaker and discarded. Each of 320 previously prepared plastic sample bottles was then filled with 10 ml of gelatin, capped, and placed in a freezer.

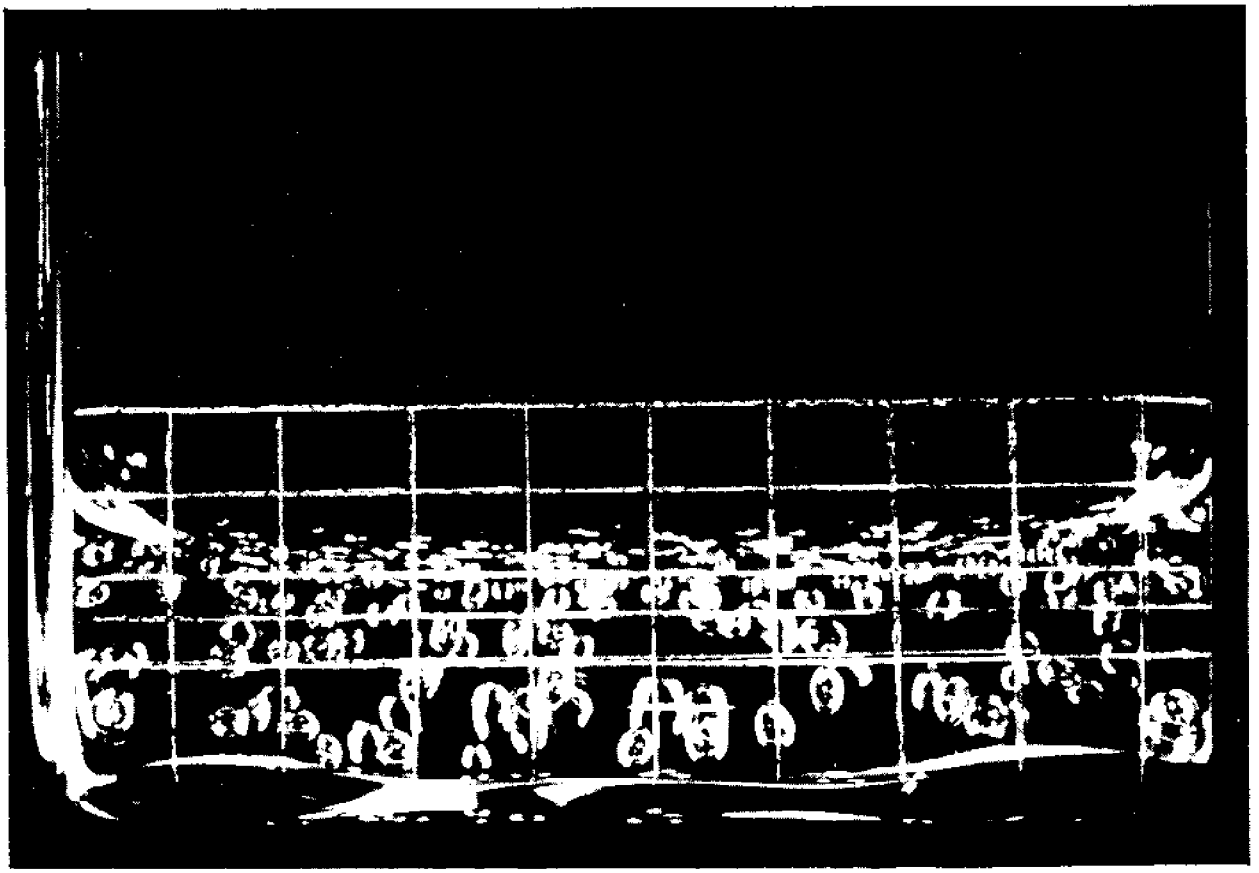

Figure 2.2. Gelatin in counting chamber 4

To conduct an experiment, a sample of frozen gelatin was taken from the freezer and placed in a 40°C waterbath. After 18 minutes, the cap was removed and the bottle was gently swirled four times. Twenty minutes total time in the waterbath was generally sufficient to allow complete melting of the gelatin, but in some cases it was necessary to wait an additional minute for the sample to become liquified.

A clean pipet was used to withdraw gelatin from the center of the bottle, the first pipet full of gel being discarded. The solution was drawn again, and each of the counting chambers was filled to the 4 mm line in the following order: CS4, CS1, CS3, and CS2. Counting chambers CS1 and CS3 were then transferred to an ice-water bath where they were allowed to stand for 10 minutes in order to gel completely. Counting chambers CS2 and CS4 were allowed to remain initially in the sol state. The four chambers were then suspended in the glass holding dish, which had been previously filled with water at a temperature of 20.0°C. The dish was placed into the pressure chamber and the endplate bolted into place. A dissecting microscope was moved into position and adjusted so that the samples could be viewed and photographed throughout the dive.

The generalized pressure schedule used in these experiments is shown in Figure 2.3. The experiment began with the introduction of dry nitrogen gas

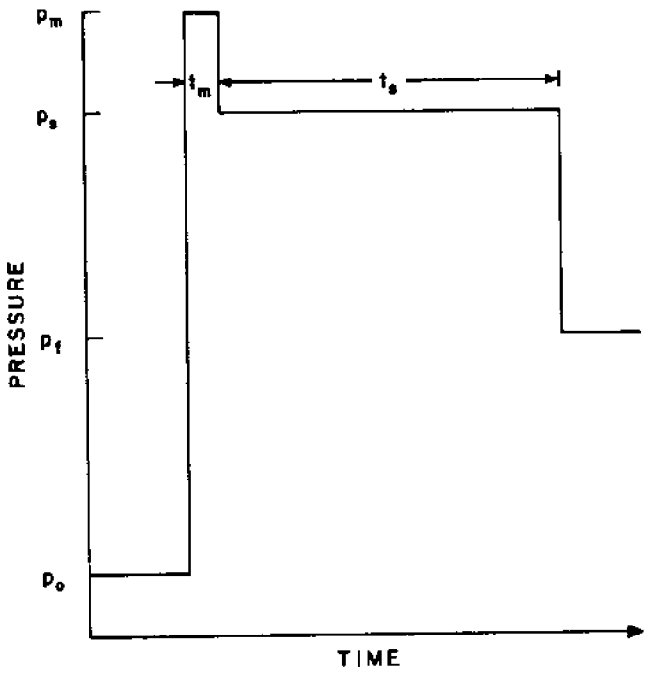

Figure 2.3. Generalized pressure schedule used in the gelatin experiments

into the pressure vessel at a rate of 0.23 bar/sec until the desired maximum pressure p_m was reached. This maximum pressure was maintained for a time t_m, at which point the pressure was reduced to the saturation pressure p_s and held constant for a time t_s. During this saturation period, the solution in counting chambers CS2 and CS4 gelled. Following saturation, the chamber was decompressed in 10 seconds to the final pressure p_f, and bubble formation was thus initiated in the gelatin samples.

Bubbles first became visible several seconds after decompression and grew rapidly during the next few minutes. Their growth was essentially complete after 10 minutes, and the resulting bubbles persisted for several days if the sample was left undisturbed. The typical diameter of a nitrogen bubble was around 1 mm, and the bubbles were uniformly distributed in the lower 3 mm of the counting cells. The number of bubbles occurring in a counting cell was generally less than 500. They were of uniform size and randomly distributed throughout the sample. The bubble density was never so high that coalescence occurred.

Five minutes after decompression, the number of bubbles in each sample chamber was counted three times; if the tallies were not in agreement a fourth count was made. To avoid any possible effects of surface contamination or rapid gas flow in the miniscus, only bubbles in the lower 3 mm of the sample chambers were included. In a few cases in which the number of bubbles was very large or the bubbles were large and distorted, the chamber was recompressed to 5.25 bar to reduce bubble size and facilitate counting. In dives which resulted in extremely large bubble numbers only one tally was made.

After the counting was finished, a series of photographs was taken of the counting chambers to provide a permanent record of the experimental results.

Upon completion of the experiment, the counting chambers were removed from the pressure chamber, and the gelatin was washed out with hot water. Immediately before their next use, the chambers were washed with a cotton-tipped applicator dipped in a dilute soap solution, emptied, and flushed at least three times with tap water. Following an additional flushing with distilled water, the chambers were filled with acetone and shaken, the acetone was dumped, and the chambers were placed upside down to dry on a clean paper towel.

2.2. Preliminary experiments

A most useful property of the gelatin model is its ability to yield reproducible data over time periods exceeding one year. This allows extended research programs to be conducted and the results confirmed by multiple and easily reproducible experiments.

As an initial test of the repeatability of the gelatin model, four dives using identical pressure schedules and adhering to the protocol outlined in section 2.1 were conducted in a one-week period. The results of these experiments are shown in Table 2.1. The average number of bubbles per sample produced by this pressure schedule was 66.13, with a standard error in the mean of 2.45. As an additional test of the stability of this model, a similar experiment was conducted by each new operator to use the equipment. In all cases it was found that after mastering the technique, the operator could obtain consistent bubble numbers for a given pressure schedule from sample to sample and from dive to dive. The longer term repeatability of the gelatin measurements may be inferred from the data reported in section 2.3, where measurements made at time intervals of many months are found to be in agreement.

TABLE 2.1. TRIAL RESULTS OF FOUR GELATIN MODEL EXPERIMENTS

Trial No.	No. of bubbles per sample			
	CS1	CS2	CS3	CS4
1	62	64		66
2	87	62	66	85
3	62	52	55	60
4	73	66	66	66

2.2.1. Assignment of errors

As indicated in section 1.3, the bubbles produced in these experiments originated from cavitation nuclei. It has been found that the number of bubbles produced by a given pressure schedule depends upon the number of nuclei

larger than some critical size. Thus, while the ultimate size of a bubble will depend upon both the bubble density in the sample and the quantity of dissolved gas, the threshold supersaturation pressure required for the growth of any given nucleus into a gross bubble will depend only on the properties of the fluid and the constituents of that nucleus, and not upon interactions with other nuclei. The occurrence of bubbles in a sample may therefore be regarded statistically as a Poisson process, and the distribution of bubble numbers resulting from independent measurements is expected to follow a Poisson distribution. As is well known, the error associated with a single measurement of a variable having a Poisson distribution is the square-root of the observed number, i.e., $\sqrt{N}$.

The validity of this error assignment is demonstrated by the data in Table 2.1. The average number of bubbles per sample is 66.13 with a standard deviation of 9.17 and a standard error in the mean of 2.45. Using the assumption of Poisson statistics to assign an error of $\sqrt{66.13}$ to each of 15 data points yields an error in the mean of 2.17.

Unless otherwise noted, the errors reported in this study were calculated assuming Poisson statistics. The error ε assigned to a single measurement of N bubbles is thus $\sqrt{N}$; the error resulting from combining n individual measurements N_j is computed as

$$\varepsilon^2 = \sum N_j/n(n - 1) \ . \qquad (2.1)$$

2.2.2. Gelatin saturation time

As discussed in section 2.1, the gelatin samples used in this study were contained in glass cells filled to a depth of 4 mm. The time required to saturate these samples with nitrogen gas was investigated with a series of dives in which bubbles were counted for various saturation periods. The results of this study are shown in Figure 2.4. It is seen that the bubble number at first increases rapidly with increasing exposure time, levels out at about 5.25 hours, and then declines until an equilibrium state is reached at around 14 hours.

In order to complete individual dives conveniently, a saturation time t_s of 5.25 hours was chosen for standard use. Because the slope dN/dt_s vanishes at this point, the resulting bubble numbers are not strongly influenced by small changes in t_s. Unless otherwise noted, the value of t_s used in this work is 5.25 hours.

2.2.3. Temperature effects

The weak gelatin mixtures employed in these experiments were found to melt at 26°C. Since the chamber temperature was usually near 24°C, this low melting temperature was not a problem, but it did serve to limit the temperature extremes encountered in this work from the initial 20°C of the water bath to the 26°C gelatin melting point. The temperature of the gelatin was normally 24°C and was routinely monitored and recorded during all experiments. The effect of temperature on bubble number within the range from 20°C to 26°C was investigated by performing a series of similar dives in which the gelatin

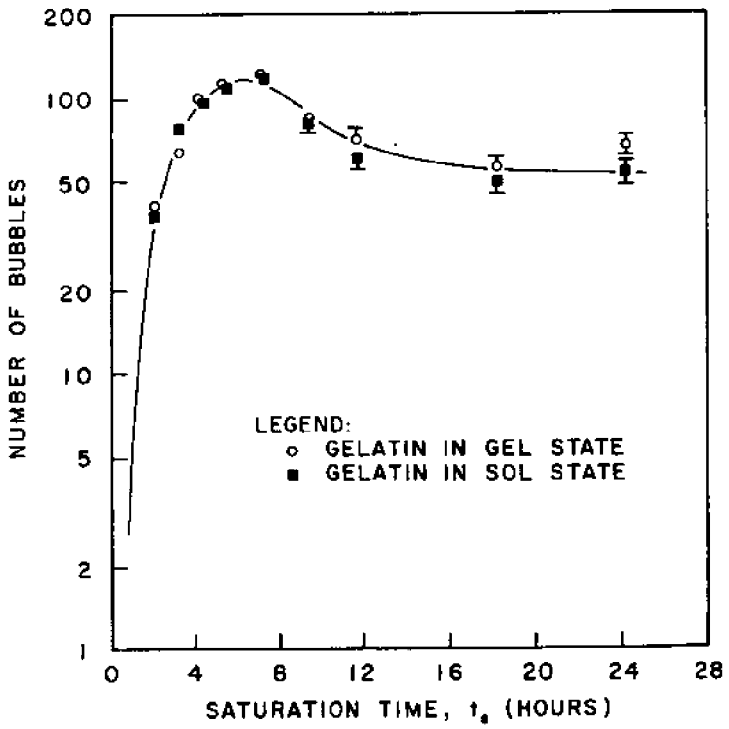

Figure 2.4. Bubble number as a function of saturation time

temperature varied from day to day in response to changes in the ambient temperature. The results of this investigation are given in Table 2.2. These data indicate that the variations in temperature were small and that these small fluctuations did not significantly alter the bubble counts.

TABLE 2.2. EFFECT OF TEMPERATURE ON BUBBLE NUMBER

Date	Temperature (°C)				Number of bubbles per sample
	$T(0)$	$T(t_m)$	$T(t_s)$	$T(t_f)$	
6 Aug 73	20.0	21.7	24.8	24.0	15.6
7 Aug 73	20.0	21.9	25.0	24.0	15.6
9 Aug 73	20.0	22.0	25.0	24.0	21.6
13 Aug 73	19.8	21.5	24.7	24.0	19.0
13 Aug 73	19.8	21.4	24.2	23.9	17.0
20 Aug 73	19.8	21.2	24.8	24.1	22.0
22 Aug 73	19.9	21.6	25.0	24.1	18.0
24 Aug 73	19.8	21.4	25.1	24.3	27.0

2.2.4. Compression rate

The rate of compression from the initial ambient pressure p_o to the maximum pressure p_m was standardized at 0.23 bar/sec. This compression rate is referred to as "rapid." The effects of small changes in this rate on bubble numbers were negligible. The magnitude of the largest rapid compression occurring in a pressure schedule is known as the "crushing pressure." This was normally equal to the difference between the maximum and initial pressures,

$$p_{crush} = p_m - p_o \quad . \tag{2.2}$$

To determine whether large changes in the compression rate affect the bubble numbers, a series of dives using a "slow" compression rate was performed by increasing the pressure by 1 bar every 30 minutes. It was found that slow-compression dives yielded an order of magnitude more bubbles than the corresponding rapid-compression dives. The data comparing fast and slow compression dives are presented in Figure 2.5. In section 4.3 the theoretical effects of compression rate on bubble number are discussed, and the large difference in bubble yield between fast and slow compression is explained.

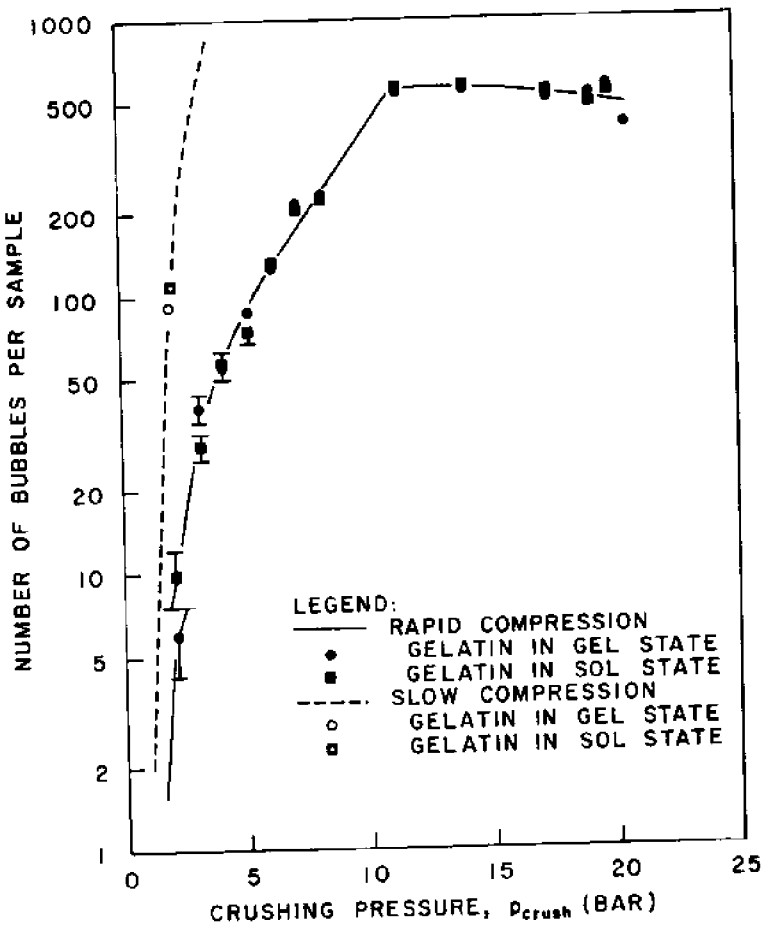

Figure 2.5. One-atmosphere-envelope for gelatin batch A

2.3. Saturation-excursion dives

The most decisive results obtained from the gelatin experiments are reported in this section. In this series of dives the pressure was rapidly raised to the maximum value p_m, and the gelatin was allowed to saturate with gas at the same pressure, $p_s = p_m$. The gelatin was then decompressed to the final pressure p_f, and the resulting number of bubbles was counted. The objective of these experiments was to determine how the bubble numbers depend upon the saturation and supersaturation pressures.

For this type of dive profile the change in pressure Δp occurring during decompression is identical to the supersaturation pressure, $p_{ss} = \Delta p = (p_s - p_f)$. All compressions were normally done at the rapid rate of *0.23 bar/sec*, while decompressions were accomplished in 10 seconds, i.e., at a rate of $0.17\ (p_s - p_f)$ *bar/sec*.

Two independent sets of data are presented in this section. The first group of experiments (Yount and Strauss, 1976), conducted in April and May of 1973, utilized gelatin mixed on 16 March 1973. This set of gelatin samples is referred to as batch A. The second group of experiments (Yount et al., 1977) used samples from gelatin batch D, mixed on 4 June 1976. These dives were done in the fall of 1976 as part of the filtration experiments discussed in the following section.

Figures 2.5, 2.6, and 2.7 show the results of dives in which the crushing pressure is equal to the supersaturation pressure, $p_{crush} = p_{ss}$. Since these

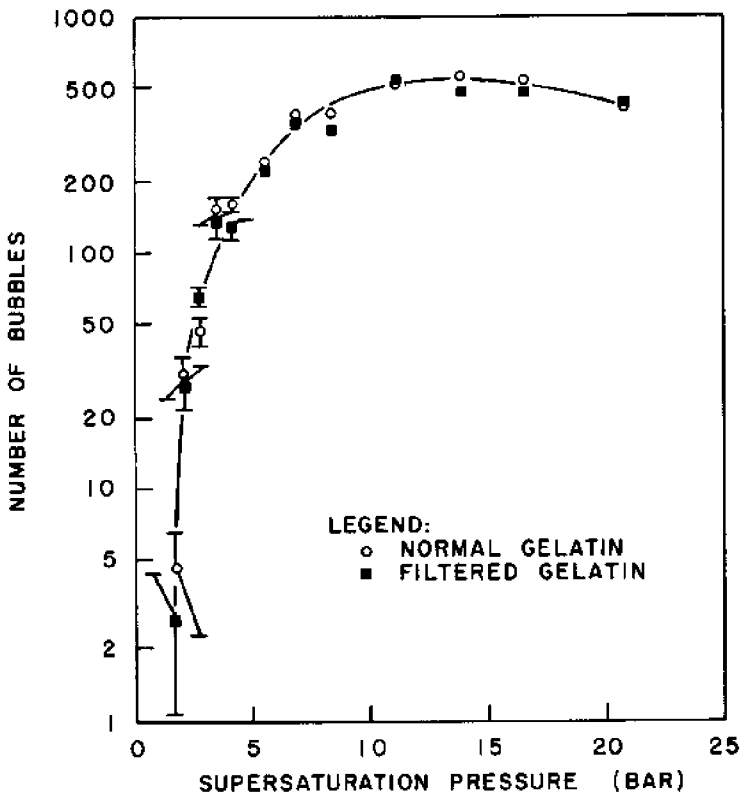

Figure 2.6. One-atmosphere-envelope for gelatin batch D

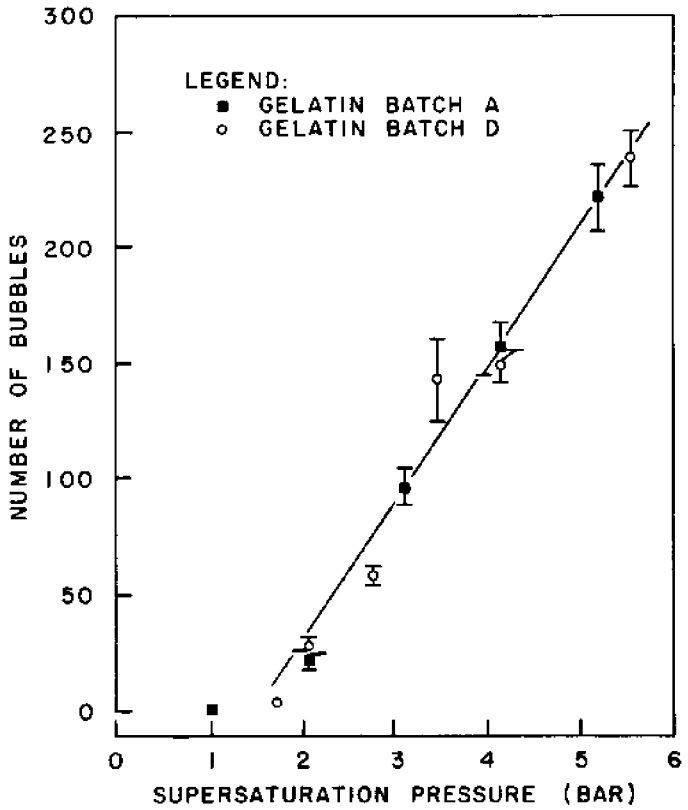

Figure 2.7. Low pressure end of the one-atmosphere-envelope

pressure profiles begin and end at an absolute pressure of one atmosphere, the resulting data define a curve known as the "one-atmosphere-envelope." As seen in Figure 2.7, in the range between zero and six atmospheres the number of bubbles produced by this type of pressure schedule increases linearly with increasing pressure. The close agreement between gelatin batch A and batch D in this low pressure range is not an intrinsic feature of the cavitation process, but instead reflects the fact that batch D was specially prepared to produce bubble counts similar to those of batch A. The bubble count continues to rise sharply in the pressure range from seven to twelve atmospheres, beyond which it levels off and then declines slowly. Included in Figure 2.5 is the one-atmosphere-envelope for "slow" compression dives as described in subsection 2.2.5.

The results of three additional sets of experiments for each of the two types of gelatin are shown in Figures 2.8 and 2.9. In these studies p_s was held constant and p_{ss} was varied. Data points thus produced trace out the relationship between the bubble number and the supersaturation pressure for a fixed value of the saturation and crushing pressures; these curves are therefore referred to as "loci of constant p_s" or "loci of constant p_{crush}."

The data in Figures 2.8 and 2.9 can be shown in a more useful form by plotting the saturation and supersaturation pressures required to form a fixed number of bubbles (Yount et al., 1977). This is done graphically from either Figure 2.8 or Figure 2.9 by constructing a series of lines parallel to the abscissa which correspond to fixed numbers of bubbles, by establishing the

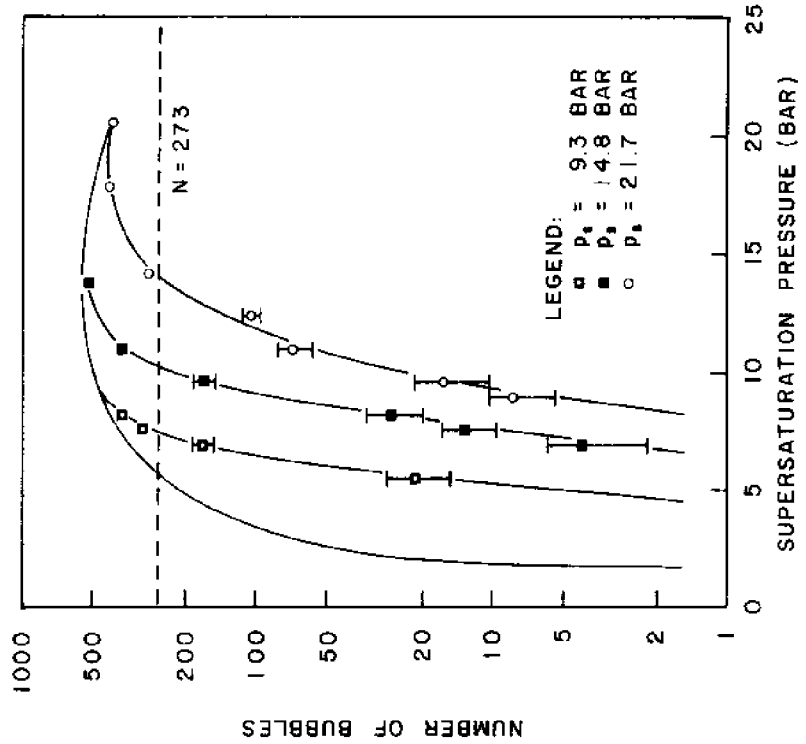

Figure 2.9. Loci of constant p_s for gelatin batch D

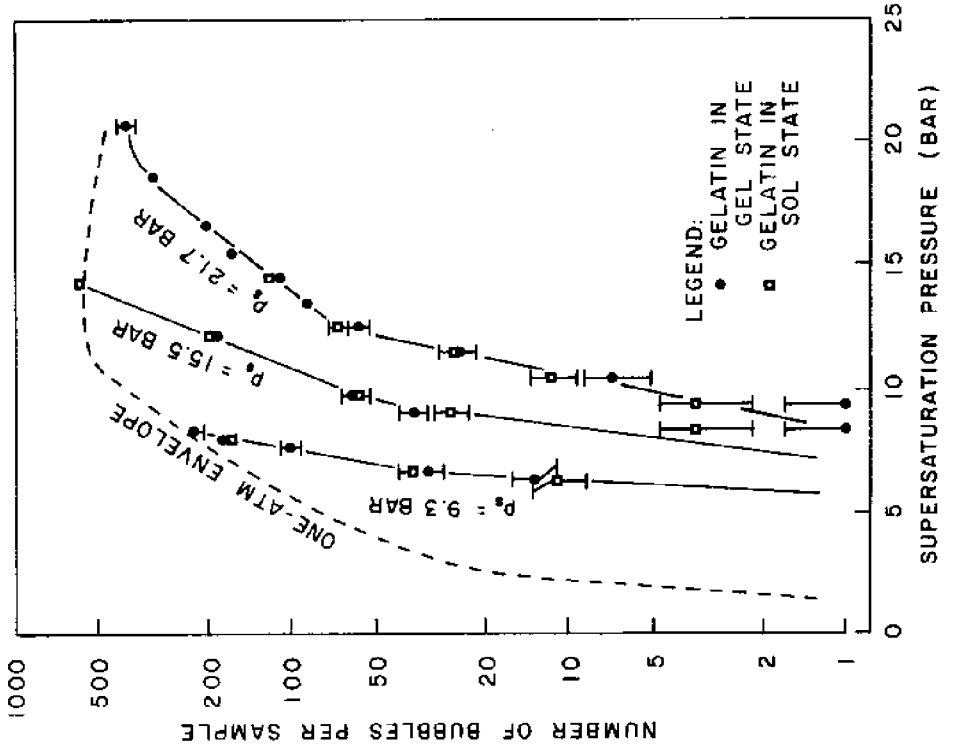

Figure 2.8. Loci of constant p_s for gelatin batch A

intercept of these lines with each of the three loci of constant p_g and the one-atmosphere-envelope, and by then reading the corresponding supersaturation pressures from the abscissa scale. As an example, the $N = 273$ line shown in Figure 2.9 crosses the one-atmosphere-envelope at 6.1 bar, and the 8.3, 13.8, and 20.7 bar loci of constant p_{crush} at supersaturation pressures of 7.7, 10.8, and 14.5 bar, respectively. These four (p_{crush}, p_{ss}) points may now be plotted to define a curve of constant bubble number. Isopleths of bubble number for the two sets of gelatin data are shown in Figure 2.10.

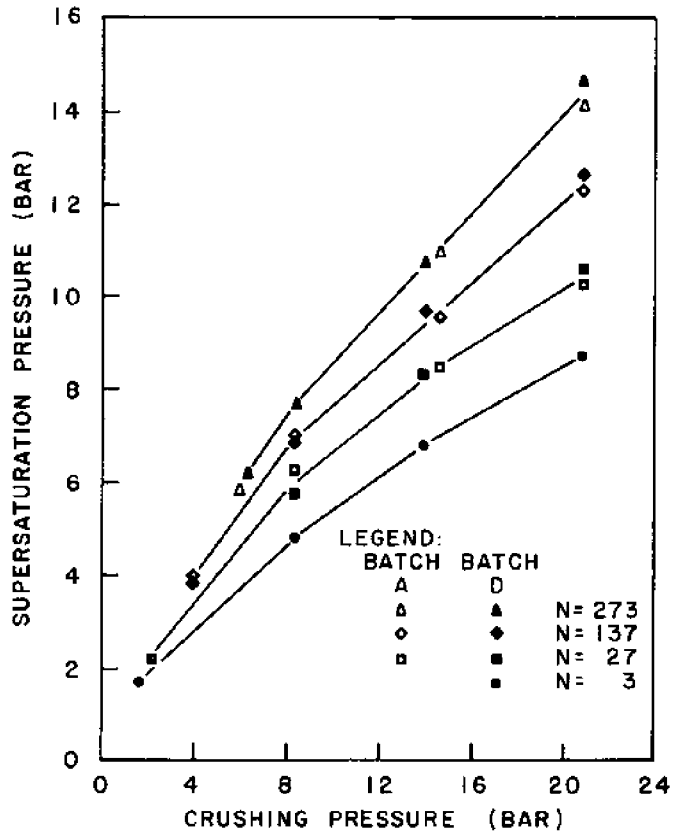

Figure 2.10. Isopleths of constant bubble number

From examination of Figure 2.10 it is seen that the supersaturation pressure required to form a fixed number of bubbles increases with the crushing and saturation pressures. From interpolation of the data in Figure 2.10 it is possible to determine what combination of supersaturation and saturation pressures will yield a given number of bubbles.

2.4. Filtration experiments

In order to establish the initial size of the nuclei responsible for the bubbles observed in the gelatin experiments, a series of dives was performed in which the gelatin samples were filtered before compression (Yount et al., 1977). The protocol used in these tests was similar to that previously described, with the exception that immediately after being thawed, the gelatin was pipeted into a filter-holding syringe and in this manner passed through

a "Nuclepore" filter. These filters have holes etched to an accuracy of +0/-20%; a photomicrograph of such a filter is shown in Figure 2.11.

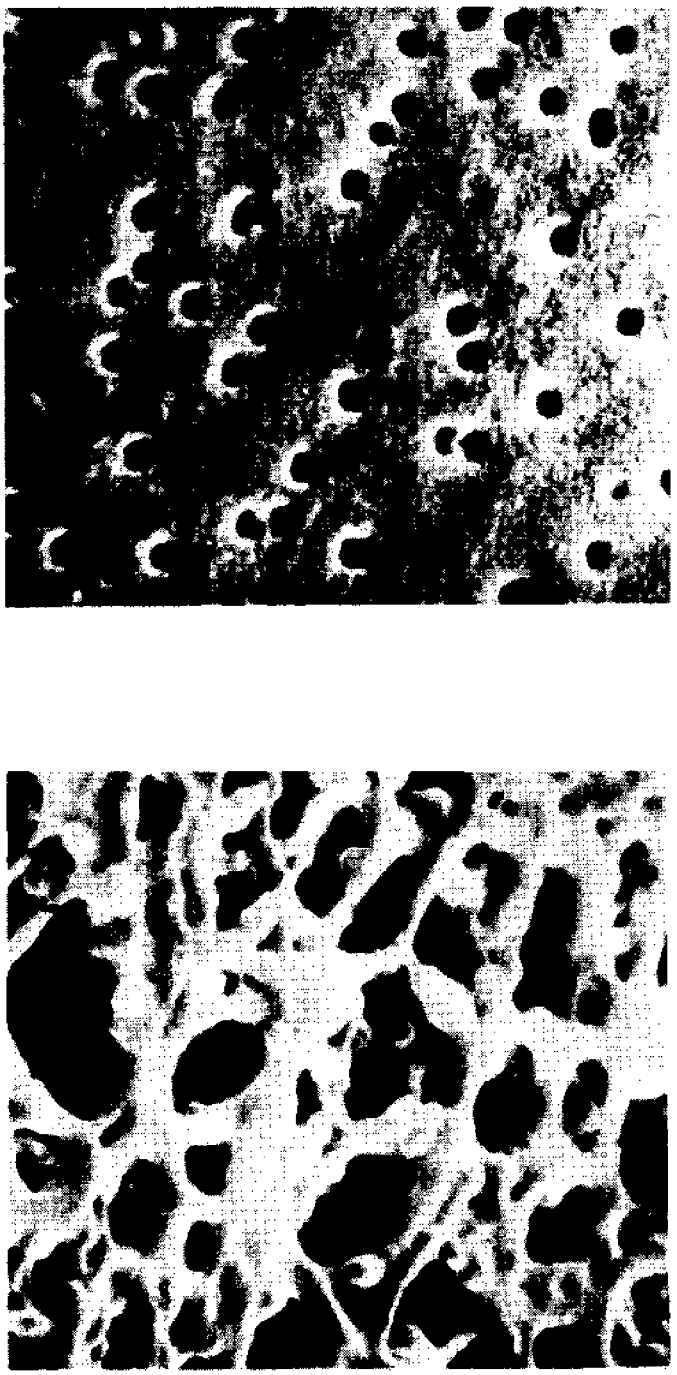

Figure 2.11. Scanning electron micrographs show smooth, flat surface and uniform, straight-through cylindrical pores of 10 μm "thin," 0.4 μm pore size Nuclepore membrane (top) with rough, tortuous paths of a 150 μm "thick," 0.45 μm pore size cellulosic filter

Experiments were conducted with filters having nominal pore diameters of 3.0, 1.0, 0.8, 0.6, and 0.4 μm. It was not possible to pass the gelatin through a 0.2 μm diameter filter. After filtration the samples were subjected to a standard one-atmosphere-envelope pressure schedule, $p_{crush} = p_{ss}$, and the resulting number of bubbles was counted. An unfiltered sample was included as a control in each of these experiments. The results are shown in Figure 2.12.

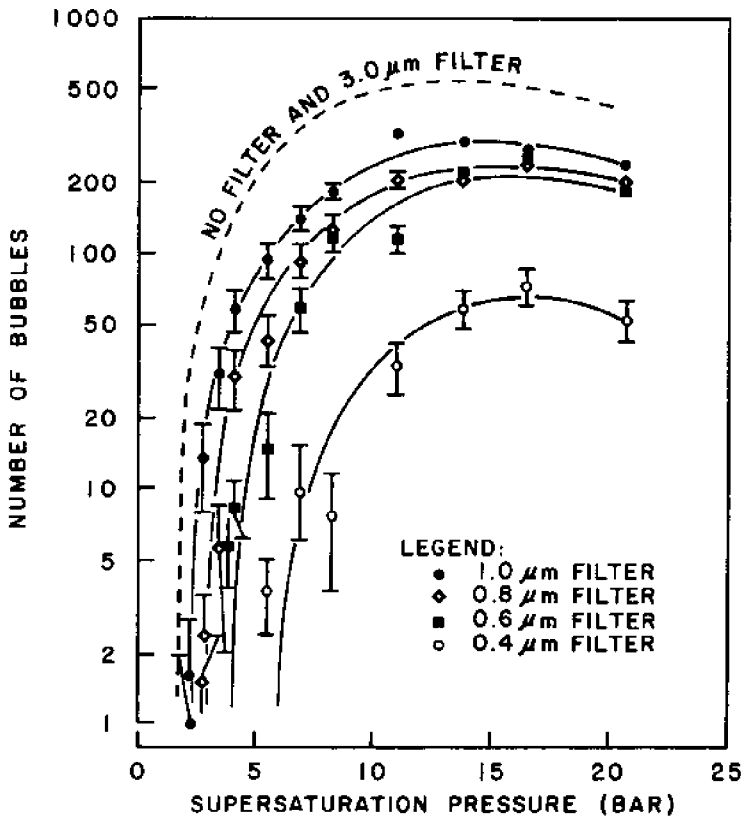

Figure 2.12. Gelatin filtration data

From examination of Figure 2.6 it can be seen that passing the gelatin through a 3.0 μm filter had no effect on the observed bubble numbers. Evidently, the nuclei responsible for the observed bubble formation in gelatin initially had diameters of less than 3 μm. For gelatin passed through the 1.0 μm filter, two differences from the unfiltered data are noted: the threshold pressure for bubble formation is shifted from 1.6 bar to 2.4 bar, and the maximum number of bubbles is lowered by about a factor of two. For gelatin passed through the 0.8 μm, 0.6 μm, and 0.4 μm filters, the threshold pressure is increased to 3.0, 4.0, and 6.1 bar, respectively, and the maximum number of bubbles is further reduced.

The systematic increase of the threshold pressures with decreasing filter size observed in this experiment establishes the important concepts of critical radius and the ordering theorem. In analogy with the result for pure bubbles discussed in subsection 1.1.2, it is assumed that for a pressure history resulting in a supersaturation pressure p_{ss}, there exists a critical

radius r_c such that any nucleus having a radius larger than r_c will grow into a gross bubble, while nuclei of lesser size will remain small. The "ordering theorem" (Yount et al., 1977) states that if at some time nucleus 'a' is larger than nucleus 'b,' then at any time in the future both nuclei will still be present in the sample and nucleus 'a' will still be larger than nucleus 'b.' When applied to a large number of nuclei, this theorem states that if at some point in time when there are N nuclei larger than nucleus 'a,' then at any time in the future there will remain N nuclei larger than nucleus 'a.' This theorem is applicable when nuclei change in size in a continuous manner, such as during the application of a pressure spike, but not when nuclei are selectively or discontinuously deleted from the sample by an external agent, such as a filter. When an experiment is performed that results in a supercritical supersaturation pressure, the ordering theorem states that the number of bubbles produced in the sample will be given by the integral

$$N(r_c) = \int_{r_c}^{\infty} n(r)dr \ , \tag{2.3}$$

where $n(r)$ is the size distribution of nuclei in the sample when the critical radius has the value r_c.

The ordering theorem can be used to determine the initial distribution of nuclear sizes in the gelatin samples. From the data presented in Figure 2.12, it is seen that the threshold for bubble formation in gelatin passed through a 0.5 μm radius filter is 2.4 bar. This represents a direct determination that the critical radius for a 2.4 bar one-atmosphere-envelope dive is 0.5 μm. From the number of bubbles counted at 2.4 bar for the one-atmosphere-envelope for unfiltered gelatin, also shown in Figure 2.12, it is concluded that there were initially 54 nuclei larger than 0.5 μm. To reach this conclusion only the ordering theorem has been assumed. From the examination of the remaining filtration data the number of nuclei initially larger than 0.4 μm, 0.3 μm, and 0.2 μm in radius may be established. The observed number of nuclei initially larger than these radii are illustrated in Figure 2.13.

An excellent fit to these data is provided by the exponential function

$$N(r) = 776 \exp(-r/0.186) \ , \tag{2.4}$$

where r is measured in μm. This equation is the integral size distribution of those nuclei which produce gross bubbles,

$$N(r_c) = \int_{r_c}^{\infty} n(r)dr = \int_{0}^{\infty} n(r)dr - \int_{0}^{r_c} n(r)dr \ , \tag{2.5}$$

where $n(r)$ is the differential nuclear size distribution in number per cm per ml. Taking the derivative of equation 2.5 yields the expression

$$dN(r)/dr = -n(r) \ . \tag{2.6}$$

Applying this result to equation 2.4 yields

$$n(r) = 4{,}172 \exp(-r/0.186) \ ; \ 0.2 \ \mu m < r < 0.5 \ \mu m \ . \tag{2.7}$$

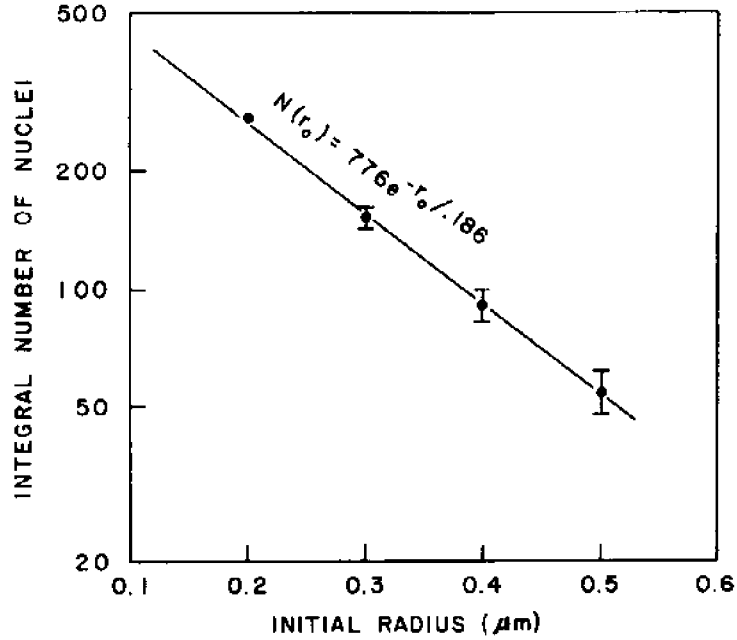

Figure 2.13. Initial distribution of nuclear radii

This is the distribution of initial nuclear sizes in the gelatin as determined by the filtration experiments. The only assumptions entering into this measurement have been the ideas of critical radius and the ordering theorem as combined in equation 2.3. In this sense, the result is model independent and does not rely upon any detailed knowledge of the physics of the nuclei.

The other significant feature of the filtration data shown in Figure 2.12 is the anomalous decrease in bubble number in the filtered samples relative to the unfiltered controls. As an example of this effect, it is expected from the observed distribution of nuclear sizes that the 0.5 μm radius filter would remove 54 nuclei from the gelatin sample. For one-atmosphere-envelope dives to pressures greater than the 2.4 bar threshold observed for this size filter, the number of bubbles produced in the filtered samples might be expected to be 54 less than that observed in the control. This is not the case. It is seen from the data that the 0.5 μm filter curve lies between 140 and 250 bubbles per ml below the unfiltered control.

This anomalous behavior is attributed to the non-ideal action of the filters used in these experiments. While it is a necessary condition that a nucleus have a size less than the filter pore size to pass through the filter, this is not sufficient to insure its passage. When a given amount of gelatin is filtered there will be nuclei smaller than the pore size originally present in the sample that will not pass through the filter. In this sense the action of the filter is non-ideal. The physical cause of this non-ideal behavior is believed to be the partial clogging of individual pores with debris from the filtrate. This partial clogging reduces the effective size of some of the filter pores and, thus, prohibits the passage of some nuclei that an unclogged filter would transmit. A more complete discussion of the physics of partially blocked filters is given in Yount et al. (1977a).

A quantitative description of the amount of non-ideal behavior exhibited by a filter is expressed by the filter efficiency factor. This number is defined as the ratio of the number of objects that pass through the actual filter to the number that would pass through an ideal filter. It is to be expected that this efficiency factor will depend on the size of the objects being filtered, becoming small for objects near the pore size, and tending toward unity as the objects become much smaller than the filter pores. This is because small objects passing through a pore are not impeded if that pore is partially obstructed, while larger structures may be stopped.

Filter efficiency factors for the gelatin data are computed from the formula

$$f = \frac{N}{N_O - N_1} , \tag{2.8}$$

where N is the observed number of bubbles for a particular filter and pressure combination, N_O is the number of bubbles in the unfiltered control at this pressure, and N_1 is the number of nuclei in the sample larger than the filter size. The computed efficiency factors as a function of filter size and pressure are presented in Table 2.3. It is seen that for a fixed pressure the efficiency drops as the filter size decreases, and that for a given filter size the factor increases with increasing pressure. The first observation shows that small pores clog more rapidly than larger ones, which is expected. The second observation may be understood by remembering that the larger bubble numbers seen at higher pressures imply that smaller nuclei are growing into bubbles. These smaller nuclei are less affected by the clogs in the filter pores, and the filter efficiency thus rises.

TABLE 2.3. FILTER EFFICIENCY FACTORS

P_{ss} (bar)	Initial nuclear radius (μm)			
	0.5	0.4	0.3	0.2
8.6	.50	.43	.37	.05
10.4	.53	.48	.40	.13
13.8	.57	.52	.45	.16
17.2	.58	.55	.49	.23
20.7	.64	.60	.55	.27

It should be noted that the imperfect nature of the filtration process used in these experiments does not challenge the arguments regarding the initial size distribution of nuclei as developed in the beginning of this section. In this work it was assumed only that no nuclei larger than the pore size passed through the filter. While the non-ideal nature of the filtration prohibited some nuclei from passing through the actual filter that would have passed through an ideal filter, it did not permit nuclei to remain in the

sample that ideally would have been filtered out. The conclusions about nuclear size are thus unaffected.

The observed nuclear size distribution given by equation 2.4 allows the isopleths of constant bubble number to be interpreted in terms of initial nuclear radii. As an example, a bubble number of 273 is seen to correspond to an initial nuclear radius of 0.2 μm; the *N = 273 isopleth* in Figure 2.10 is therefore associated with the supersaturation pressure required to induce a nucleus of 0.2 μm initial radius to grow into a bubble after having been rapidly compressed by an amount p_{crush}. Similar (p_{crush}, p_{ss}) relationships for 0.5 μm, 0.4 μm, and 0.3 μm nuclei can be found by determining isopleths of constant bubble numbers of 54, 90, and 150, respectively. The measured values of (p_{crush}, p_{ss}) points are plotted in Figure 2.14.

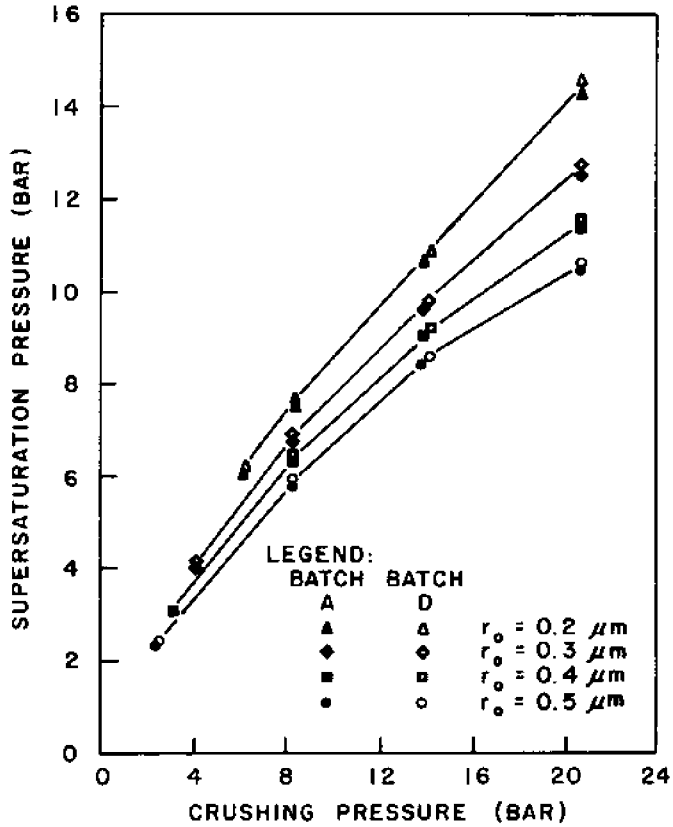

Figure 2.14. Pressure reduction limits as a function of crushing pressure

2.5. Denucleation

The data presented in Figure 2.10 demonstrate that the number of bubbles formed in response to a fixed supersaturation decreases as the crushing pressure rises. If it is assumed that the critical radius for bubble formation depends only on the supersaturation pressure and not the absolute pressure, then this result implies, through use of the ordering theorem, that the

application of a rapid compression shifts the size distribution of nuclei toward smaller radii. In order to test the validity of this hypothesis, a set of dives was conducted in which p_s and p_{ss} were held constant, but a pressure spike was applied to the gelatin samples prior to the beginning of the saturation period. Since both the saturation and supersaturation pressures were constant, the critical radius for bubble formation at the final pressure remained constant and was independent of the magnitude or duration of the pressure spike. Any change in bubble number induced by the pressure spike must therefore have as its cause a shift in the distribution of nuclear sizes.

The dive profile used in these tests is shown in Figure 2.3. The samples were compressed at the rapid rate of *0.23 bar/sec* to a maximum pressure p_m of 21.7 bar, and this pressure was held for a time t_m. The chamber was then decompressed in 10 seconds to the saturation pressure p_s of 11.3 bar, where the samples were allowed to stand for a time period of $(5.25 - t_m)$ hours. The total length of the experiment was thus held constant at about 5.25 hours. After saturation the samples were decompressed to ambient pressure, and the resulting number of bubbles was counted. All of these dives utilized samples from gelatin batch A. These experiments are somewhat similar to those of Harvey et al. (1944), who showed that the threshold for ultrasonic cavitation can be similarly increased by the application of a pressure spike.

The results of this program are shown in Figure 2.15. The number of bubbles produced when the pressure spike was held for one second is 275 per ml. The number of bubbles produced in a 1.0-11.3-1.0 bar one-atmosphere-envelope dive is about 1,210 per ml. The pressure spike thus reduced the bubble yield by a factor of 4.4. As t_m increased, the number of bubbles decreased sharply for the first two minutes and then leveled out at 39 bubbles per ml. The ultimate effect of the pressure spike was to reduce the bubble yield to 3.2 percent of its nominal amount. Since p_s and p_{ss}, and thus r_c, remained unchanged, it was concluded that *the rapid application of hydrostatic pressure to the gelatin resulted in the modification of the original nuclear size distribution.*

These experiments suggest that gelatin might be completely denucleated by the rapid application of sufficiently large pressure. To check this conjecture, tests were conducted in which gelatin was subjected to very large hydrostatic pressures by centrifugation. The gelatin was thawed in the usual manner, pipeted into the bottom of a centrifuge tube, and then gelled in an ice-water bath. The remainder of the tube was filled with cold distilled water, covering the gel to a depth of about 4 cm. The tube was then spun at 25,000 rpm for 15 minutes in an ultra-centrifuge, the water exerting a minimum hydrostatic pressure of 1,000 bar upon the gelatin during this period. After being spun, the water was emptied from the tube, and the gelatin was remelted. Normal dives were then conducted with the centrifuged gelatin.

For pressures up to the 21.7 bar limit of the chamber, the centrifuged samples produced no bubbles. Samples drawn from either the top or bottom of the treated gelatin sol in the tube failed to nucleate in all cases. As an additional check that the nuclei were being crushed rather than physically removed from the samples, gelatin adulterated with 0.2 μm polystyrene spheres was subjected to the same treatment. The spheres were not centrifuged out of

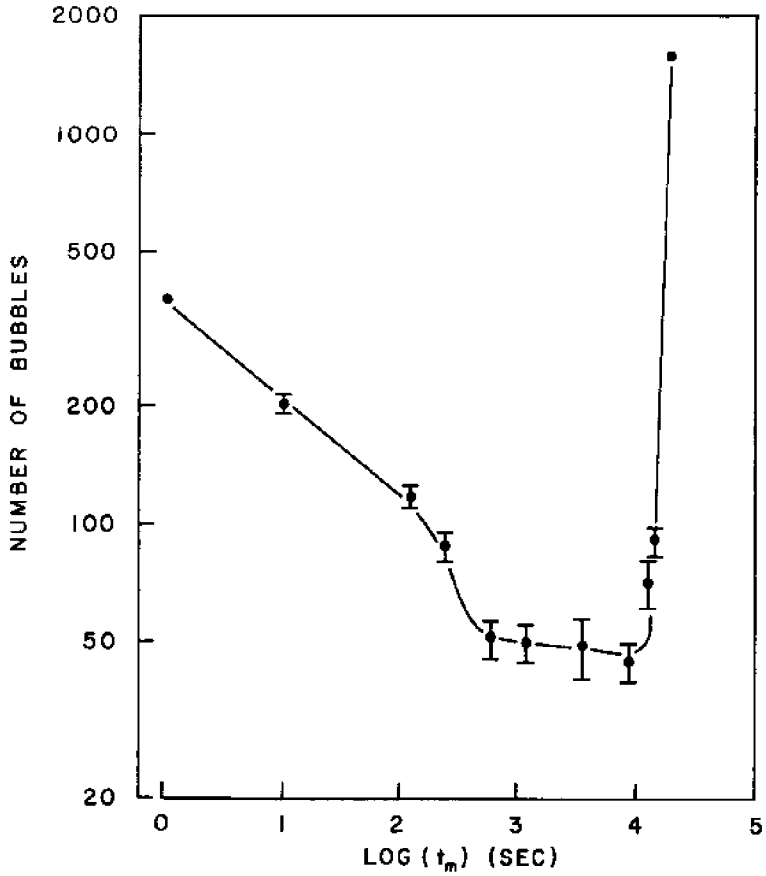

Figure 2.15. Number of bubbles as a function of time at maximum pressure

the sample. The rapid application of large hydrostatic pressure to the gelatin is thus an effective method of reducing the size of nuclei sufficiently to suppress bubble formation at supersaturation pressures of up to 20.7 bar.

Gelatin sol denucleated by centrifuging remains denucleated for periods greater than two days, the maximum that has been tested. The gelatin may be frozen and stored for many months without the reappearance of detectable nuclei. The observation that gelatin denucleated prior to the beginning of the standard dive protocol remains denucleated afterward demonstrates that the nuclei studied in the gelatin model experiments are not introduced into the samples during freezing, melting, or pipeting.

2.6. Summary of the gelatin experimental results

The gelatin experiments reported in this chapter provide data from which the following conclusions concerning the physical nature of cavitation nuclei are drawn:

1. The nuclei are associated with gas phases. This is inferred from the fact that the application of modest hydrostatic pressures will markedly

affect both the nucleation thresholds (section 2.4) and the bubble numbers (section 2.3), and that large pressures will effectively denucleate a sample (section 2.5). Because solids and liquids are little affected by such pressure changes, the nuclei must be associated with gas phases. This result is not new; it was first demonstrated by Harvey et al. (1944).

2. The nuclei are gas permeable. The data presented in subsection 2.2.5 show that the compression rate can greatly affect the final bubble numbers. This suggests that the gas within a nucleus is normally not isolated from the surrounding fluid, but can diffuse through the liquid-gas interface. This conclusion is supported by the observation of Strauss and Kunkle (1974) that bubbles can be produced in gelatin by isobaric switching of the ambient gas from nitrogen to helium. This sensitivity to atmospheric composition demonstrates conclusively the gas-permeable nature of the nuclei.

3. The nuclei are stable. As reported in section 2.5, gelatin may be effectively denucleated. This may be achieved either by modifying the nuclei within the gelatin, as by the application of large hydrostatic pressure, or by removing the nuclei from the sample by processes such as filtration. Once a sample has been denucleated, it remains that way for a period in excess of two days. This shows that cavitation nuclei are not being continuously replaced; hence, they must be stable, physical structures and not ephemeral products of kinetic processes such as random motion of the water molecules or ionization by cosmic rays.

4. Initially, the nuclei have an exponential size distribution given by equation (2.4).

5. A rapid compression modifies the nuclear size distribution.

CHAPTER 3. MODELS OF GAS CAVITATION NUCLEI

In this chapter several proposed models of gaseous cavitation nuclei are briefly reviewed and their validity in light of the results of the gelatin experiments is examined.

3.1. Classification of nuclear models

The basic problem to be overcome in stabilizing a gaseous cavitation nucleus is to prevent the collapse of the nucleus due to outward diffusion of the internal gas. For the similar case of the perfusion-limited collapse of a bubble in a saturated fluid held at constant ambient pressure, equation (1.15) gives the time rate of change in radius as

$$dr/dt = (6RT\alpha S\gamma/r)/(4\gamma/r + 3p_{amb}) \quad . \tag{1.15}$$

For a nucleus to be stable dr/dt must, by definition, vanish. This can be accomplished in four ways:

1. Provide a source to replace gas lost from the nucleus.
2. Arrange for the perfusion constant α to vanish.
3. Make the radius arbitrarily large.
4. Oppose the fluid surface pressure $2\gamma/r$ with an independent pressure or reduce the total surface tension at the liquid-gas interface to zero.

Each of these hypothetical operations has been used as the basis for one or more models of cavitation nuclei.

Nuclear models of the first kind make no attempt to prevent the outflow of gas from the nucleus, but instead provide a supply to replace that which is lost. Mathematically, these models add a source term to the gas flow equations.

The simplest of such mechanisms was suggested by Plesset (1969), who argued that solid, hydrophobic spheres would act as cavitation nuclei. The spheres are viewed as being immersed in a continuous fluid in which thermodynamic fluctuations at the solid-liquid interface act to produce a thin shell of gas surrounding the sphere. Plesset's model thus uses statistical fluctuations as a gas source.

This model has recently been re-examined by Yount and Kunkle (1975), who assumed that shell thicknesses of less than the diameter of a water molecule are not physically meaningful. A finite shell thickness of this size would lower the probability of shell formation by many orders of magnitude, indicating that the theoretical cavitation threshold for this model is about 1,000 bar. This is not very different from the result predicted for homogeneous nucleation. The Plesset model was tested experimentally by Kunkle and Yount (1975), who added sub-micron poly-styrene spheres to gelatin. In no case was it found that these spheres acted as cavitation nuclei. Evidently, the nuclei studied in the gelatin experiments were not smooth hydrophobic spheres.

Nuclear models of the second kind prevent the diffusion of gas from a nucleus by assuming the liquid-gas interface to be impermeable. A model of this type was first introduced by Fox and Herzfeld (1954), who postulated the existence of nuclei composed of gas bubbles enclosed in impermeable, elastic skins of protein molecules. So long as the skin remains impermeable and intact, the size of such a nucleus depends only on the instantaneous value of the ambient pressure. It follows that the cavitation threshold should be independent of any previously applied ambient pressure. This prediction proved to be inconsistent with the subsequent experiments of Strasberg (1956, 1959), which showed that the critical pressure for the onset of ultrasonic cavitation in water varies smoothly upon the magnitude of a previously applied crushing pressure. Because of this conflict, Herzfeld (1957) abandoned the organic skin model. Since the gelatin experiments clearly showed the cavitation nuclei to be permeable, they directly ruled out the applicability of impermeable-skin nuclear models.

Nuclear models of the third kind are characterized by gas-fluid interfaces with infinitely large radii of curvature; that is, flat surfaces. In practice this is accomplished by filling a crevice in a solid body with gas and by arranging the contact angles of the solid-liquid gas system in such a manner as to cause the curvature of the liquid-gas interface vanish. The stabilization of gas in crevices is the mechanism responsible for the majority of the bubbles observed in common supersaturated fluids, such as champagne, beer, and tonic water. Most of the bubbles in these systems do not originate in the fluid, but rather on the walls of the container. Harvey et al. (1944) generalized this observation of bubble formation in solid crevices on container walls to nucleation within fluids by postulating that cavitation nuclei are small solid particles containing gas-filled crevices.

The crevice model has been recently re-examined theoretically by Yount (1979b). He found that the model is viable in general, but that it fails to account properly for the results from gelatin studies. In particular, the crevice model as developed by Apfel (1970) is, according to its author, not applicable to supersaturation problems such as the gelatin experiments. Strasberg's version of this model (1959) was compared by Yount (1979b) to the gelatin data and found to fail. Thus, neither of the existing crevice models can properly explain the gelatin results.

In addition to the particular problems in describing nucleation in gelatin with the crevice model, several fundamental observations suggest that this mechanism is not applicable to aqueous media in general. Sirotyuk (1970) found that the complete removal of solid particles from a sample of water increased the cavitation strength by at most 30 percent, demonstrating that most of the cavitation nuclei present in high purity water are not associated with solid particles. Bateman and Lang (1944) attempted to introduce nuclei into liquids by mixing in solid impurities, experimenting with charcoal, blood corpuscles, dialyzed colloidal ferric hydroxide, ivory black, and sodium bicarbonate. The net result of the experiments was that the addition of solid impurities to liquids had little effect on the cavitation threshold. Bernd (1963) noted that gas phases stabilized in crevices are not usually truly stable, but tend to dissolve slowly. This instability is caused by imperfections in the geometry of the liquid-gas interface, which is almost never exactly flat. While it may be possible to realize conditions in which a gas phase is truly stabilized in

a crevice, for this configuration to remain stable following a rapid compression of many atmospheres seems to be an untenable assumption.

Cavitation experiments have produced two additional results which indicate that cavitation nuclei are not of the crevice type. In the filtration experiments reported in section 2.4 it was found that the size of a nucleus is strongly correlated with the critical supersaturation pressure required for bubble formation. In the context of the crevice model this result implies that crevices of a given size and shape are associated uniquely with particles of a single size. Because it seems likely that the type of fissures occurring in small particles would also occur in larger ones, this experimental result argues against the applicability of the crevice model to gelatin. In addition, both Strasberg (1959) and Bernd (1963) noted that the threshold pressure for ultrasonic cavitation in water can be increased by permitting the water to stand quietly for many hours, and Bernd showed that this increase can be consistently explained by the rise of the largest nuclei to the surface of the water. Because solid particles generally will not float, these experiments again indicate that cavitation nuclei are at least not exclusively of the crevice variety.

In summary, nuclear models of the third kind consist essentially of gas phases stabilized in crevices in solid particles. While the crevice conjecture represents a viable nuclear model, none of the existing mathematical treatments make predictions that are supported by the gelatin experiments. In addition to problems with the mathematical development of this model, experimental studies show little or no correlation between the cavitation strength of a liquid and the number of solid impurities in the sample. The nuclei found within gelatin, water, and most common fluids are most probably not of this type.

Nuclear models of the fourth kind consist of gas bubbles in which the surface tension of the surrounding medium is opposed by a third constituent of the system. The basic operational principle of this class of models is to reduce the net interfacial surface tension to zero. Several methods of achieving this result have been proposed.

If the medium surrounding a bubble has a non-vanishing shear modulus, it will be capable of mechanically supporting holes larger than some critical radius. The material can be viewed as having sufficient mechanical strength to support inclusions under pressure, a common example being foam rubber in which the individual cells can withstand pressures of many atmospheres without collapsing. Gent and Tompkins (1969) studied the nucleation and growth of bubbles in elastomers and found that gas phases could be stabilized by this mechanism. This model is not applicable to gas bubbles in either water or gelatin, however, since the shear modulus of water vanishes, while that of gelatin is negligible in comparison with the pressure $2\gamma/r$ when r is of a typical nuclear size.

A second mechanism, suggested by Akulichev (1966), is to oppose the surface pressure of the fluid with the force arising from an electric surface charge of ions residing at the liquid-gas interface. The Coloumb repulsion between these ions pushes them outward against the fluid and thus counteracts the surface tension. The applicability of the ionic model to water and gelatin has been experimentally tested. Sirotyuk (1970) showed that the cavitation

strength of water does not depend on its conductivity due to dissolved ions and concluded that the ion model is not characteristic of the nuclei found in water. In experiments in which salts were added in solution to gelatin samples, Kunkle and Yount (1975) found no correlation between bubble number and the free ion concentration of gelatin. This lack of correspondence is evidence that the nuclei in gelatin are not of the ionic type.

The third example in this class, and the main subject of this work, is the surfactant stabilized model. Here a layer of surface-active molecules residing at the liquid-gas interface of a bubble opposes the surface tension of the surrounding fluid and at equilibrium causes the net interfacial tension to vanish. This mechanism is consistent with Sirotyuk's (1970) observation that "the stabilization of gas bubbles acting as cavitation nuclei in water is always attributable to the presence of surface-active substances in the water." In agreement with the results of the gelatin experiments, the surfactant nucleus is gaseous, permeable, and stable. Furthermore, mathematical models based upon the hypothesis are able to quantitatively replicate the results of the gelatin experiments. For these reasons, it is felt that the surfactant model is the best choice from the available candidates to represent the nature of the cavitation nuclei found in gelatin and water.

3.2. A comparison of three models of surfactant-stabilized nuclei

The surfactant-stabilized nucleus is a gas bubble enclosed in a skin of surface-active molecules. Three mathematical models of the system have been introduced: the Impermeable Organic Skin model of Fox and Herzfeld (1954) (FH model), the Varying Permeability model of Yount (1979b) (VP model), and the Surfactant Stabilized model (SS model) detailed in Chapter 4 of this work. These models have some points in common, but they also have many differences. This is partly because each seeks to explain the nature of the system at a more fundamental level than its predecessor. In this section the three models are compared and their salient features discussed.

The principle components of the surfactant nucleus are the nuclear skin and the gas cavity which it encloses. Any model must at least implicitly account for certain physical properties of this system. In particular, it must: (1) outline the general structure of the nucleus; (2) identify the type and structure of the skin; (3) stipulate an equation of state for the surfactant material; (4) discuss the gaseous permeability of the skin; and (5) determine the stability of the system. The manner in which each of the three proposed models deals with these properties is discussed below.

1. General structure of the system. In all three models the nucleus is assumed to be spherical. The skin is of uniform thickness, and this thickness is small compared with the nuclear radius.

2. Type and structure of the skin. The skin of the FH model is composed of one or more layers of soluble organic molecules, the VP model uses one or more layers of insoluble surfactant molecules, and the SS model employs a monolayer of insoluble surfactant molecules.

3. Surfactant equation of state. The most detailed treatment of the surfactant equation of state is given in the SS model. In this model the tension of the skin, Π, is assumed to depend on the surface area per surfactant molecule, A. The functional dependence $\Pi(A)$ is derived from experimental measurements of common surface-active substances. The value of Π can vary between zero and an upper limit of Π_{max}. This upper limit is related explicitly to the desorption of energy of the surfactant and the dynamic state of the system.

The VP model also assumes that Π depends on A and has an upper limit Π_{max}, but it does not explicitly employ an equation of state relating Π to A. The value of Π is permitted to assume whatever value is required to maintain the mechanical equilibrium of the system. It is assumed that the compressibility of the skin is sufficiently small that a negligible amount of work is done in a compression of the skin to its limiting tension, and that the nuclear radius remains nearly constant during the skin compression. The functional dependence $\Pi(A)$ used in this model is thus arbitrarily close to the form

$$\Pi(A) = \Pi_{max}\ H(A_{min}) \tag{3.1}$$

where $H(A)$ is Heavyside's unit step function. Comparison of this equation with the SS model's force-area relationship shows that the surfactant used in the VP model is a special type of that used in the SS model.

The value of Π_{max} used in the VP model is found empirically to depend on the equilibrium size of the nucleus, r_o, in the approximate manner

$$\Pi_{max}/\gamma_o \approx 1.00 + 1.40\ r_o\ , \tag{3.2}$$

where the initial radius r_o is expressed in micrometers. If Π_{max} is assumed to be determined only by the chemical nature of the surfactant material, then this result indicates that nuclei of different initial sizes are stabilized with different surfactants or differing mixutres of surfactant materials. If Π_{max} depends mostly on the nuclear curvature, or other non-chemical effects, then this inference is not valid.

The organic skins used in the FH model obey the particularly simple equation of state

$$\Pi = Constant\ . \tag{3.3}$$

Changes in the nuclear radius are calculated using the equation given by Love (1944) for an ideal elastic shell. Yount (1979b) has demonstrated that the application of this equation is equivalent to constraining Π to be constant and employing equation (4.8) for the mechanical equilibrium of the system to calculate differential changes in the nuclear radius.

4. Permeability of the skin. The permeability of the skin in the SS model depends on the fractional area of the liquid-gas interface covered by surfactant molecules. The specific resistivity r thus depends on the molecular area A and may have any value between zero and infinity. When the surfactant molecules are packed closely together and the skin tension is therefore near the maximum, the diffusive resistivity is very large; when the

molecules are farther apart, so that the tension decreases, the resistivity approaches zero.

The VP model, as its name implies, also considers the diffusive resistance of the surfactant skin to be variable. In this case, however, only two values are considered: $r = 0$, a fully permeable skin, or $r = \infty$, a fully impermeable skin. This change in permeability is attributed physically to the changing area per surfactant molecule, but it should be noted that the change in resistivity occurs after the skin tension has reached its maximum value and is being held constant. The diffusive resistivity in this model thus does not depend explicitly on the skin tension, but instead is determined by a change in the ambient pressure.

In the FH model the diffusive resistance of the skin is always infinite. This impermeability is of crucial importance to this model because it is necessary to maintain a pressure differential between the internal gas and the ambient environment. The impermeable nature of the nucleus contradicts the experimental results of Strasberg (1956) and this contradiction caused Herzfeld (1957) to withdraw the model.

5. Stability of the nuclear skin. The organic compounds employed in the FH model are assumed to be soluble in the fluid surrounding the nucleus. For such soluble compounds the concentration of molecules at a liquid-gas interface is determined by the rate of diffusion of molecules from the skin into the fluid. For sufficiently slow changes in the nuclear radius, the molecular concentration at the interface will remain fixed at the equilibrium value. The value of Π therefore depends only on the chemical properties of the liquid-surfactant-gas system, and not on the size of the nucleus.

The surface-active materials used in the VP and SS models are assumed to be nearly insoluble in the surrounding field. These molecules are bound by strong electro-chemical interactions, and work must be done to remove them from the interface.

In the SS model the desorption energy of the surface-active molecules is explicitly related to the maximum allowable skin tension. If an attempt is made to further compress a nucleus whose skin is already stressed to the maximum tension, individual molecules are lost from the skin at a rate sufficient to maintain Π at a value less than or equal to Π_{max}. Molecules desorbed from the skin into the fluid are assumed to be permanently inaccessible to the system.

The molecular stability of the VP model is similar to that of the SS model in that material is removed from the interface when a nucleus is additionally compressed beyond the point when Π first equals Π_{max}. In this model, however, molecules are stored in the system and are available for use in any subsequent re-expansion of the skin. This may be accomplished by assuming, for example, that the lost molecules are either trapped inside the nucleus or form into a multilayer sheet. No attempt is made to derive the value of Π_{max} from the chemical properties of known surfactants or from geometric considerations.

The three models outlined above may be regarded as successively more detailed treatments of the same physical system. The FH model can be viewed

as a special case of the VP model in which only the impermeable equations are considered, while the VP model itself is in many ways a special case of the SS model. Through a suitable choice of the parameters associated with the SS model it is possible to replicate several features of the VP model, including the surfactant equation of state and the permeable-impermeable nature of the nuclear skin. Important differences between these two models remain, however. The values of Π_{max} are generally larger in the SS model than in the VP model for a nucleus of the same initial size. For identical dive profiles, correspondingly more molecules are removed from the skin of a VP nucleus than an SS model nucleus. While the material desorbed from the SS model nuclear skin is permanently lost, the molecules removed from the skin of a VP nucleus are stored and may be used to partially repopulate the skin during decompression. This skin restoration does not occur in the SS model.

The most basic difference between the SS and VP models, however, involves the computational methods employed in their construction. The VP model is an analytic approximation model in the sense that it simplifies some of the relevant physics in order to produce results in closed-form expressions. Examples of the type of approximations used in the VP model are the surfactant force curve in equation (3.1) and the idealized permeable-impermeable nature of the skin. In contrast, the SS model is a differential model that calculates the response of the system to changes in its environment by numerical techniques. The physical behavior of the components of the SS model can be stipulated to whatever accuracy is desired. As an example, the approximation to the surfactant force curve used in the VP model is replaced by an analytic equation; if additional accuracy is desired, this equation can be replaced by the data on an individual surfactant. This model therefore provides a deeper view into the basic physics of the surfactant nucleus than does the VP model, and it enables the study of some phenomena, such as bubble nucleation in non-saturated fluids and non-saturation decompression schedules, that have not been addressed by the VP model.

CHAPTER 4. THE SURFACTANT STABILIZED MODEL

In this chapter the equations describing the Surfactant Stabilized model are presented. The relevant physics is introduced in section 4.1, the algorithm developed to solve these equations discussed in section 4.2, and the model predictions compared with the gelatin data in section 4.3.

4.1. The mathematical structure of the Surfactant Stabilized model

As discussed in Chapter 3, the Surfactant Stabilized model considers a cavitation nucleus to be a gas phase enclosed in a gas-permeable monomolecular skin of surface-active molecules. It is assumed that the parameters describing the nucleus are angularly isotropic and thus spacially dependent on a single radial variable. This is equivalent to assuming that the nucleus is spherical and that the surfactant skin is uniform in composition and thickness. A cross-section of the nucleus is shown in Figure 4.1. The nuclear radius r is defined to be the radius of the liquid-gas dividing surface. The surfactant skin has an inner radius of r_1, an outer radius of r_2, and a thickness of $t_{skin} \equiv r_2 - r_1$. In all cases considered in this work, it is assumed that the thickness of the skin is much less than the nuclear radius ($t_{skin} << r$) and that the same radius can be used for both the gas-surfactant and surfactant-liquid interfaces ($r_1 \approx r_2 \approx r$).

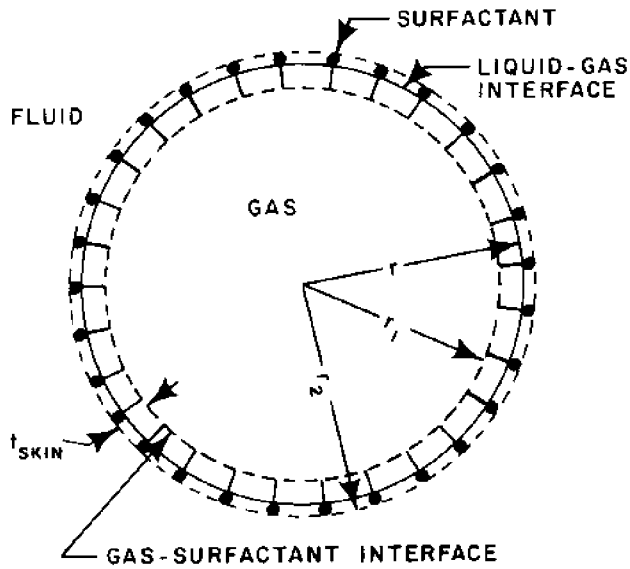

Figure 4.1. Cross-sectional view of a surfactant-stabilized nucleus

The nucleus is assumed to be filled with a single species of gas. The amount of gas is N moles, and the internal gas pressure is p. The equation of state relating r, N, and p is taken to be the second-order virial expansion of the ideal gas law,

$$pV = NRT(1 + pB_p + p^2C_p) \quad , \tag{4.1}$$

where V is the internal volume of the nucleus, R is the universal gas constant, T is the gas temperature, and B_p and C_p are the first two virial coefficients of the gas. The gas temperature is taken to be constant and equal to the temperature of the surrounding fluid, hence

$$\frac{\partial T}{\partial t} = \frac{dT}{dt} = 0 \ . \tag{4.2}$$

The amount of gas contained in the nucleus is not necessarily constant; it varies as gas diffuses into or out of the nucleus through the surfactant skin. Because the nuclei are observed to be much smaller than the minimum size given by equation (1.12b) for diffusion-limited gas transfer, the role of gas flow is perfusion-limited. The flow rate is given by the equation

$$\frac{dN}{dt} = 4\pi r^2 \alpha [U(r) - U_O] \ , \tag{4.3}$$

where $U(r)$ is the concentration of gas in the fluid just beyond the surfactant skin, U_O is the concentration necessary to establish equilibrium with the gas in the nucleus, and α is a proportionality parameter. The value of α is not constant, but varies in response to changes in the skin. Equation (1.5b) sets the relationship between p and U_O to be

$$U_O = Sp \ , \tag{4.4}$$

where S is Henry's solubility constant.

The fluid around the nucleus is exposed to an ambient pressure of $p_{amb}(t)$. The amount of gas dissolved in the fluid, i.e., the gas tension, will vary with both time and position in the sample. It is assumed that the scale length for spatial changes in the gas tension is large compared with the size of the nucleus. This allows the nucleus to be viewed as being contained within an isotropic, quasi-infinite sphere of fluid in which the equilibrium gas tension varies with time. This region, referred to as the "nuclear domain," is shown in Figure 4.2.

Within the nuclear domain, variations in the gas tension are related primarily to the flow of gas through the nuclear skin. The gas concentration in this region $U(\rho,t)$ is therefore spherically symmetric, depending only on time and the radial distance ρ from the center of the nucleus. Outside of the nuclear domain the gas tension W is independent of nuclear processes and is determined by the global geometry of the fluid sample and the ambient pressure history.

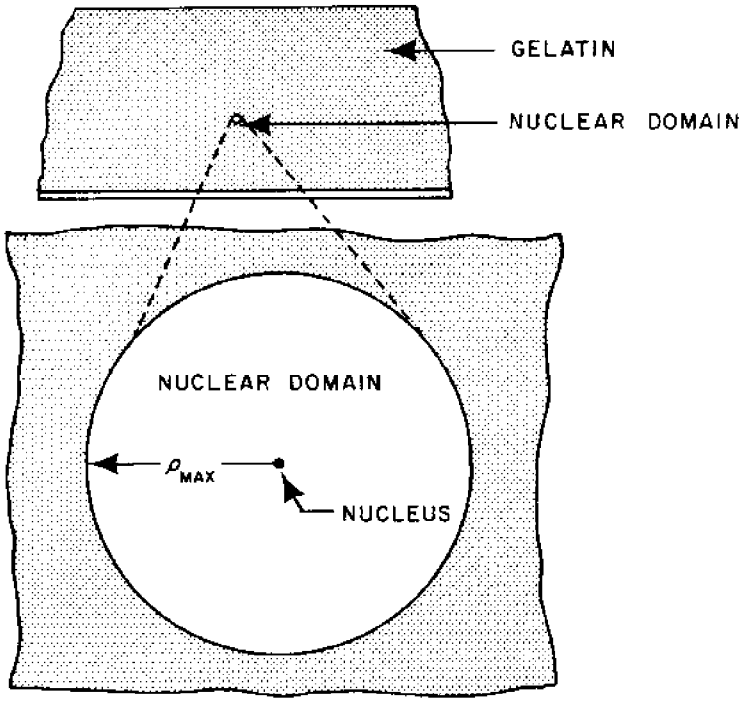

Figure 4.2. The nuclear domain

The transport of gas through the fluid within the nuclear domain is modeled by the Fickian diffusion equation

$$\frac{\partial U}{\partial t} = D\nabla^2 U + \vec{v} \cdot \nabla U \ , \tag{4.5a}$$

where D is the diffusion constant and $\vec{v}$ is the velocity of the fluid. The boundary conditions on this equation are that at large radial distances $U(\rho,t)$ becomes equal to the asymptotic concentration $W(t)$,

$$\lim_{\rho \to \infty} U(\rho,t) = W(t) \ , \tag{4.5b}$$

that the rate of gas transport in the fluid at the interface is equal to the gas flux through the skin,

$$D \left. \frac{\partial U(\rho,t)}{\partial \rho} \right|_{r} = \alpha[U(r;t) - Sp(t)] \ , \tag{4.5c}$$

and that the initial distribution of gas in the nuclear domain is given by the function $g(\rho)$,

$$U(\rho,0) = g(\rho) \ . \tag{4.5d}$$

The asymptotic gas concentration $W(t)$ must be found by an independent calculation.

The surface tension of the liquid around the nucleus exerts a pressure on the liquid-gas interface of $2\gamma/r$. The surfactant molecules oppose the surface tension of the fluid, lowering it by an amount Π. The total surface pressure is thus

$$p_{surface} = 2(\gamma - \Pi)/r \ . \tag{4.6}$$

The value of Π depends on the type and number of surfactant molecules in the skin, as well as upon r and dr/dt. The physics of surfactant monolayers at liquid-gas interfaces is discussed in subsection 4.1.1, where the functional form of Π is investigated. Tolman (1949) showed from thermodynamic considerations that the value of the surface tension should be affected by the curvature of a surface. His result is

$$\gamma = \gamma_o/(1 + 2\delta/r) \tag{4.7}$$

where δ is on the order of 10^{-8} cm. The smallest nuclear radius encountered in this work is larger than 4×10^{-6} cm, a curvature which reduces the surface tension by 0.5 percent. In view of this result, the simplifying assumption is made that γ is a constant and independent of the nuclear radius.

It is postulated that the nucleus is in mechanical equilibrium at all times. This means that the vector sum of the forces acting at any point is always close to zero. Therefore, the difference between the total inward and outward pressures must vanish. Hence,

$$p_{amb} + 2(\gamma - \Pi)/r = p \tag{4.8a}$$

and

$$2\ (\gamma - \Pi) = r(p - p_{amb}) \ . \tag{4.8b}$$

This equation differs from the corresponding relationship for the equilibrium of a bubble by the addition of the $2\Pi/r$ term, which is due to the surfactant skin.

Equations (4.1), (4.3), and (4.8) may be combined and differentiated to yield

$$dp = dp_{amb} - \frac{dr}{r}\,(p - p_{amb}) - \frac{2}{r}\frac{d\Pi}{dr}\,dr \ , \tag{4.9a}$$

and

$$[V - NRT(B_p + 2pC_p)]dp + pdV = RT(1 + pB_p + p^2C_p)dN \ . \tag{4.9b}$$

Equation (4.9b) may be simplified by introducing the new variables $\overline{V}$ and $\overline{R}$ defined by

$$\overline{V} \equiv V - NRT(B_p + 2pC_p) \ , \tag{4.10a}$$

$$\overline{R} \equiv R(1 + pB_p + p^2C_p) \ . \tag{4.10b}$$

Note that for an ideal gas, B_p and C_p vanish by definition, so that $\overline{V}$ becomes equal to V and $\overline{R}$ becomes equal to R. Substituting $\overline{V}$ and $\overline{R}$ into equation (4.9b) yields

$$dp = (\overline{R}TdN - pdV)/\overline{V} \ . \tag{4.11}$$

Substituting this last result in equation (4.9a), one obtains

$$dr(p - p_{amb}) + r\left(dN\frac{\overline{R}}{\overline{V}}T - p\frac{dV}{\overline{V}}\right) - rdp_{amb} + 2d\Pi = 0 \ . \tag{4.12}$$

Solving this equation for dr yields

$$dr = r\left[dN\frac{\overline{R}}{\overline{V}}T - dp_{amb}\right]\Bigg/\left[pr^3\frac{4\pi}{\overline{V}} - 2\frac{d\Pi}{dr} - (p - p_{amb})\right] \ . \tag{4.13}$$

Finally, dividing by dt and substituting for dN/dt with equation (4.3) produces the desired expression,

$$\frac{dr}{dt} = \left[3\overline{R}T\alpha(U(r) - Sp)\frac{V}{\overline{V}} - r\frac{dp_{amb}}{dt}\right]\Bigg/\left[3p\frac{V}{\overline{V}} - (p - p_{amb}) - 2\frac{d\Pi}{dr}\right] \ . \tag{4.14}$$

Equation (4.14) relates the instantaneous values of the parameters with the differential increment of the radius. Evidently, for a permeable nucleus of finite size held at constant ambient pressure to be stable in the sense that dr/dt is zero, it is necessary that $U(\rho)$ be equal to Sp, and p be equal to p_{amb}:

$$p = p_{amb} \ , \tag{4.15a}$$

and

$$U(\rho,t) = Sp_{amb} \ . \tag{4.15b}$$

When put in equation (4.8), this condition for nuclear stability clearly requires that the total surface pressure vanish. A necessary and sufficient condition for the stability of a surfactant-stabilized nucleus in an isobaric environment is that the total surface pressure be zero, which implies the relationship

$$\Pi = \gamma \ . \tag{4.16}$$

A nucleus existing in a saturated fluid held at constant pressure such that equations (4.15) and (4.16) are satisfied is said to be in "stable equilibrium." Because Π is a function of the single variable A, the interfacial area per surfactant molecule, the condition stated by equation (4.16) is equivalent to demanding that the surface area of the nucleus be equal to the product of the number of surfactant molecules and the particular molecular area $A\gamma$ which results in a value of Π equal to γ. The equilibrium size of a surfactant-stabilized nucleus is thus determined uniquely by the chemical nature of the surfactant material and by the number of such molecules in the nuclear skin.

4.1.1. Physics of insoluble surfactant monolayers at liquid-gas interfaces

The definitive property of surface-active substances is their ability to reduce the free energy of an interface. If the surface tension of a pure two-component system is γ_o, the addition of a surfactant to the interface will reduce the surface tension by an amount Π to a final value of γ. Hence, these quantities are related by the expression

$$\Pi = \gamma_o - \gamma \ . \tag{4.17}$$

The parameter Π is universally known as the "surface pressure of the surfactant." The name is a misnomer, since the units are actually those of a tension or compression and not a pressure. The surface pressure is not necessarily constant; it can vary with the concentration of surface-active molecules on the interface, increasing as the mean distance between molecules decreases. The most important quantity involved in the functional dependence of Π is the average area per surface-active molecule. In many cases Π is a function only of this area,

$$\Pi = \Pi(A) \ , \tag{4.18}$$

where A is commonly measured in square-angstroms, i.e., in units of 10^{-16} cm^2.

The surfactants of interest in this work are those that reside at liquid-gas interfaces. Such molecules are composed of two functional parts: a polar group at one end and a non-polar hydrocarbon chain at the other. If the separation between these two regions is more than a few angstroms, each group will be chemically unaffected by the other, and each will independently seek energy equilibrium within the system, which is Langmuir's principle of independent action. By definition, it is energetically favorable for the polar group to be immersed in water and the hydrocarbon tail in other hydrocarbons or in gas. If the spacing between these two chemical groups exceeds the thickness of the liquid-gas interfacial region, then such a molecule resident at the dividing surface will be aligned with its polar head in the fluid and the hydrocarbon tail in the gas, as shown in Figure 4.3. To move the molecule entirely into the liquid, work must be done to pull the hydrocarbon tail through the interface and into the fluid. Similarly, to move the molecule into the gas, work is required to translate the polar head out of the liquid and through the interfacial region.

A schematic potential energy diagram for the surfactant-liquid-gas system is shown in Figure 4.4. The work required to desorb or evaporate a molecule, E_{sol} and E_{evap}, respectively, will in general depend on the concentration of similar molecules in the surrounding liquid or gas. For the special case of nearly insoluble substances, the concentration of surfactant molecules in the liquid and gas is nearly zero, and the evaporation and desorption energies are sensibly concentration independent. The surface-active molecules considered in the SS model are assumed to be nearly insoluble in both water and gas, and that the energies E_{sol} and E_{evap} are taken to be constant. A lower limit to the values of these energies may be established from thermodynamic arguments. If the surfactant molecules are assumed to be in thermodynamic equilibrium, then they have an average thermal energy of 1/2 kT in the radial direction. For the molecules to be kept at the interface it is clearly necessary that both E_{sol} and E_{evap} exceed the average thermal kinetic energy, which is about 2.0 x 10^{-14} erg at room temperature.

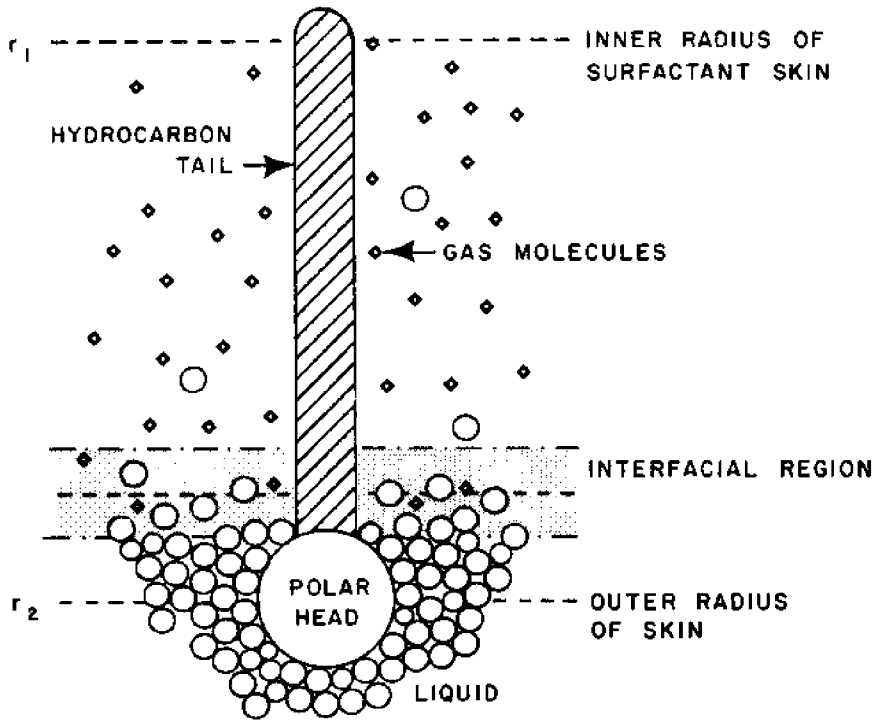

Figure 4.3. Ideal orientation of a surfactant molecule at the liquid-gas interface

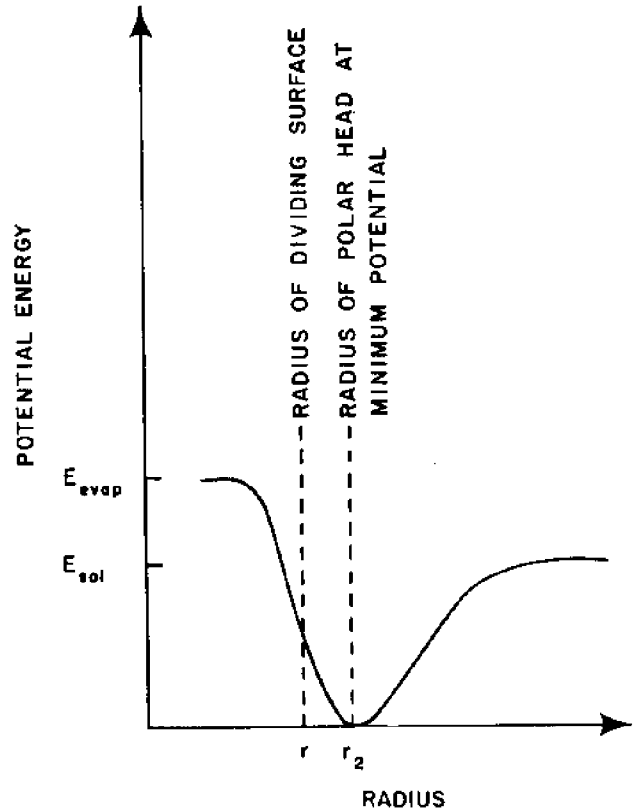

Figure 4.4. Schematic potential energy diagram of a surfactant molecule at a liquid-gas interface

The form of the $\Pi(A)$ relation for surfactants has been the subject of much laboratory work, beginning with the studies of insoluble oil films on water by Pockels in 1891. The usual method employed in determining $\Pi(A)$ is to spread a known amount of material on a fluid surface to form a monomolecular layer. A thin linear wire is used to compress the film, and as the monolayer is compressed the force exerted on the wire rises. The area per molecule A is found by dividing the area covered by the film by the number of molecules. The value of Π is computed by dividing the force by the length of the wire. While simple in concept, the work is difficult in practice. Gaines (1966) gave a complete discussion of the techniques used in making these measurements.

A schematic force-area diagram characteristic of long-chain insoluble surfactants is shown in Figure 4.5. Following the nomenclature of Gaines (1966), this curve may be divided into three monolayer states: gaseous, expanded, and condensed. In the gaseous region the surface area per molecule is much larger than the geometric cross-section area of a molecule,

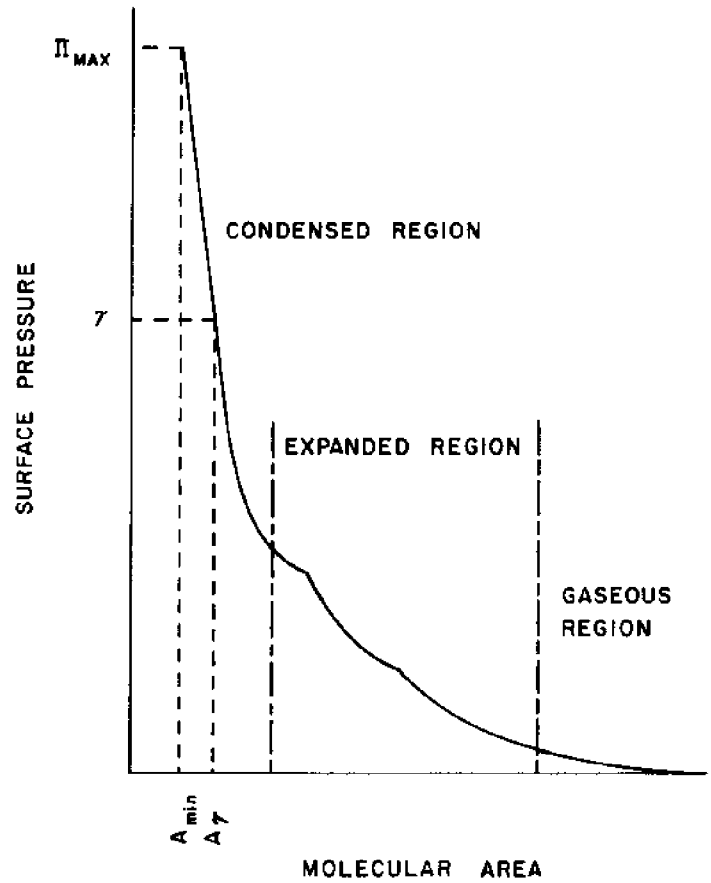

Figure 4.5. Force-area diagram of a hypothetical surface-active substance

$$A >> A_o \ , \tag{4.19}$$

where A_o is the minimum possible molecular area. The molecules may be viewed as forming a two-dimensional ideal gas with average molecular energy kT; the equation of state for this idealized system is

$$\Pi A = kT \ . \tag{4.20}$$

This equation can be made more realistic by allowing for the finite area of each molecule,

$$\Pi(A - A_o) = kT \ . \tag{4.20}$$

which is the two-dimensional equivalent of the van der Waal's equation of state for non-ideal gases. It has been shown by Adam and Jessop (1926) and by Adam (1928) that the behavior of many real materials approaches this equation at sufficiently large values of A.

The condensed state is of primary interest in this work since it is here that large values of the surface pressure ($\Pi \simeq \gamma_o$) are encountered. In this domain A is nearly equal to A_o, and the surfactant molecules are almost solidly packed together. As seen in Figure 4.5, the dependence of Π on A becomes very sharp as A approaches A_o, with the slope $d\Pi/dA$ increasing rapidly. An equation of state representative of surfactant materials in the condensed state has been empirically determined by fitting the observations of saturated lecithins by Phillips and Chapman (1968) with various mathematical functions. The two-parameter representation

$$\Pi(A) = C_1 e^{-A/A_1} \tag{4.22}$$

fits these data very well, as can be seen in Figure 4.6. The $\Pi(A)$ curves for other condensed monolayers, such as fatty alcohols and acids, are, however, more complicated. A rigorous treatment of these materials at moderate values of Π ($\Pi \simeq 20$ *dyne/cm*) would require a more detailed equation of state than an exponential, but for large values of Π, most surfactants are satisfactorily modeled by this equation. Because the high-tension region of the $\Pi(A)$ curve is of primary interest in this study, it is assumed that equation (4.22) represents the proper form of the $\Pi(A)$ relationship for the surfactant material used in the SS model and that this equation adequately describes the $\Pi(A)$ curve for all values of A.

The behavior of monolayers in the expanded state is characterized by several shallow curves in the $\Pi(A)$ diagram, which usually include one or more critical points, possibly signifying phase transitions in the surfactant material. Films in this region behave very much like two-dimensional liquids or super-liquids, and this region is often subdivided into several discrete states, such as the liquid-expanded, intermediate, and liquid-condensed states recognized by Harkins (1952). There is controversy over the molecular arrangements and phase transitions which lead to the observed behavior. For purposes of the Surfactant Stabilized model, the behavior of the monolayer in this region is of little practical interest since the model is relatively insensitive to the exact nature of this portion of the $\Pi(A)$ curve. It is only required that $\Pi(A)$ monotonically decreases as A increases through the expanded and gaseous regions.

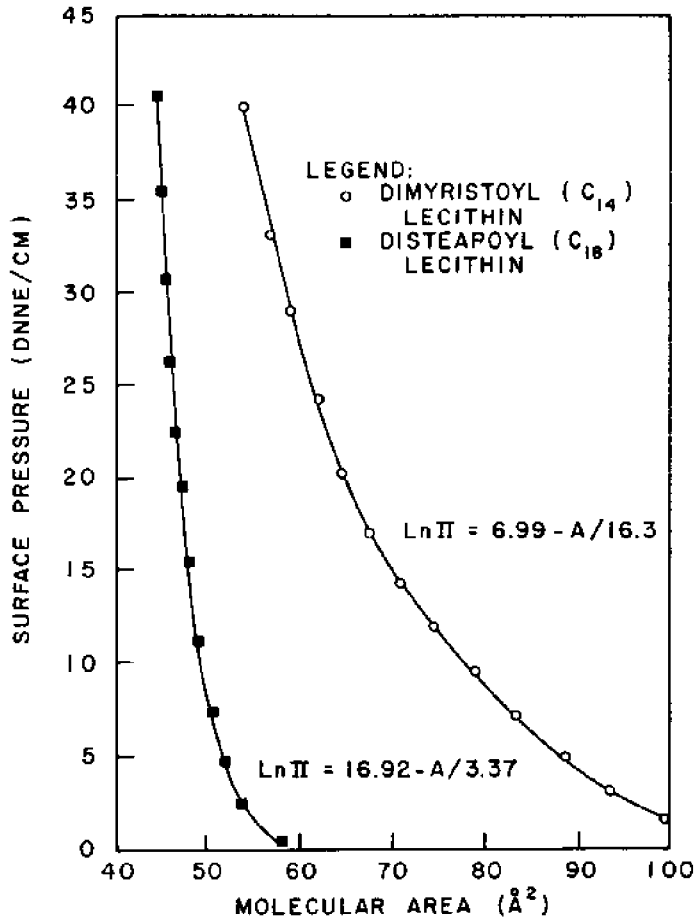

Figure 4.6. Force-area diagrams of two surfactants (Data points measured from Phillips and Chapman, 1968)

Equation (4.22) gives the functional form of the $\Pi(A)$ relation adopted in this work. The maximum value of Π predicted by this equation is that which occurs at the minimum possible area, $\Pi(A_o)$. In practice the maximum value of the surface pressure is limited by the stability of the surfactant skin to values well below $\Pi(A_o)$. The upper limit to Π, Π_{max}, is reached when it becomes energetically favorable for the surfactant molecules to desorb into the surrounding fluid rather than to be further compressed.

To develop an analytic expression for the limit Π_{max} that is applicable to a stationary monolayer, consider the work done in the compression of the monolayer by an amount equal to the area of a single molecule:

$$\Delta W = \Pi(A)A \ . \tag{4.23}$$

If the energy ΔW is larger than the desorption energy E_{sol}, then the work done in decreasing the surface area of the skin by an amount A will be less if a molecule leaves the skin than if all the molecules are further compressed. The

upper limit to Π for a stationary monolayer is thus determined by the critical relationship

$$\Pi_{max} = E_{sol}/A_{min} \ , \tag{4.24}$$

where A_{min} is that area which satisfies the equation

$$\Pi(A_{min}) = C_1 e^{-A_{min}/A_1} = E_{sol}/A_{min} \ . \tag{4.25}$$

As is intuitively expected, Π_{max} is greater for materials having larger desorption energies.

The value of Π_{max} given by equation (4.24) is that characteristic of a stationary monolayer. In laboratory work it has been found that the limiting value of Π depends on the rate at which the skin is compressed, Π_{max} increasing with increasing values of the molecular compression rate (dA/dt). The measurements reported by Rabinovitch et al. (1960) of Π_{max} (dA/dt) for stearic acid are reproduced in Table 4.1; these data indicate that the functional dependence of Π_{max} on dA/dt for this particular nonstationary monolayer can be expressed as

$$\Pi_{max} = 15 + 1.54 \times 10^{10}\sqrt{dA/dt} \ dyne/cm \ . \tag{4.26}$$

The constant appearing in this equation may be identified with the E_{sol}/A_{min} term in equation (4.24). The general expression for Π_{max} is thus

$$\Pi_{max} = E_{sol}/A_{min} + B_1\sqrt{dA/dt} \ , \tag{4.27}$$

where B_1 is a parameter characteristic of the surfactant-fluid combination. The value dA/dt to be used in this equation is the rate that occurred just before Π_{max} was reached. The value of Π_{max} therefore depends on the dynamic state of the nucleus under consideration.

TABLE 4.1. OBSERVED DEPENDENCE OF Π_{max} ON dA/dt

$\sqrt{dA/dt}$ (cm/sec)	Π_{max} (dyne/cm)
2.01×10^{-9}	48
5.96×10^{-10}	23
--	15

Source: Rabinovitch et al. (1960)

If an attempt is made to adjust the system such that Π exceeds Π_{max}, molecules will desorb from the skin into the liquid. It is assumed that this loss will occur at a rate sufficient to insure that Π is less than or equal to Π_{max} at all times. This is tantamount to assuming that the time scale for changes in the nuclear parameters are long compared with the time required for molecules to leave the skin. This later time may be estimated from the thickness of the skin (~10 nm) and the average thermal velocity in the radial direction as

$$\Delta t \simeq t_{skin}/v = t_{skin}\sqrt{kT/m} \simeq 10^{-10} \text{ sec} , \qquad (4.28)$$

where the molecular weight has been assumed to be 300 amu. Because this time is short compared with the most rapid changes in internal parameters encountered in this work, $q_j/(dq_j/dt)$ greater than 10^{-3} sec, the above assumption is clearly justified. The stability limit Π_{max} is evidently a true upper limit to Π, and for the systems and materials studied in this work Π is always less than or equal to Π_{max}.

Equations (4.22) and (4.27) give that functional form of the $\Pi(A)$ relation used in the SS model. A given surface-active substance is specified by the four parameters A_1, B_1, C_1, and E_{sol}. Because the type of surfactant material actually occurring in the nuclei is not known *a priori*, these four parameters must be deduced from observations. The knowledge of these parameters gained from model fitting will eventually permit the tentative identification of the surface-active material involved in these nuclei.

4.2. Numerical integration of the SS model equations

The differential equations (4.9) along with the surfactant equations of state (4.22) and (4.27), and the diffusion equations (4.5) form a set of coupled, non-linear, second-order partial differential equations which describe the dynamical behavior of the SS model. A closed-form analytic solution to this set of equations has not yet been developed; indeed, experience with such problems indicates that the discovery of such a solution would be downright miraculous. In the absence of an analytic solution, an algorithm has been developed to integrate the equations numerically. When used in a computer program, this algorithm traces the physical parameters describing the nucleus through a given pressure profile. The program is designed to permit comparison of the SS model with the results of the gelatin model experiments. This is done by following a nucleus through a standard pressure profile and by determining whether it remains of sub-micrometer size or grows into a gross bubble.

The algorithm is composed of three parts: the first computes the gas tension in the general vicinity of the nucleus; the second computes the gas tension in the nuclear domain; and the third integrates equations (4.9) given the current value of $U(\rho)$. By separating the large-scale depth variations of the first calculation from the radial variations of the second, the combined problem is greatly simplified. Each of the three procedures is examined below.

4.2.1. Calculation of the ambient pressure and of the gas tension in the gelatin

The generalized pressure profile used in the SS model, shown in Figure 4.7, is composed of a number of linear pressure changes. These segments are

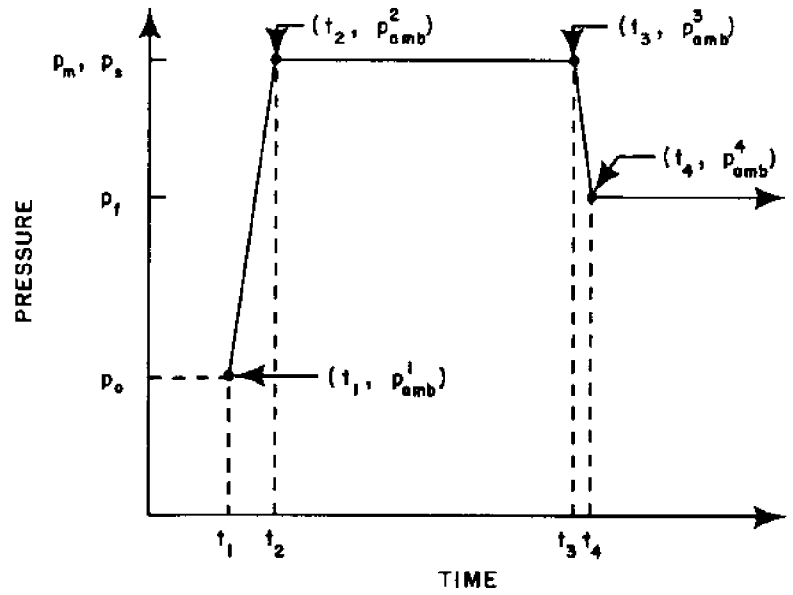

Figure 4.7. Generalized ambient pressure profile used in the model calculations

determined by a set of time and pressure points (t_j, p^j_{amb}), the ambient pressure at time t_j being p^j_{amb}. By convention t_1 is zero and time is therefore measured as elapsed time since the beginning of the dive. The ambient pressure at any arbitrary time is calculated from the equation

$$p_{amb}(t) = p^j_{amb} + (t - t_j) \frac{dp_{amb}}{dt} , \tag{4.29}$$

where the value of j is chosen such that t falls within the time span t_j to t_{j+1} and where

$$\frac{dp_{amb}}{dt} = \frac{p^{j+1}_{amb} - p^j_{amb}}{t_{j+1} - t_j} . \tag{4.30}$$

By construction, the derivative dp_{amb}/dt is normally constant and changes value only at the critical points t_j, at which times it may suffer a discontinuous change. To avoid problems caused by this behavior, the numerical integration must be arranged such that the critical instants t_j are reached at the end of the time steps and, hence, that the value of dp_{amb}/dt does not change during an integration step.

The nuclei studied in this program are assumed to be located within an infinitely wide gelatin slab 4 mm thick. The top surface of the slab is open to the atmosphere, and the bottom surface is covered by an impermeable wall. The calculation of the gas tension $W(Z,t)$ within the gelatin is done by the standard numerical technique of diffusion through thin layers. The calculation assumes that the gelatin slab is divided into N_{tau} thin layers as shown in Figure 4.8. The gas tension in the j^{th} layer at time t is $W_j(t)$. The j^{th}

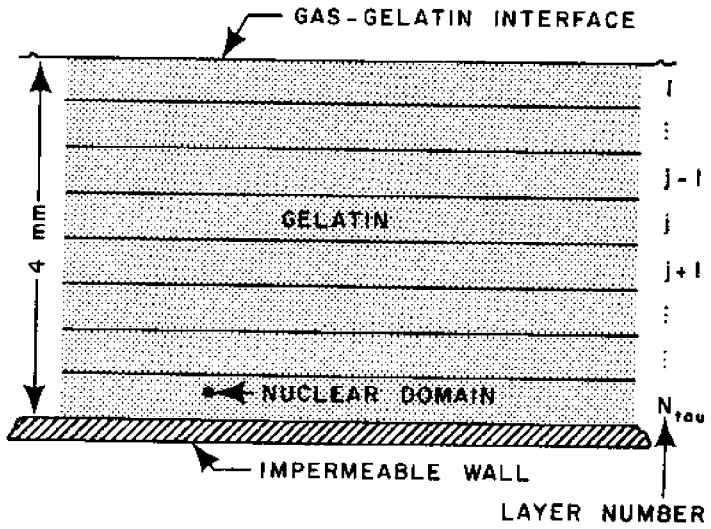

Figure 4.8. Division of the gelatin slab into N_{tau} layers

layer is a distance Z centimeters below the surface given by

$$Z = 0.4(j - 1/2)/N_{tau} = DZ(j - 1/2) \ , \tag{4.31a}$$

where

$$DZ = 0.4/N_{tau} \tag{4.31b}$$

is the thickness of a single layer in cm. The gas flux into the j^{th} layer through the interface between the j^{th} and $j+1^{th}$ layers is approximated by Fick's law of diffusion,

$$F = D[W_{j+1}(t) - W_j(t)]/DZ \ . \tag{4.32}$$

The total rate of gas flow into the j^{th} layer must include the gas diffusing through the interface with the $j+1^{th}$ layer. The net rate of gas transport into this layer is then

$$\frac{dN_j}{dt} = D\{[W_{j+1}(t) - W_j(t)] - [W_j(t) - W_{j-1}(t)]\}/DZ \ . \tag{4.33}$$

Maintaining this gas flux for a time Δt will change the gas concentration in the j^{th} cell by an amount

$$\Delta W_j = \Delta t \frac{dN_j}{dt} \frac{1}{DZ} \ . \tag{4.34}$$

The linearized expression for the gas concentration in the j^{th} cell at time $(t + \Delta t)$ is then

$$W_j(t + \Delta t) = W_j(t) + \Delta W_j$$
$$= W_j(t) + \Delta t D[W_{j+1}(t) + W_{j-1}(t) - 2W_j(t)]/DZ^2 \ . \qquad (4.35)$$

There are two regions in which this equation does not apply, these being the $j = 1$ and $j = N_{tau}$ layers. In the case of the $j = N_{tau}$ layer, the flux through the interface with the $j+1^{th}$ layer is zero because this region is an impermeable wall. Hence,

$$W_{N_{tau}}(t + \Delta t) = W_{N_{tau}}(t) + \Delta t D[W_{j-1}(t) - W_j(t)]/DZ^2 \ . \qquad (4.36)$$

For the first layer, the interface between the j^{th} and $j+1^{th}$ layers is the gelatin-gas dividing surface. The flux of gas through this interface is modeled by the perfusion equation

$$F = D\{D_1[Sp_{amb}(t) - W_1(t)]\} \ , \qquad (4.37)$$

where the constant D_1 is defined to be the gas uptake parameter and has the units of an inverse length. The value of D_1 depends on the combination of liquid and gas, but not on the pressure or gas concentration. The total flux into the first layer is now given by the equation

$$\frac{dN_1}{dt} = D\{D_1[Sp_{amb}(t) - W_1(t)] + [W_2(t) - W_1(t)]/DZ\} \ . \qquad (4.38)$$

The gas concentration becomes

$$W_1(t + \Delta t) = W_1(t) + \Delta t D\{D_1[Sp_{amb}(t) - W_1(t)]DZ + W_2(t) - W_1(t)\}/(DZ)^2 \ . \qquad (4.39)$$

Equations (4.35), (4.36), and (4.39) allow the gas concentration at any point within the gelatin to be calculated by time-step integration, given the initial gas concentration $W_j(0)$ and the ambient pressure profile $p_{amb}(t)$. For the purpose of these model calculations, it is assumed that at time zero the gelatin is fully saturated with the ambient gas. The initial condition on $W_j(t)$ is therefore

$$W_j(0) = Sp_{amb}(0) \equiv Sp_o \ . \qquad (4.40)$$

4.2.2. Calculation of the gas tension in the nuclear domain

The nuclear domain, as defined in section 4.1, is a spherical volume centered on the nucleus enclosing that portion of the gelatin acting directly on the nucleus. It is assumed that the size of this sphere is small compared with the thickness of the integration layers in the gelatin slab, but large compared with the nuclear radius. The depth dependence of the gas tension can then be neglected locally, while the tension at the outer boundary of the nuclear domain is insensitive to gas exchange with the nucleus itself. The radius of the nuclear domain, ρ_{max}, is thus bounded by

$$DZ >> \rho_{max} >> r \ . \qquad (4.41)$$

In practice the optimum size for ρ_{max} is found to be about 25 times the initial radius of the nucleus,

$$\rho_{max} = 25 r_o \ , \tag{4.42}$$

and that the model calculations are relatively insensitive to the value of ρ_{max}.

For the larger nuclei studied in this project, r_o is 1 μm, and ρ_{max} is then 25 μm. The layer thickness DZ used in the diffusion calculation is 500 μm. Thus, in all cases considered in this work the choice of ρ_{max} given by equation (4.42) satisfies the conditions in equation (4.41). This is to say that it is legitimate to perform the diffusion calculations by separating the problem into nuclear and non-nuclear domains as first suggested in section 4.1.

The procedure for calculating the gas tension in the nuclear domain is similar to that described in subsection 4.2.1 for diffusion in the gelatin slab. As shown in Figure 4.9, the nuclear domain is divided into n thin shells, the gas concentration in the j^{th} shell at time t being $U_j(t)$. The flux of gas flowing into the j^{th} shell through the interface with the $j+1^{th}$ shell is given by Fick's law:

$$F = D[U_{j+1}(t) - U_j(t)]/D\rho \ , \tag{4.43}$$

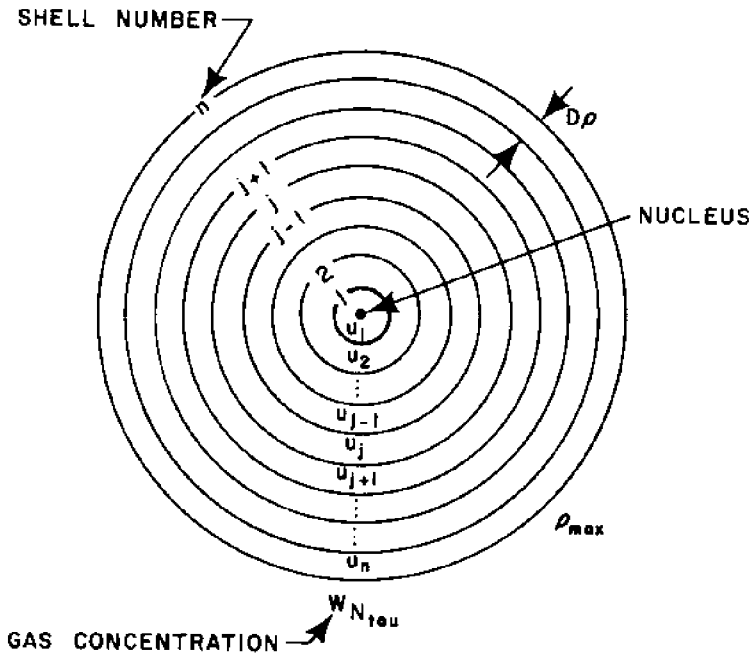

Figure 4.9. Division of the nuclear domain into n thin shells

where

$$D\rho = [\rho_{max} - r(t)]/n \tag{4.44}$$

is the thickness of the individual shells. The total rate at which gas enters the j^{th} shell is then

$$\frac{dN_j}{dt} = 4\pi D\{[r(t) + jD\rho]^2[U_{j+1}(t) - U_j(t)] + [r(t) + (j - 1)D\rho]^2[U_{j-1}(t) - U_j(t)]\}/D\rho \ ; \ 2 < j < n \ . \tag{4.45}$$

Maintaining this gas flow for a time interval Δt will change the concentration of gas in this shell by an amount:

$$\Delta U_j = \Delta t \frac{dN_j}{dt} \frac{1}{V_j} \ , \tag{4.46}$$

where the volume of the j^{th} shell is

$$V_j = \frac{4}{3}\pi\{[r(t) + jD\rho]^3 - [r(t) + (j - 1)D\rho]^3\} \ . \tag{4.47}$$

The gas concentration at time $(t + \Delta t)$ is then

$$U_j(t + \Delta t) = U_j(t) + \Delta U_j \ . \tag{4.48}$$

There are two regions in which this equation is not applicable. In the outermost shell, j is equal to n and the value of U_{j+1} is therefore not well defined. The gas flux through this outermost interface is taken to be

$$F = D[WN_{tau}(t) - U_n(t)]/D\rho \ , \tag{4.49}$$

where $WN_{tau}(t)$ is the gas concentration at the bottom of the gelatin slab, as determined by equation (4.36). The net rate at which gas enters the n^{th} shell is thus given by the equation

$$\frac{dN_n}{dt} = 4\pi D\{[r(t) + nD\rho]^2[WN_{tau}(t) - U_n(t)] + [r(t) + (n - 1)D\rho]^2[U_{n-1}(t) - U_n(t)]\}/D\rho \ . \tag{4.50}$$

The remaining special region is the first shell, where the inner interface is the liquid-surfactant dividing surface. The gas flux across this interface is modeled by the perfusion equation

$$F = (H \cdot D \cdot D_1)\ [Sp(t) - U_1(t)] \ , \tag{4.51}$$

where D_1 is the gas uptake parameter and H is the fractional area of the interface accessible for gas diffusion. The factor H must be included because a portion of the liquid-gas interface is blocked with surfactant molecules. The resistivity of the monolayer to gas diffusion is assumed to depend linearly on the fractional area covered by surfactant material. If the interface were densely packed with molecules, then the value of H would approach zero, but if no molecules were present, then H would be unity. The use of the fractional area assumption to model the resistivity of a monolayer to gas transport has been investigated by Barnes et al. (1970), who showed that it results in the minimum possible resistance.

The expression for H adopted for use in the SS model is

$$H = 1 - (A_{min} - A_{diff})/A \ , \tag{4.52}$$

where A_{min} is the minimum allowable molecular surface area as defined by equation (4.25), and A_{diff} is the area available for gas diffusion at maximum skin tension. That the value of A_{diff} does not vanish reflects the fact that a monolayer of surfactant molecules packed together at minimum area does not form a perfectly impermeable skin, but instead reduces the permeability to a small but finite value. Measurements of the diffusive resistance of monolayers at the air-water interface to the transport of various gases have been reported by Hawke and Alexander (1962) and Blank (1962). The parameter A_{diff} is not known *a priori* and must be determined by fitting the model to the data. In practice, the value of A_{diff} is found to have little effect on the results of saturation dives, and its magnitude is established largely from analysis of non-saturation experiments, such as the crushing-time study reported in section 2.5.

The total rate at which gas enters the first shell is given by

$$\frac{dN_1}{dt} = 4\pi D\{Hr^2 D_1[Sp - U_1] + [r + D\rho]^2[U_2 - U_1]/D\rho\} \ . \tag{4.53}$$

Equations (4.45), (4.50), and (4.53), along with equation (4.48), allow the gas concentrations $U_j\ (t + \Delta t)$ to be calculated, given the values of $U_j(t)$, $W_{N_{tau}}(t)$, $p(t)$, and $H(t)$. As in subsection 4.2.1, it is assumed that at time zero the material in the nuclear domain is fully saturated with gas. The initial values of $U_j(t)$ are therefore

$$U_j(0) = Sp_{amb}(0) \equiv Sp_o \ . \tag{4.54}$$

An examination of equation (4.44) shows that the spacing between the shells in the nuclear domain is not constant, but varies as the nucleus changes size. Because the radius of the inner boundary of the nuclear domain varies with time while the size of the outer boundary is held fixed, the position of each shell is time dependent. If, during a time Δt, the nuclear radius changes by an amount Δr, the radius of the outer surface of the j^{th} shell, $\rho_j(t)$, moves to the new position given by

$$\rho_j(t + \Delta t) = \rho_j(t) + \Delta r(1 - j/n) \ . \tag{4.55}$$

The volume of the j^{th} shell also varies in response to the change in radius, the new value being given by

$$V_j(t + \Delta t) = \frac{4}{3}\pi[\rho_j(t + \Delta t)^3 - \rho_{j-1}(t + \Delta t)^3] \ . \tag{4.56a}$$

The change in volume caused by a small variation in radius Δr is denoted by ΔV_j, which is related approximately to Δr by the equation

$$\Delta V_j = V_j(t + \Delta t) - V_j(t)$$

$$\cong 4\pi\Delta r[\rho_j^2(t)(1 - j/n) - \rho_{j-1}^2(t)(1 - j/n - 1/n)] \ . \tag{4.56b}$$

Now consider the first shell. If Δr is less than zero, then ΔV_1 is greater than zero, and the volume of this shell is increased by the decrement in radius. In order to fill the new shell with fluid, an amount of material ΔV_1 must be obtained from the old $j = 2$ shell. The gas concentration in the new $j = 1$ shell is therefore given by the weighted average

$$U_1(t + \Delta t) = [V_1(t)U_1(t) + V_1U_2(t)]/V_1(t + \Delta t) \ . \tag{4.57}$$

Similarly, the new $j = 2$ shell must now be filled with material from the old $j = 2$ and $j = 3$ shells, which produces a new concentration of

$$U_2(t + \Delta t) = \{[V_2(t) - \Delta V_1]U_2(t) + [\Delta V_1 + \Delta V_2]U_3(t)\}/V_2(t + \Delta t) \ . \tag{4.58}$$

The process of filling the j^{th} new shell with material from the j^{th} and $(j-1)^{th}$ old shells will in general yield a new gas concentration of

$$U_j(t + \Delta t) = \left\{\left[V_j(t) - \sum_{\ell=1}^{j-1}\Delta V_\ell\right]U_j(t) + U_{j+1}(t)\sum_{\ell=1}^{j}\Delta V_\ell\right\}\Big/V_j(t + \Delta t) \ . \tag{4.59}$$

For the special case of the n^{th} shell, we obtain

$$U_n(t + \Delta t) = \left\{\left[V_n(t) - \sum_{\ell=1}^{n-1}\Delta V_\ell\right]U_n(t) + W_{N_{tau}}(t)\sum_{\ell=1}^{j}\Delta V_\ell\right\}\Big/V_n(t + \Delta t) \ . \tag{4.60}$$

In equations (4.59) and (4.60), it is assumed that the change in radius is sufficiently small that the inequality

$$\sum_{\ell=1}^{j-1}\Delta V_\ell \leq V_j(t) \tag{4.61}$$

is always satisfied; this assures that all of the material needed to fill the new j^{th} shell can be found in the old j^{th} and $(j+1)^{th}$ shells.

The entire procedure for calculating $U_j(t + \Delta t)$ is carried out in two separate steps. In the first step, equations (4.48), (4.45), and (4.50) are used to calculate the change in concentration due to gas diffusion during the

time interval Δt. Equations (4.59) and (4.60) are then used to compute the variations due to the change in nuclear radius occurring during the same time interval.

4.2.3. Calculation of differential variations in the internal parameters

The internal parameters describing the nucleus at a given time are the nuclear radius $r(t)$, the internal gas pressure $p(t)$, the amount of gas in the nucleus $N(t)$, and the number of surfactant molecules in the skin $N_{mol}(t)$. The parameters $r(t)$, $p(t)$, and $N(t)$ are related through the equation of state in equation (4.1). Equation (4.8) places a constraint among r, p, and the surface pressure Π, while equation (4.22) gives the functional dependence of Π on A, the surface area per surfactant molecule. The parameters A, N_{mol}, and r are connected through the geometric relationship

$$4\pi r^2 = AN_{mol} \ . \tag{4.62}$$

The concentration difference appearing in equation (4.3) can be evaluated by replacing $U(r,t)$ with $U_1(t)$, as determined by equation (4.53). The parameter α in equation (4.3) may be identified with the leading terms in equation (4.51),

$$\alpha(t) = D \cdot D_1 \cdot H(t) \ . \tag{4.63}$$

The derivative $d\Pi/dr$ in equation (4.14) can be calculated using the definitions in equations (4.22) and (4.62),

$$\frac{d\Pi}{dr} = - \frac{\Pi(A)}{A_1} \frac{d}{dr} \frac{4\pi r^2}{N_{mol}} \ . \tag{4.64}$$

Writing out the derivative, this equation becomes

$$\frac{d\Pi}{dr} = - \frac{\Pi}{A_1} \frac{8\pi r}{N_{mol}} - \frac{4\pi r^2}{(N_{mol})^2} \frac{dN_{mol}}{dr} \ . \tag{4.65}$$

The dN_{mol}/dr term in equation (4.65) is associated with the desorption of surfactant molecules from the nuclear skin into the surrounding fluid. In subsection 4.1.1 it was indicated that molecules will leave the skin if and only if Π exceeds the critical value Π_{max}. This limiting skin tension may be associated with that particular value of A which satisfies the equation

$$\Pi(A_{min}) = \Pi_{max} \ . \tag{4.66}$$

Thus, a small change in the radius δr will result in a loss of molecules if and only if it results in a new value of A, $\bar{A}$, that is less than or equal to A_{min}. Evidently, if A is greater than or equal to A_{min}, then an increment in the radius will result in a larger value of the molecular area, and no material will be lost as a result of this process. Hence,

$$\frac{dN_{mol}}{dr} = 0 \ ; \ dr > 0 \ . \tag{4.67}$$

If δr is less than zero and if the value of $\bar{A}$ produced by this perturbation is greater than A_{min}, then there is again no molecular loss:

$$\frac{dN_{mol}}{dr} = 0 \; ; \; A \geq A_{min} \; . \tag{4.68}$$

In the case that A is equal to A_{min} and δr is less than zero, the value of $\bar{A}$ that would be predicted using equation (4.62) with N_{mol} fixed is less than A_{min}. In this situation molecules will be lost from the interface. It is assumed that the rate of molecular loss is sufficiently fast that the value of A can never be significantly less than A_{min}. The decrement in radius will therefore result in the desorption of enough molecules to maintain A equal to A_{min} and Π equal to Π_{max}, or in mathematical terms,

$$\frac{d\Pi}{dr} = 0 \; ; \; dr < 0 \text{ and } A = A_{min} \; . \tag{4.69}$$

Substituting this result into equation (4.65) yields

$$\frac{dN_{mol}}{dr} = \frac{2N_{mol}}{r} \; ; \; dr < 0 \text{ and } A = A_{min} \; . \tag{4.70}$$

When a surfactant molecule desorbs from the nuclear skin into the surrounding fluid, it is assumed to be permanently lost from the system. More explicitly, it is postulated that there is no significant accretion of surfactant molecules from the fluid to the skin. Because molecules running into the nucleus may be incorporated into the skin if Π is less than Π_{max}, this assumption might not be valid over long time intervals. Hence, it is assumed only that the time scale for molecules to be reacquired is long compared with the 5.25-hour duration of most gelatin experiments.

Equation (4.14) can now be used to estimate the change in radius Δr occurring during the short time interval Δt:

$$\Delta r \approx \frac{dr}{dt} \Delta t \; . \tag{4.71}$$

For this approximation to be valid, the value of dr/dt must be sensibly constant during the time step. Because the right-hand side of equation (4.14) depends mainly on the values of the internal parameters, a useful estimate of the longest time step that may accurately be used in equation (4.71) can be derived by demanding that none of the internal parameters change significantly during this interval. This may be expressed analytically as choosing Δt such that each of the parameters of interest q_j satisfies an equation of the form

$$\left(\frac{dq_j}{dt} \Delta t \right) \Big/ q_j \leq \delta \; , \tag{4.72}$$

where δ is an arbitrary accuracy parameter. Smaller values of δ will result in shorter time steps and better accuracy in the approximations.

In practice Δt is calculated by choosing the smallest member of the set Δt_j, defined, in part, by

$$\Delta t_j = \delta q_j \Big/ \frac{dq_j}{dt} \; ; \; j = 1,4 \; . \tag{4.73}$$

The variables that must be considered in computing the time interval are: (q_1,r), (q_2,p), (q_3,N), and (q_4,Π). An additional constraint on the choice of Δt is that it be small enough that the diffusion calculations in equations (4.48) and (4.36) will be done correctly. The calculations will proceed accurately only if Δt is less than or equal to $0.5\ DX^2/D$ where DX is the thickness of an individual integration layer. It can be assured that the use of equations (4.48) and (4.36) to compute $U_j(t)$ and $W_j(t)$ is valid by placing elements in the set Δt_j of

$$\Delta t_5 = 0.5\ DZ^2/D \tag{4.74a}$$

and

$$\Delta t_6 = 0.5\ D\rho^2/D \; . \tag{4.74b}$$

Two further additions to the set Δt_j are necessary. The first is the time remaining until the next change in dp_{amb}/dt, which is given by

$$\Delta t_7 = t_k - t \; , \tag{4.75a}$$

where k is chosen such that

$$t_k > t \geq t_{k-1} \; . \tag{4.75b}$$

As described in subsection 4.2.1, this constraint is necessary to insure that dp_{amb}/dt does not change discontinuously during the time step. The final limitation on Δt is that which is necessary to prevent discontinuous changes in $d\Pi/dr$. As shown by equations (4.68) and (4.70), such an abrupt change can occur only as A decreases to A_{min}. If dr/dt is greater than zero, or dr/dt is less than zero and A is equal to A_{min}, then this discontinuity will not occur. These situations therefore place no constraint on Δt, and the value of Δt_8 is thus set to the value of Δt_5. In the case that dr/dt is less than zero and A is greater than A_{min}, the interval Δt_8 is calculated by estimating when A will become equal to A_{min}, which occurs about when the equation

$$4\pi\left(r + \frac{dr}{dt}\,\Delta t_8\right)^2 = A_{min}N_{mol} \tag{4.76}$$

is satisfied. The element Δt_8 is therefore taken to be

$$\Delta t_8 = \frac{r - \sqrt{A_{min}N_{mol}/4\pi}}{dr/dt} \tag{4.77a}$$

if dr/dt is less than zero and A is greater than A_{min}, or

$$\Delta t_8 = \Delta t_5 \tag{4.77b}$$

if dr/dt is greater than zero or dr/dt is less than zero and A is greater than A_{min}.

The longest time step consistent with the choice of δ can now be found by determining the minimum element of Δt_j. The values of the internal parameters r, p, and N at time $(t + \Delta t)$ can be estimated using the equations

$$q_j(t + \Delta t) = q_j(t) + \Delta t \frac{dq_j(t)}{dt} , \tag{4.78}$$

where the current values of dq_1/dt, dq_2/dt, and dq_3/dt are given by equations (4.14), (4.9a), and (4.9c), respectively. A more accurate estimate can be made by numerically calculating the second derivatives and by including these terms in the expansion. This leads to

$$q_j(t + \Delta t) = q_j(t) + \Delta t \frac{dq_j(t)}{dt} + \frac{1}{2} \Delta t^2 \frac{d^2q_j(t)}{dt^2} , \tag{4.79}$$

where

$$\frac{d^2q_j(t)}{dt^2} = \left[\frac{dq_j(t)}{dt} - \frac{dq_j(t - \Delta t)}{dt} \right] \Big/ \Delta t . \tag{4.80}$$

The number of surfactant molecules in the skin at time $(t + \Delta t)$ can be computed using equations (4.67), (4.68), and (4.70). This gives

$$N_{mol}(t + \Delta t) = N_{mol}(t) \tag{4.81a}$$

if dr/dt is less than zero or dr/dt is greater than zero and A is greater than A_{min}, and it gives

$$N_{mol}(t + \Delta t) = N_{mol}(t) + 2 \frac{N_{mol}}{r} \Delta r \tag{4.81b}$$

if dr/dt is less than zero and A is less than or equal to A_{min}.

Equations (4.29), (4.30), (4.35), (4.48), (4.59), (4.79), and (4.81) allow the complete state of the nucleus and environment to be determined at time $(t + \Delta t)$, given the condition of the system at time t. The only additional requirement is an orderly system for performing the calculations. An outline of the algorithm developed for use in this study is described below. Using this algorithm it is possible to trace accurately an initially stable nucleus through any given pressure profile and to determine in detail its condition at any later time.

4.2.4. The calculational algorithm

The following algorithm organizes the work to be done in computing the state of the nuclear system at time $(t + \Delta t)$, given the complete condition of the system at time t and the ambient pressure profile.

1. Use equations (4.9a), (4.9c), and (4.14) to calculate dr/dt, dp/dt, and dN/dt, respectively.

2. Use equations (4.73 through 4.77) to determine the current value of the eight elements of Δt_j.

3. Set Δt to be the smallest element of Δt_j.

4. Calculate $r(t + \Delta t)$, $p(t + \Delta t)$, and $N(t + \Delta t)$ using equation (4.79).

5. Compute the values of $\overline{R}(t + dt)$ and $\overline{V}(t + dt)$ from the definitions in equation (4.10).

6. Use equations (4.29) and (4.30) to determine $p_{amb}(t + \Delta t)$ and $dp_{amb}(t + \Delta t)/dt$.

7. Using equations (4.35), (4.36), and (4.38), calculate the gas concentrations $W_j(t + \Delta t)$.

8. Compute $\Pi(t + \Delta t)$ and $N_{mol}(t + \Delta t)$ from equations (4.22), (4.62), and (4.81), and then use equation (4.52) to find $H(t + \Delta t)$.

9. Determine the second derivatives d^2q_j/dt^2 from equation (4.80).

10. Use equations (4.59) and (4.60) to calculate the change in $U_j(t)$ due to the change in radius occurring during the time step.

11. Compute $U_j(t + \Delta t)$ from equation (4.48) and from equations (4.45), (4.50), and (4.53).

12. Use equation (4.27) to calculate $\Pi_{max}(t + \Delta t)$.

By repeating this sequence it is possible to determine the state of the nucleus and environment at any time. The accuracy of the calculations is determined by the parameter δ, and they can be made arbitrarily exact by reducing δ to a sufficiently small value.

A computer program employing this algorithm has been developed for use in model calculations. In this program it is assumed that at time zero the system is in stable equilibrium as defined in section 4.1. The initial conditions on the internal parameters are therefore

$$p = p_{amb} = p^1_{amb} \ , \tag{4.82a}$$

$$\Pi = \gamma \ , \tag{4.82b}$$

$$N = pV/[RT(1 + pB_p + p^2C_p)] \ , \tag{4.82c}$$

and

$$d^2q_j/dt^2 = 0 \ . \tag{4.82d}$$

The initial value of the nuclear radius r_o is a free parameter, subject only to the constraints that it be much smaller than the layer thickness DZ and much larger than the skin thickness t_{skin}.

In Table 4.2 the values of the various physical constants used in this program are tabulated. In all of the work reported in this publication it is assumed that the gas is nitrogen and the surrounding fluid is gelatin. The diffusion properties of nitrogen in gelatin are assumed to be similar to those of nitrogen in water. The surface tension of the gelatin used in the experiments has been reported by Yount (1977a) as 51 ± 5 *dyne/cm* for gelatin batch A and 55 ± 5 *dyne/cm* for gelatin batch D. The intermediate value of *54 dyne/cm* will be used in all future computational work.

TABLE 4.2. PHYSICAL CONSTANTS USED IN MODEL CALCULATIONS

	Constant	Value	Reference
T	Temperature	295°K	Subsection 2.2.3
R	Universal gas constant	8.31×10^7 erg/deg mole	
B_p	First-order virial coefficient	-1.94×10^{-4} bar^{-1}	Gray (1963)
C_p	Second-order virial coefficient	2.10×10^{-6} bar^{-1}	Gray (1963)
γ	Gelatin-nitrogen surface tension	54 dyne/cm	Subsection 4.2.4
S	Solubility	6.7×10^{-13} mole/cm dyne	Gerrard (1976)
D	Diffusion coefficient	1.8×10^{-5} cm^2/sec	Bartels (1971)
D_1	Gas uptake constant	183 cm^{-1}	Blank (1962)

4.3. Results of SS model calculations

The results of numerical calculations performed using the SS model are reported in this section. The goal of this computational program was to determine the values of the five constants that describe the surfactant skin: A_1, C_1, A_{diff}, E_{sol}, and B_1. This has been accomplished by using the SS model as

represented by a computer program to model the results of the gelatin experiments reported in Chapter 2. The work may be conveniently divided into three parts, each part serving to determine one or two of the five unknowns. In subsection 4.3.1 the calculations of decompression thresholds for nuclei initially in stable equilibrium are used to find A_1 and C_1; the parameters E_{sol} and B_1 are found through an analysis of rapid compression saturation-excursion dives in subsection 4.3.2; and in subsection 4.3.3 the value of A_{diff} is deduced from a study of crushing-time experiments.

The calculations reported in this section were performed on the PDP 11/40 Computer of the University of Hawaii Institute for Astronomy. The analysis of a single dive profile required between 3 and 10 minutes on this machine, and data from about 700 such dives were computed in this program. Several types of profiles were considered, including simple decompressions from ambient pressure, decompressions following rapid compression and prolonged exposure at the maximum pressure, and decompressions following variable compressions and prolonged exposures at various levels not necessarily equal to the maximum pressure. These are discussed below.

4.3.1. Calculation of decompression thresholds

The threshold pressure for bubble formation is defined to be the maximum pressure reduction to which an initially stable nucleus may be rapidly subjected without its growing into a gross bubble. In practice, a useful definition of a "gross bubble" is found to be a gas phase larger than twice the initial radius of the nucleus. Because of the exponential character of the surfactant force curve, this quadrupling of the nuclear surface is usually sufficient to reduce Π to a very small value. At this point the nucleus acts much like a true bubble free of surfactant constituents, and equation (1.20) therefore may be evaluated to determine if it will continue to grow. In all of the cases studied in this work, it was found that after increasing in size by a factor of two, the nuclear radius was larger than the critical radius for bubble growth. The above definition of a "gross bubble" was thus found to be satisfactory.

The pressure profile employed in the decompression threshold calculations consisted of a single pressure step that was accomplished in 10 seconds, during which time the ambient pressure was decreased from the initial saturation pressure p_s to the final pressure p_f. The supersaturation pressure p_{ss} is therefore equal to the pressure change Δp:

$$p_{ss} = \Delta p = p_s - p_f \cdot \tag{4.83}$$

Following decompression the numerical integration was continued for a length of time sufficient to determine if bubble growth would occur.

By examining equation (4.14), it is seen that the nuclear radius will increase if and only if the inequality

$$\frac{dp_{amb}}{dt} > 3\bar{R}T\delta[U(r,t) - Sp]\frac{V}{\bar{V}}\frac{1}{r} \tag{4.84}$$

is satisfied. The validity of this inequality defines a "rapid decompression." If dp_{amb}/dt is sufficiently small that the condition fails, then the nucleus will not grow during decompression. The SS model thus predicts the existence of a minimum decompression rate necessary to induce bubble growth. Because $d\Pi/dr$ is less than zero when A is greater than A_{min}, equation (4.14) indicates that the nuclear size will increase during the decompression, as one might expect. Examination of equation (4.67) shows that no molecules will be lost during a decompression. For this reason the upper limit to Π of Π_{max} plays no role in decompression threshold computations, and it is therefore possible in this case to omit from consideration the two parameters that determine Π_{max}, namely, E_{sol} and B_1. It follows that only three parameters characteristic of the surfactant material are of interest in the study of decompression thresholds: A_1, C_1, and A_{diff}.

Computed pressure reduction limits for nuclei stabilized by a skin composed of dicapryl lecithin are plotted in Figure 4.10. The force-area curve for this

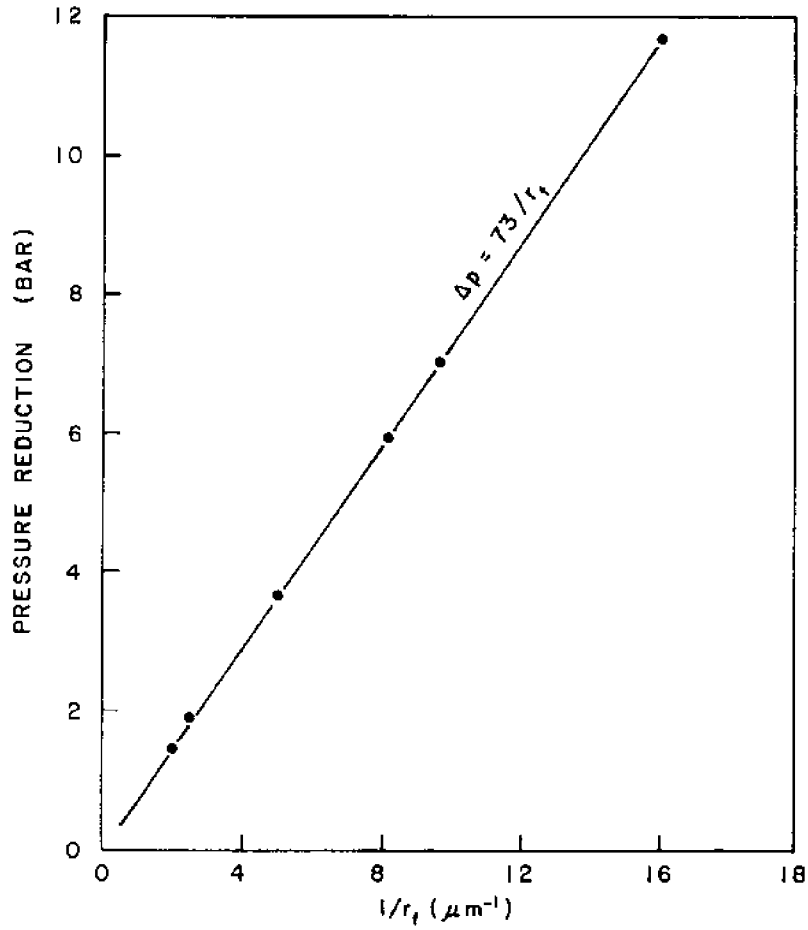

Figure 4.10. Calculated relationship between the equilibrium nuclear radius and the minimum pressure reduction required for bubble growth

substance is shown in Figure 4.6; the characteristic parameter values are $C_1 = 1{,}105$ *dyne/cm*, $A_1 = 16$ Å^2. The decompression thresholds for this material are seen to be inversely proportional to the initial radius, and an excellent parameterization of the computed points is provided by the function

$$\Delta p = 72.7/r_o \text{ dyne cm}^{-2} \quad . \tag{4.85}$$

The surprisingly simple mathematical form of this result is found to be a general feature of the SS model and has been obtained also from the VP model (Yount et al., 1977b; Yount, 1979b). Decompression thresholds for all of the surface-active compounds studied in this program were found to be of the mathematical form

$$\Delta p = \xi/r_o \quad , \tag{4.86}$$

where the slope parameter ξ is determined by the chemical nature of the particular material being studied and depends only on the values of C_1 and A_1.

Computations done in this program enable us to draw two further conclusions concerning decompression thresholds. These are:

1. The pressure reduction limits do not depend on the initial ambient pressure p^1_{amb}, which in this case is equal to the saturation pressure p_s. This is illustrated in Figure 4.11, where Δp is plotted as a function of p_s for a

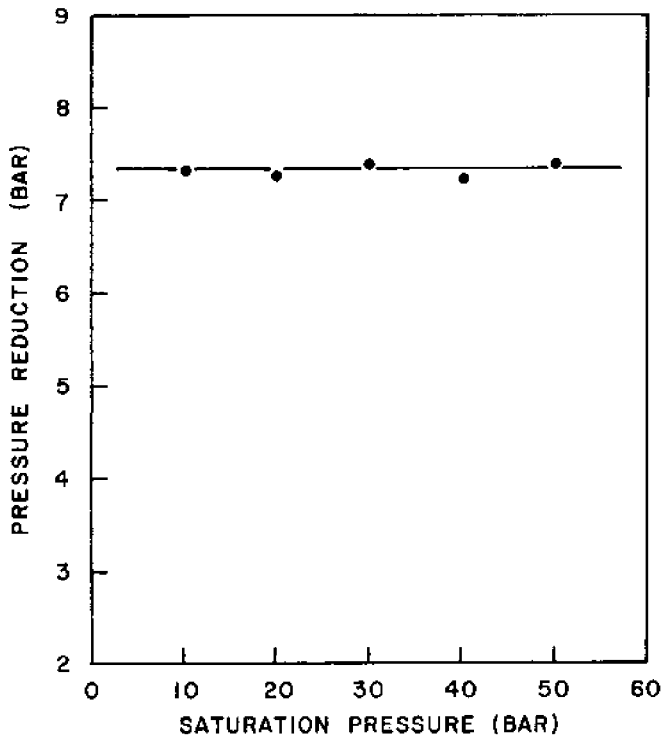

Figure 4.11. Calculated dependence of the pressure reduction limit on the saturation pressure for a 0.1-μm nucleus

0.1-μm nucleus. This remarkable prediction was made earlier by Yount and Strauss (1976), who based their arguments on the crevice model of Harvey et al. (1944). It also follows from the VP model (Yount et al., 1977b; Yount, 1979b). The prediction was tested by Yount and Strauss (1976) by decompressing gelatin mixed at 6.9 bar with water that had stood for several days at high pressure. The bubble formation threshold measured from $p_{amb} = 6.9$ bar was $\Delta p = 0.83$ bar--the same as that found from atmospheric pressure.

2. The value of the parameter A_{diff} has little effect on the decompression thresholds. The data in Figure 4.12 demonstrate the dependence of Δp on A_{diff} for a 0.1-μm nucleus. This lack of sensitivity to A_{diff} is due to the fact that the fractional area for gas diffusion through the nuclear skin does not depend strongly on A_{diff} unless A is near A_{min} [see equation (4.52)]. Because the decompressions studied in this article always begin from the equilibrium state and only result in larger values of A, the inequalities

$$A > A\gamma > A_{min} , \tag{4.87}$$

are satisfied throughout the decompression, where $A\gamma$ is defined by the equation

$$\Pi(A\gamma) = \gamma . \tag{4.88}$$

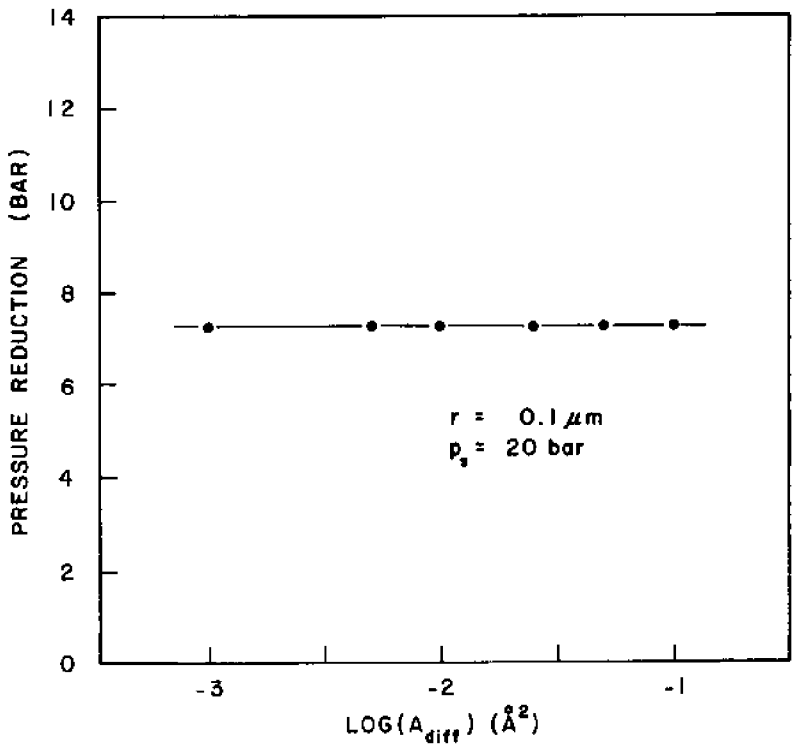

Figure 4.12. Calculated dependence of the pressure reduction limit on the minimum area for diffusion A_{diff}

The value of A is never close to A_{min}, and the diffusive properties of the nucleus are therefore not strongly dependent on A_{diff}.

In Figure 4.13 graphs of Δp versus $1/r_o$ are shown for the six hypothetical surfactant materials having force-area curves displayed in Figure 4.14. In each case the decompression thresholds are of the form given by equation (4.86).

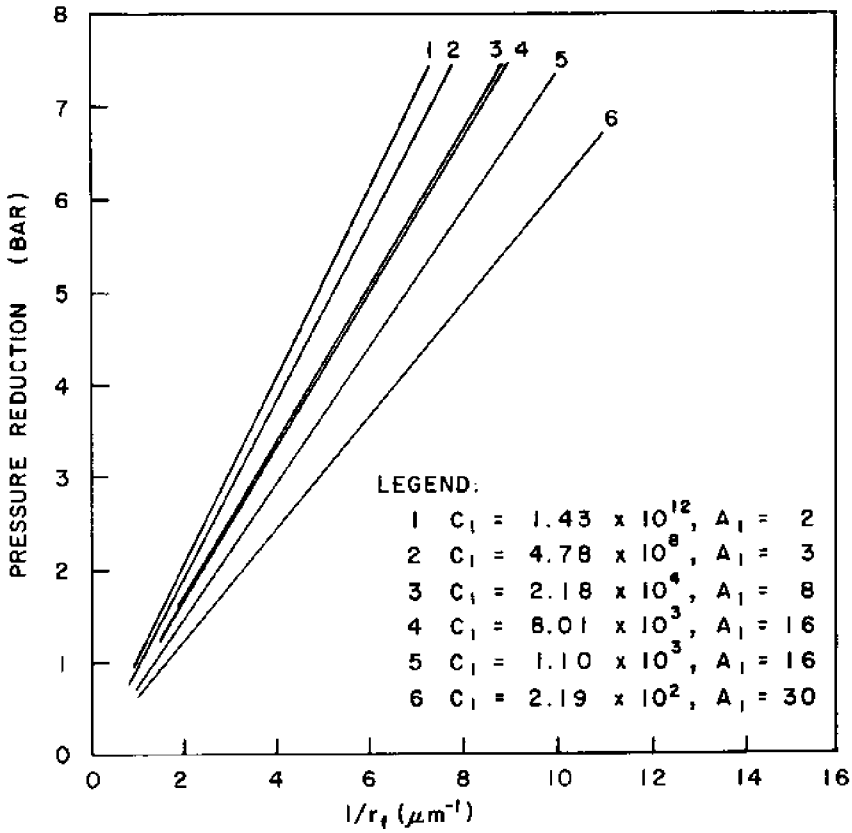

Figure 4.13. Calculated dependence of the pressure reduction limit on the equilibrium nuclear radius for six surfactants

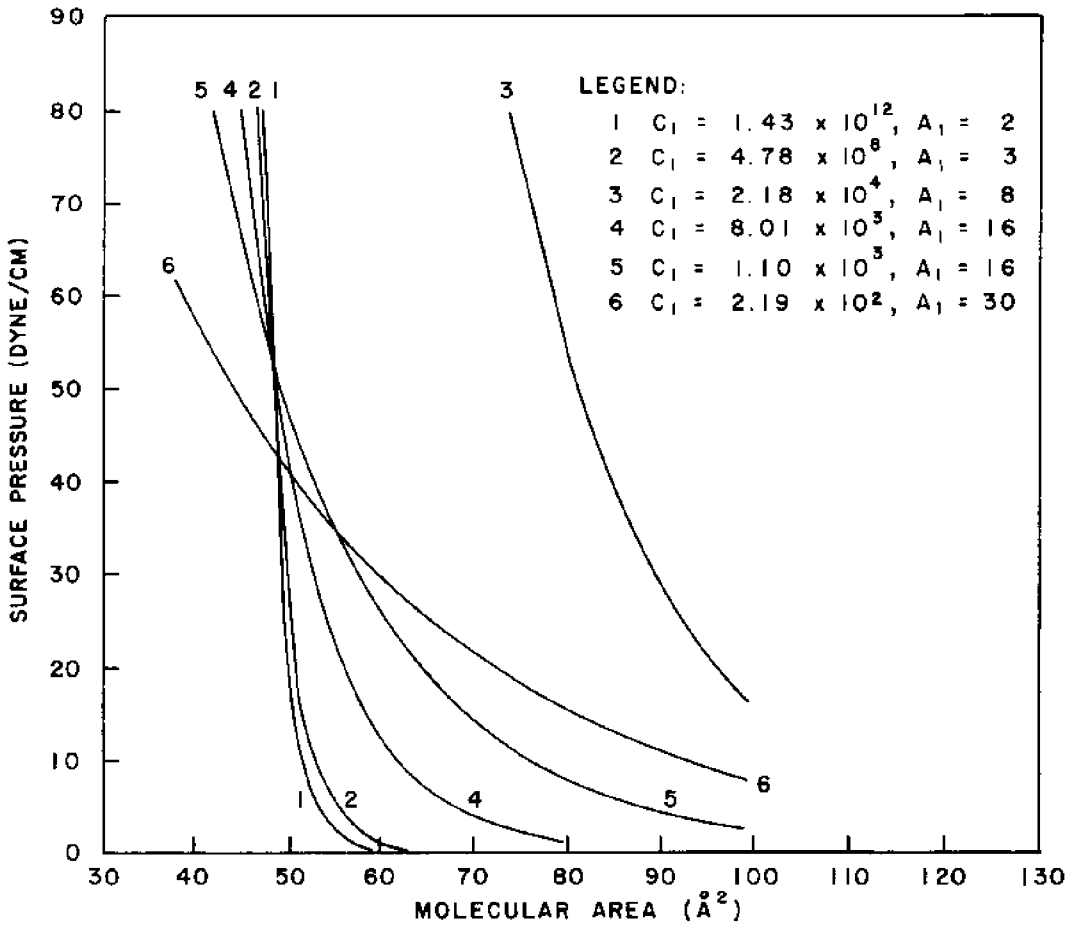

Figure 4.14. Force-area diagrams of six hypothetical surfactants

Examination of these graphs shows that the value of the slope parameter δ depends on the steepness of the corresponding surfactant force-area curve. This relationship is displayed explicitly in Figure 4.15, where the steepness parameter s, defined by the equation

$$s = \ell n(A\gamma/A_1) \ , \tag{4.89}$$

is plotted versus the slope ξ. This curve may be used to determine the value of ξ for a surfactant having known values of C_1 and A_1. It should be noted that a given choice of ξ uniquely determines the value of C_1 and the ratio $A\gamma/A_1$, but it does not place a constraint on A_1 itself.

Examination of equation (1.20) shows that a bubble has a slope parameter of 2γ--in this case *108 dyne/cm*. As shown in Figure 4.15, the decompression threshold of a surfactant-stabilized nucleus is always below this value. This result is not striking since the surfactant molecules are expected to counteract partially the surface tension of the water and thus reduce the amount of work necessary to increase the size of the nucleus. The quantity of work done

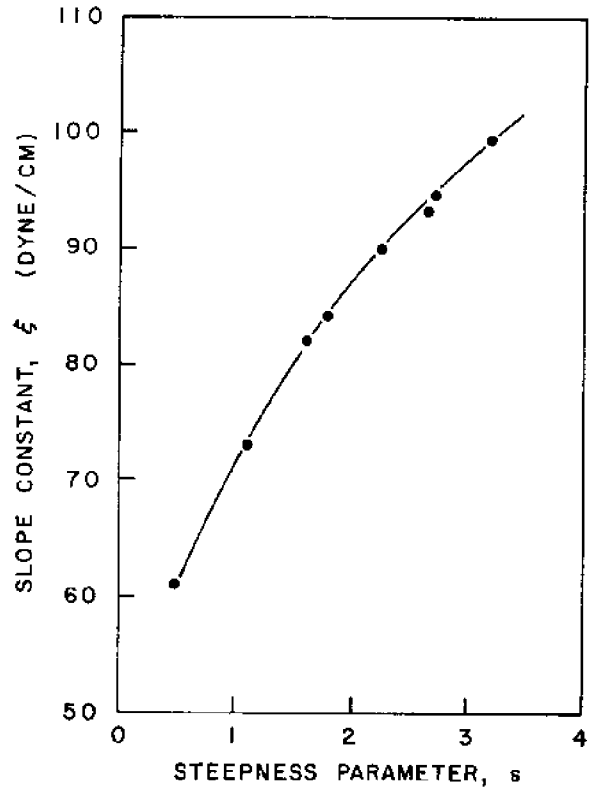

Figure 4.15. Dependence of the slope constant ξ on the steepness parameter s

by the skin in the complete expansion of a nucleus initially in stable equilibrium is given by the integral

$$\Delta W = \int_{r_o}^{\infty} 8\pi r \Pi(r) dr = N_{mol} \int_{A_\gamma}^{\infty} \Pi(A) dA = 4\pi r_o^2 \gamma \frac{A_1}{A_\gamma} . \tag{4.90}$$

Evidently, as $A_1/A\gamma$ increases the quantity of energy stored in the skin increases, and the value of ξ thus decreases. In the limiting case of an incompressible skin, A_1 vanishes and the skin plays no role in the expansion; the slope parameter is therefore equal to that of a bubble

$$\lim_{s \to \infty} \xi(s) = 2\gamma . \tag{4.91}$$

In the case of an ideal elastic skin the ratio $A_1/A\gamma$ is arbitrarily large, and Π is constant at the equilibrium value of γ. Equation (4.8b) becomes

$$dp = dp_{amb} , \tag{4.92}$$

and it is seen that an arbitrarily small decrease of the ambient pressure will result in gas supersaturation leading to growth of the nucleus. Evidently the decompression threshold vanishes in this case, and the lower limit to $\xi(s)$ is given by

$$\lim_{s \to (-\infty)} \xi(s) = 0 \ . \tag{4.93}$$

The value of the slope parameter characteristic of the nuclei studied in the gelatin experiments can be deduced from the determination of the decompression threshold for nuclei of a known size. Such a measurement was made by using a vacuum pump to decompress gelatin samples. In these experiments (Yount and Strauss, 1976) it was found that decompressing gelatin batch A samples by 0.83 bar produces a bubble yield of 5 ± 2 *bubbles per ml*. The nuclear radius associated with a bubble number of 5 may be determined from the initial size distribution given by equation (2.4) to be 0.93 μm. The observed value of ξ is then:

$$\xi = 0.83 \times 10^{6} \times 0.93 \times 10^{-4} = (77 \pm 5) \ dyne/cm \ . \tag{4.94}$$

This corresponds to an s value of (1.32 ± 0.3), from which the ratio $A\gamma/A_1$ can be computed to be (3.74 ± 1.0). The magnitude of C_1 may be calculated by using equation (4.22) as

$$\ell n C_1 = \ell n \gamma + A\gamma/A_1 = 3.99 + 3.74 = 7.73 \pm 1.0 \ , \tag{4.95a}$$

which gives

$$C_1 = 2{,}276 \ dyne/cm \ . \tag{4.95b}$$

The value of A_1 is not determined by this measurement, and its exact value is not strictly needed for further computational use. This is because the quantity of work done by the skin in response to a given change in nuclear radius depends on the ratio $A\gamma/A_1$, and not on the value of A_1 itself. The point is more clearly illustrated by using equation (4.62) to rewrite equation (4.22) in the form

$$\Pi(r) = C_1 \ exp[-4\pi r^2/N_{mo}\ell A_1] \tag{4.96a}$$

or, if no molecular loss has occurred,

$$\Pi(r) = C_1 \ exp[-(r/r_o)^2 A\gamma/A_1] \ . \tag{4.96b}$$

The derivative $d\Pi/dr$ appearing in the differential equation (4.14) therefore depends on the ratio $A\gamma/A_1$ and not on the singular value of A_1.

For computational convenience and to enable illustrative values of several parameters to be computed, a value to $A\gamma$ of 48 $\mathring{A}^2$ has been arbitrarily assigned. This area is close to that of several saturated lecithins having slope parameters similar to that observed in gelatin. It must be emphasized, however, that this value is arbitrary, and that any other physically reasonable choice of $A\gamma$ would be equally valid and yield identical computational results. Given this value of $A\gamma$, the parameter A_1 is calculated to be

$$A_1 = A\gamma/3.74 = (12.85 \pm 4.7)\mathring{A}^2 \ . \tag{4.97}$$

4.3.2. Rapid-compression saturation-excursion dives

In this subsection the results of the rapid-compression saturation-excursion dives reported in section 2.3 are analyzed to determine the value of the variables E_{sol} and B_1. For these computations an initially stable nucleus is exposed to the pressure schedule shown in Figure 4.7. The resulting values of the internal parameters are graphed in Figure 4.16 as a function of time for a typical dive. This figure shows many of the salient features of the experiments.

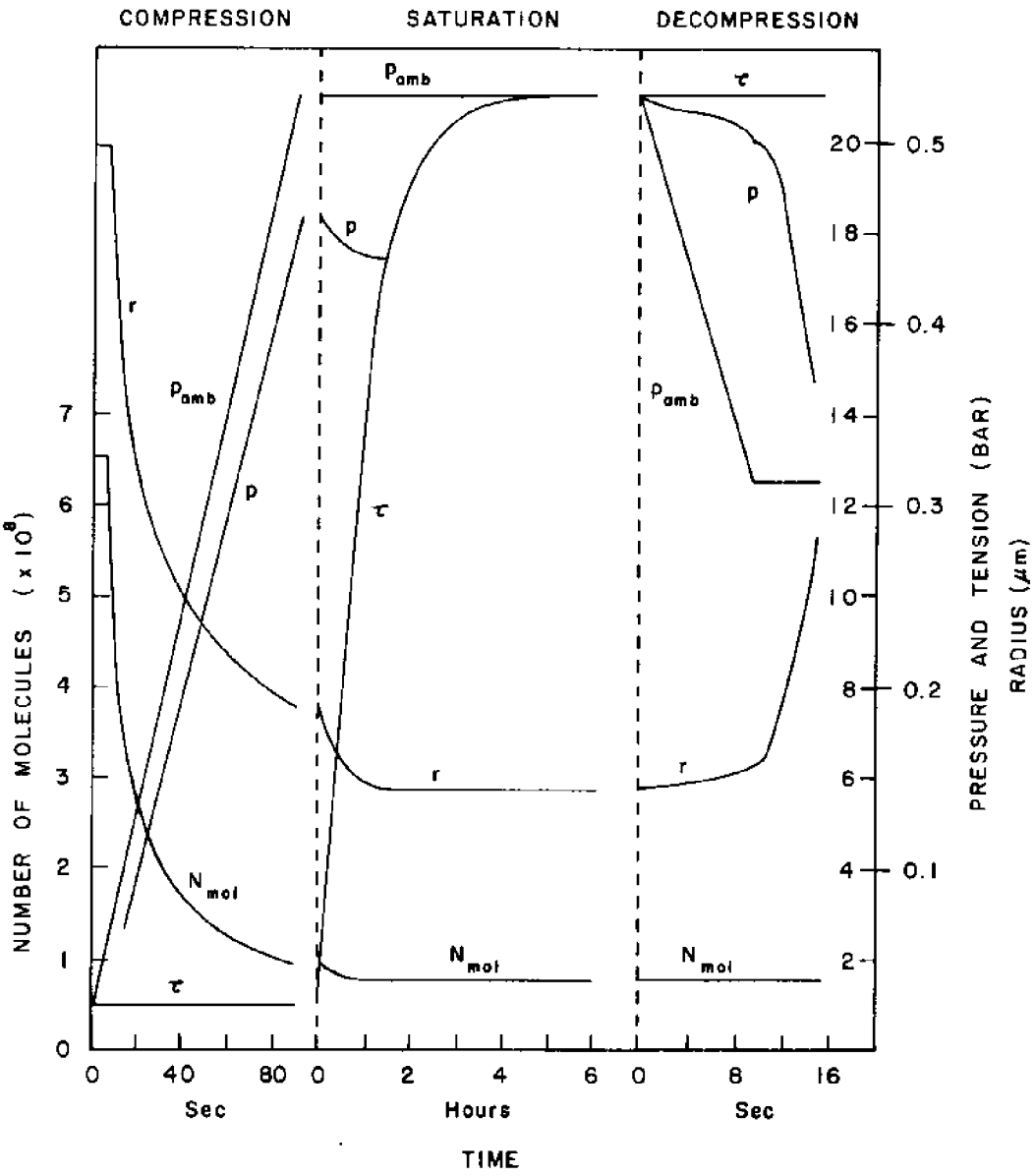

Figure 4.16. History of p_{amb}, r, p, N_{mol}, and τ during a 1 to 21.7 to 12.5 bar saturation-excursion dive

The dive begins with a rapid compression from the initial ambient pressure of 1 bar to the saturation pressure of 21.7 bar. During the first few seconds of compression, the $d\Pi/dr$ term in equation (4.14) dominates the calculation of dr/dt, forcing dr/dt, dp/dt, and dN/dt to assume relatively small values while Π increases rapidly. This initial interval is therefore characterized by small changes in r, p, and N, and by a large increase in Π. The work done upon the nucleus during this stage is used almost entirely to force the surfactant molecules closer together, thus raising the value of Π.

About seven seconds into the compression, Π reaches its maximum value of Π_{max}. At this time molecules begin desorbing from the skin into the liquid at a rate sufficient to keep Π fixed at Π_{max} [see equation (4.70)]. During the remainder of the compression, Π remains constant at Π_{max}, while the values of the internal parameters change rapidly.

Following the compression is a relatively long saturation period during which the ambient pressure remains constant. At the start of this interval the gas tension in the nuclear domain τ is equal to the initial ambient pressure of 1 bar. Throughout the subsequent six-hour exposure, τ steadily rises as gas diffuses into the gelatin slab. At the end of the saturation interval, τ is essentially equal to p_s and the gelatin slab is very nearly in diffusive equilibrium with its surroundings; that is, W_j is nearly equal to p_s.

During the initial phase of the saturation period, the pressure within the nucleus is much higher than the ambient tension, and gas diffuses out. This loss of gas forces the nucleus to contract further, in accordance with equation (4.14). Because dr/dt is less than zero and A is equal to A_{min}, the value of Π remains fixed at Π_{max} and additional surfactant molecules are lost from the skin. The loss of molecules continues until p is equal to τ. Throughout the rest of the saturation period, p remains equal to τ, and at the end of the exposure the nucleus is very nearly in stable equilibrium. The nuclear size immediately before decompression will therefore depend only upon the number of surfactant molecules left in the skin. If the initial number of molecules was N^o_{mol} and the final number N^f_{mol}, the final radius r_f may be determined from equation (4.62) to be

$$r_f = r_o \sqrt{N^f_{mol}/N^o_{mol}} \quad . \tag{4.98}$$

Using the results in subsection 4.3.1, the minimum pressure reduction necessary to induce bubble formation can be computed from the equation

$$\Delta p = 77/r_f \quad . \tag{4.99}$$

Given the values of the three parameters E_{sol}, B_1, and A_{diff}, the threshold pressures $\Delta p(r_o,p_s)$ can now be computed. In Table 2.5 the results of the gelatin model determinations of these thresholds are presented. These data are plotted in Figure 2.14, which shows how the decompression limit for a nucleus of initial size r_o depends on the crushing pressure p_{crush}, which in this case is related to the maximum pressure and saturation pressure by the equation

$$p_m = p_s = p_{crush} + 1 \ bar \quad . \tag{4.100}$$

The values of E_{sol} and B_1 are now to be found by fitting the model to the data in Table 2.5.

The effect of the parameter A_{diff} on the decompression thresholds for a fixed choice of B_1, E_{sol}, r_o, and p_{crush} is shown in Figure 4.17. The shape of this curve may be understood by an examination of Figure 4.16. During the compression phase of the dive, A_{diff} has little effect on dr/dt. This is because a change in A_{diff} causes H to increase or decrease, and the difference $[U(r,t) - Sp]$ to decrease or increase correspondingly. The product $H[U(r,t) - Sp]$ occurring in equation (4.14) thus tends to remain relatively constant, and the value of dr/dt is therefore stationary with regard to A_{diff}. At the beginning of the saturation exposure, the internal gas pressure p is higher than the ambient gas tension τ. Because p is determined primarily by isobaric gas diffusion out of the nucleus, the elapsed time until p equilibrates to τ, t_{eql}, will depend almost entirely on the ratio A_{diff}/A_{min}. If this time is short compared with the quasi-exponential rise time or τ, t_{diff}, then A_{diff} will have little effect on the number of molecules lost during the saturation. On the other hand, if t_{eql} is long in comparison with t_{diff}, the number of molecules lost will depend strongly on A_{diff}. This behavior is clearly evident in Figure 4.17. In order to minimize the effect of A_{diff} on the decompression thresholds, it is assumed that A_{diff} is sufficiently large that t_{eql} is much

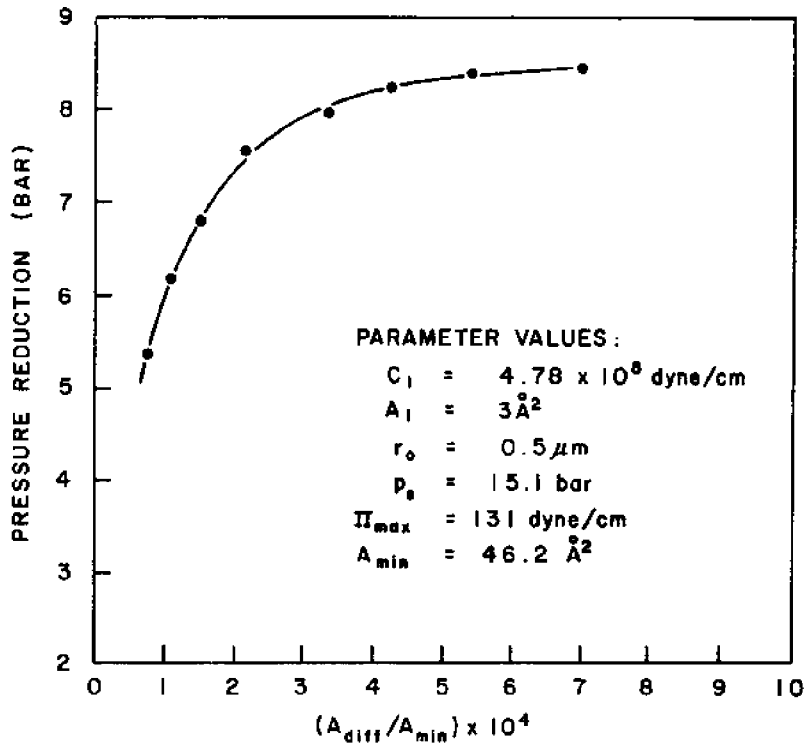

Figure 4.17. Dependence of the pressure reduction limit on the ratio (A_{diff}/A_{min})

less than t_{diff}. In the following subsection it is shown that this assumption is in fact valid and that the ratio A_{diff}/A_{min} is on the order of 5×10^{-4}. For the remainder of this subsection it is assumed that

$$A_{diff} = 5 \times 10^{-4} A_{min} = 240 \times 10^{-4} \text{ Å}^2 \quad . \tag{4.101}$$

Having determined a preliminary value of A_{diff}, the experimental results in Table 2.5 can be used to deduce the value of the parameters E_{sol} and B_1. This is done by employing the SS model to compute the value of Π_{max} necessary to produce the observed value of Δp, given the values of r_o and p_{crush}. This calculation is performed by finding an upper and a lower limit and by then employing the method of successive halving to iterate the proper value of Π_{max}. The results of these calculations are shown in Figure 4.18, where Π_{max} is plotted as a function of $\sqrt{dA/dt}$. The expected functional dependence of Π_{max} is given in equation (4.27) as

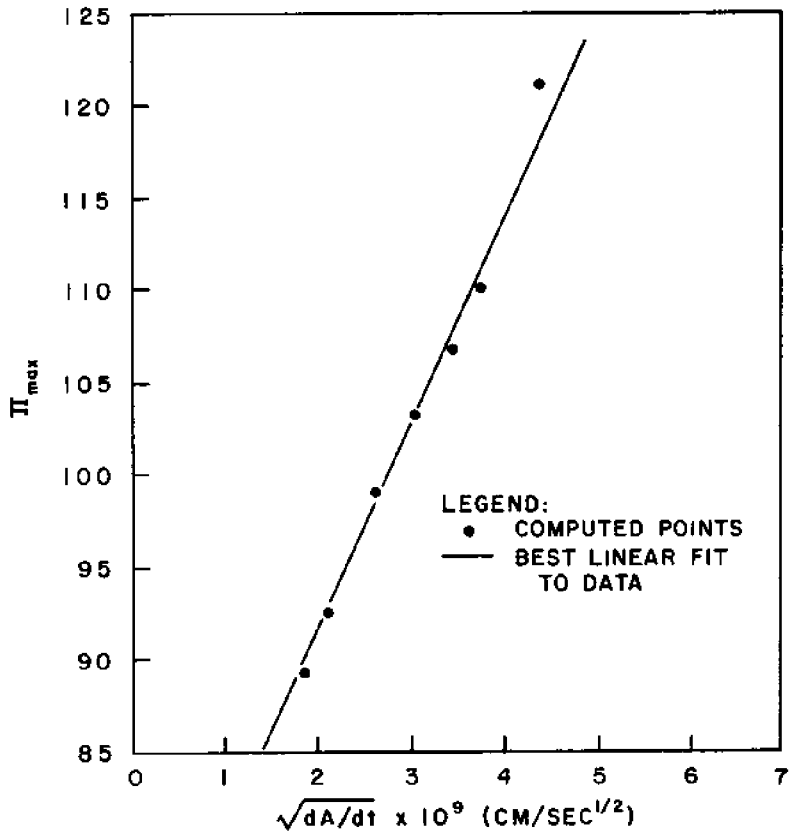

Figure 4.18. Dependence of the maximum skin tension of the rate of change in molecular area. Computed points from observed data in Table 2.5.

$$\Pi_{max} = E_{sol}/A_{min} + B_1\sqrt{dA/dt} \ .$$

From the data in Figure 4.18, the values of the parameters are found to be

$$E_{sol}/A_{min} = 69 \ dyne/cm \tag{4.102a}$$

and

$$B_1 = 1.12 \times 10^{10} \ dyne \ sec^{1/2}/cm^2 \ . \tag{4.102b}$$

Using equation (4.25), the magnitude of A_{min} can be determined to be

$$A_{min} = 45.0 \ \mathring{A}^2 \ . \tag{4.103}$$

The value of E_{sol} may now be found from equation (4.102a):

$$E_{sol} = 3.11 \times 10^{-13} \ erg = 4.45 \ kcal/mole \ . \tag{4.104}$$

The ratio $E_{sol}/(1/2)kT$ is 15.33, and the skin is therefore stable against thermal fluctuations, as required by the discussion in subsection 4.1.1. It should be noted that the observed value of B_1 is very close to that deduced from the measurements reported by Rabinovitch et al. (1960) for stearic acid.

Equation (4.99) provides the information necessary to deduce the final size of a nucleus following a rapid compression from the critical supersaturation pressure required to make the nucleus grow into a bubble. As an example, Table 2.5 shows that after a 0.5-μm nucleus has been rapidly compressed by 20.7 bar, it requires a supersaturation of 10.4 bar to make that nucleus grow into a bubble. The final radius of the nucleus just before decompression evidently is

$$r_f = \frac{77}{10.4 \times 10^6} = 0.074 \ \mu m \ . \tag{4.105}$$

In this manner it is possible to compute r_f for each of the entries in Table 2.5.

The post-compression size distribution of nuclei may now be determined by use of the ordering theorem introduced in section 2.5 and the initial nuclear size distribution. Continuing with the above example, it is found from equation (2.4) that there were initially 54 nuclei larger than 0.5 μm. Although the rapid compression reduced the equilibrium nuclear radius to 0.07 μm, the ordering theorem states that there must still be 54 nuclei larger than this new size. The post-compression nuclear size distributions obtained in this manner are plotted in Figure 4.19, along with the original distribution. It should be noted that for each value of p_{crush} there exists a critical radius such that nuclei smaller than this size will be unaffected by the compression, i.e., such that r_f is equal to r_o.

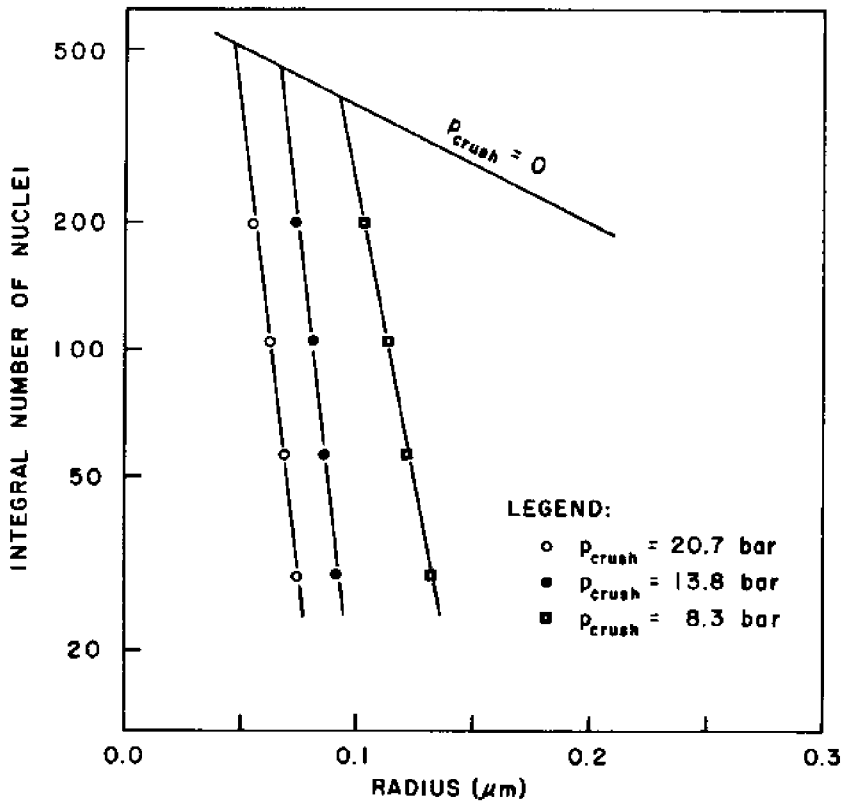

Figure 4.19. Post-compression nuclear size distributions

4.3.3. Crushing time experiments

In section 2.5 a series of gelatin experiments is described in which a pressure spike was applied to the sample before the saturation exposure. The results of this program are shown in Figure 2.13. In this subsection these data are employed, along with the previously determined values of A_1, C_1, E_{sol}, and B_1, to find the value of A_{diff}. As mentioned in subsection 4.3.2, the determination of A_{diff} is not necessarily decoupled from that of E_{sol} and B_1. If the value of A_{diff} is sufficiently small that the ratio A_{diff}/A_{min} is on the steep end of the curve shown in Figure 4.17, then an iterative procedure to determine A_{diff}, E_{sol}, and B_1 simultaneously is clearly necessary. As will be seen, the derived value lies on the flat portion of this curve, and the independent calculation of these parameters is therefore justified.

The crushing time experiments measure the number of bubbles as a function of the time at maximum pressure t_m. Because the pressure spike was always followed by a saturation exposure at lower pressure, the critical radius for bubble formation was constant throughout this program. The value of r_c can be found from equation (4.99) to have been

$$r_c = \frac{77}{10.35 \times 10^6} = 0.0744 \ \mu m \ . \qquad (4.106)$$

These experiments can now be interpreted as measuring the number of nuclei larger than 0.074 μm at the end of the dive. The initial nuclear radius corresponding to any given bubble number can be found from the nuclear size distribution given by equation (2.4). The effect of a pressure schedule that yields N bubbles is to reduce a nucleus of initial radius $r_o(N)$ to a final size of r_o. As an example, an experiment done with t_m of 120 sec produced 118 bubbles per ml. The corresponding initial radius is calculated from equation (2.4) to be 0.35 μm. It is possible to determine the value of A_{diff} from this datum by using the SS model to compute the final size of a 0.35-μm nucleus as a function of A_{diff}, keeping the parameters C_1, A_1, E_{sol}, and B_1 fixed at their previously determined values. The results of these calculations yield a value for $Adiff$ of

$$A_{diff} = 2.5 \times 10^{-2} \text{ Å}^2 \quad . \tag{4.107}$$

The number of bubbles produced by a dive having a pressure spike of arbitrary duration may be determined by calculating the modified nuclear size distribution produced by that schedule. This is done by computing the final sizes of several nuclei subjected to the same profile, and then plotting r_f against $\ell nN(r_o)$, as determined from equation (2.4). The results of such calculations for several values of t_m are shown in Figure 4.20. The effect of the pressure

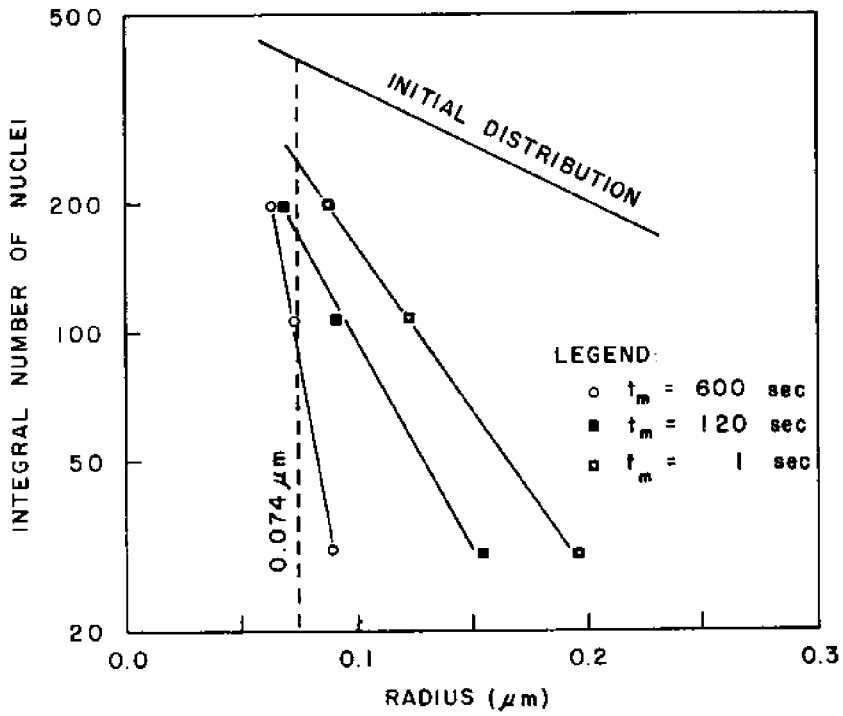

Figure 4.20. Effect of a pressure spike on the nuclear size distribution

schedule on the nuclear size distribution is to shift the curve to smaller sizes and steepen the slope. It should be noted that only those nuclei having initial sizes of less than about 0.04 μm were not affected by the crushing pressure of 20.7 bar. The number of bubbles produced by a pressure spike of arbitrary length can be found by measuring the intercept of the proper distribution with the 0.074-μm line. In Figure 4.21 the results of the SS model calculations are compared with the data from Figure 2.15, and the two are seen to be in close agreement.

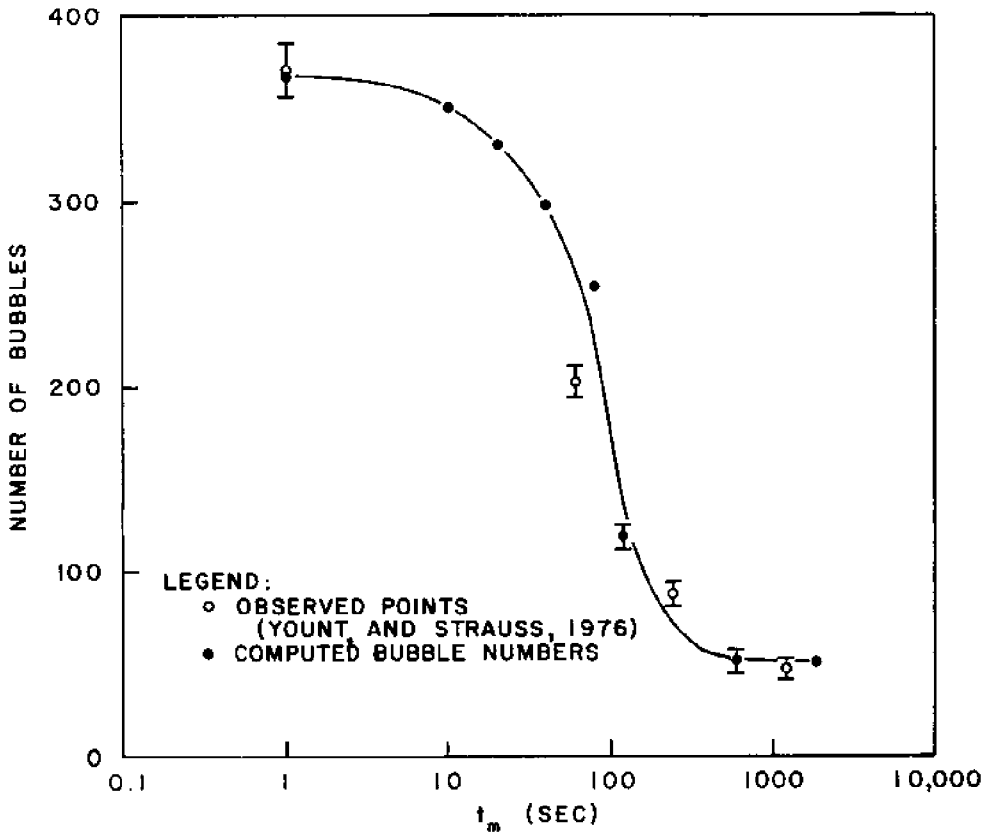

Figure 4.21. Dependence of bubble number on crushing time

CHAPTER 5. THE GROWTH AND CHEMICAL NATURE OF SURFACTANT-STABILIZED NUCLEI

In this chapter two related questions are considered: What type of surface-active material forms the skin of surfactant-stabilized nuclei, and what physical mechanisms are responsible for the occurrence of the nuclei and lead to the observed exponential size distribution? These questions are of practical significance because their answers supply information pertinent to any ability to solve problems of bubble formation by destroying existing nuclei and preventing their subsequent regrowth.

5.1. Identification of the nuclear surfactant

The analysis of the gelatin data using the Surfactant Stabilized model described in section 4.3 has yielded values of the parameters C_1, B_1, A_{diff}/A_{min}, A_γ/A_1, and E_{sol}/A_{min}. These numbers are representative of the surfactant material associated with the nuclei found in gelatin. In this section these observed results will be compared with measurements of known surfactant materials in order to identify, so far as is possible, the chemical constituent(s) of the nuclear skin.

The two most useful numbers for purposes of chemical identification are C_1 and the ratio A_γ/A_1. The values of these parameters determine the shape of the force-area curve of a given surfactant. To permit a comparison, representative values of C_1, A_1, and A_γ for individual members of several classes of insoluble surfactant materials at water-air interfaces have been determined. These are summarized in Table 5.1, along with the equilibrium spreading pressure Π_e and

TABLE 5.1. PHYSICAL PROPERTIES OF SELECTED SURFACE-ACTIVE SUBSTANCES

Material	s	A_γ (Å^2)	ℓnC_1	A_1 (Å^2)	Π_e (dyne/cm)	Solubility (mole/cm^3)
Saturated Lecithins						
C_{14} and C_{12}	1.10	48.9	6.99	16.30		
C_{18}	2.56	43.6	16.92	3.37	36	
C_{10}	1.11	48.3	7.01	16.0		
Phosphatidylethanolamines						
C_{18}	2.66	37.3	18.30	2.61		
C_{10}	0.88	41.7	6.41	17.24		
Fatty Alcohols						
C_{18} 1-Octadecanol	3.80	20.0	49.07	0.442	35	4×10^{-11}
C_{16} 1-Hexadecanol	3.80	19.3	48.90	0.431	40	

water solubility of materials when available. Examination of this table indicated that several of the saturated lecithins and phosphatidylethanolamines have characteristic values of $A\gamma/A_1$ and C_1 that agree well with the measured values. Because other surface-active substances might behave similarly, the surfactant material cannot be identified uniquely as being a saturated lecithin but it may only be concluded that this is one possibility consistent with the observations.

The parameters B_1 and E_{sol}/A_{min} provide information concerning the stability and dynamic behavior of the skin. Because observations of the maximum allowable skin tension Π_{max} are difficult to make in even the most favorable instances, understandably little information has been reported concerning the dependence of Π_{max} on the compression rate dA/dt; i.e., on the magnitude of B_1. The observed value of this parameter seems reasonable since it is close to that reported by Rabinovitch et al. (1960) for stearic acid, but it is of little use in elucidating the chemical nature of the surfactant material. The ratio E_{sol}/A_{min} determines the maximum tension to which the monolayer may be slowly compressed without collapsing. Gaines (1966) noted that this monolayer stability limit is not necessarily equal to the equilibrium spreading pressure and can even lie below the ESP. Munden and Swarbrick (1973) and Phillips and Chapman (1968) were able to compress monolayers of saturated lecithins to surface pressures well above *50 dyne/cm*, at which point the compressions were usually terminated by spillage of water over the edge of the trough rather than by collapse of the skin. The observed value of *69 dyne/cm* therefore seems reasonable when compared with the saturated lecithins.

The ratio A_{diff}/A_{min} measures the ability of the monolayer to block the flow of gas across the interface. As noted in subsection 4.2.2, the use of the fractional area hypothesis in determining the diffusive resistivity of a monolayer has been examined by Barnes et al. (1970). This group used a mechanical analog of hard spheres in a vibrating pan to estimate A_{diff}/A_{min} for water molecules diffusing through straight chain alcohols and found a limiting value of about 3×10^{-3}. Because this ratio depends strongly on the size of the molecules involved, their number, although of the same order of magnitude as the observed value of 0.5×10^{-3}, is not strictly relevant. An independent estimate of this ratio applicable to densely packed monolayers can, however, be developed from thermodynamic principles.

Consider the small portion of monolayer shown in Figure 5.1. The surface-active molecules, although packed together in a minimum area, do not densely cover the interface but instead tesselate it into a number of small openings or windows. Because the average window is smaller than a nitrogen molecule, it is only through those fenestrations made larger by thermodynamic fluctuations that gas molecules can pass. The absolute probability that a single window will be increased in area by an amount σ due to thermodynamic fluctuations is given by the Boltzmann equation as

$$p(\sigma) = ce^{-\sigma\Pi/kT} \quad . \tag{5.1}$$

where $\sigma\Pi$ is the energy associated with the fluctuation.

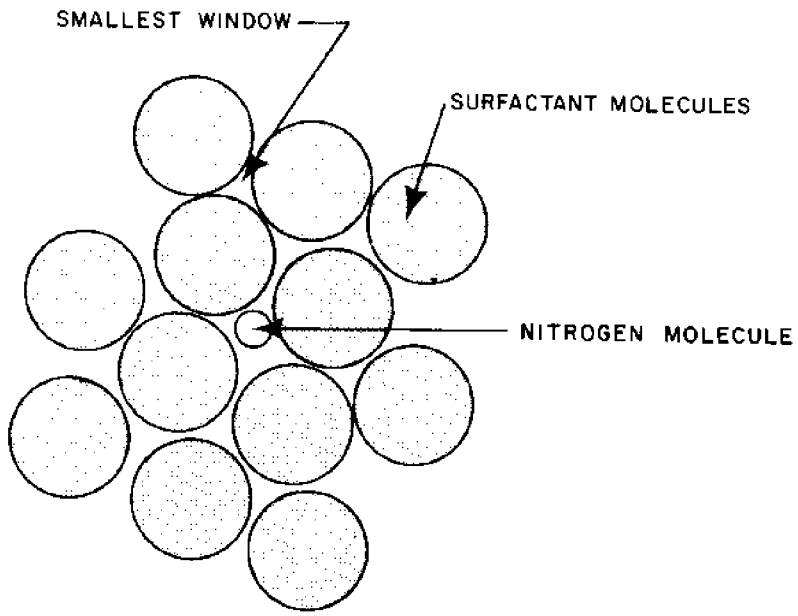

Figure 5.1. Top view of the surfactant monolayer

The constant of proportionality in equation (5.1) can be evaluated by setting the integral over all positive values of σ equal to the fractional number of fluctuations δ that result in uniform increases in area, where the value of δ lies between zero and one. That the value of δ is not unity reflects the facts that one-half of all fluctuations are decreases and that, of the positive fluctuations, only those that uniformly increase the window areas are germane, since a fenestration must be uniformly increased in size to permit passage of a gas molecule. The value of δ is therefore about 0.1, a figure arrived at by assigning multiplicatively a probability of 0.5 to each of the three constraints: (1 and 2) that in each of two principle directions there is an increase in size, and (3) that the size increase in one direction is roughly equal to that in the other direction. The value of the proportionality constant c is then given by:

$$c = \delta / \int_0^\infty e^{-\sigma\Pi/kT}\, d\sigma \simeq 0.1\ \Pi/kT\ . \tag{5.2}$$

The minimum area which must be added to a single window in order for diffusion to occur is assumed to be σ_o, but any perturbation larger than this will also work. The probability of a single opening being available for diffusion at any instant in time is therefore given by the integral

$$P = \int_{\sigma_o}^\infty p(\sigma)d\sigma = 0.1\ \frac{\Pi}{kT} \int_{\sigma_o}^\infty e^{-\sigma\Pi/kT}\, d\sigma = 0.1\ e^{-\sigma_o\Pi/kT}\ . \tag{5.3}$$

The area for diffusion associated with one such window is taken to be A_{gas}, the cross-sectional area of a gas molecule; this reflects the fact that rarely will an opening be expanded to a size large enough to admit two or more gas molecules

simultaneously. Assuming that there exists one window for each surfactant molecule, the ratio A_{diff}/A_{min} becomes

$$\frac{A_{diff}}{A_{min}} = 0.1 \frac{A_{gas}}{A_{min}} e^{-\sigma_o \Pi/kT} . \tag{5.4}$$

The value of σ_o will depend on the size and shape of both the gas and surfactant molecules. Following the example of Barnes et al. (1970), it is assumed that the molecules present circular cross-sections. If the effective cross-sectional area of a nitrogen molecule is taken to be 5.56 Å^2, while A_{min} has been assumed to be 48 Å^2, then the area σ_o is found by measurement to be 9.13 Å^2. The ratio A_{diff}/A_{min} then has the numerical value

$$\frac{A_{diff}}{A_{min}} = 0.1 \frac{5.56}{48} exp(-10.04/4.07) = 1 \times 10^{-3} , \tag{5.5}$$

where the value of Π has been taken to be 110 dyne/cm^2. Because this result depends strongly on the product $\sigma_o \Pi$ occurring in the exponential in equation (5.4) and on the value of ζ, the good agreement with the observed number is somewhat fortuitous. The important point is that the magnitude of the measured value is about what is expected from elementary considerations.

The calculation of monolayer permeation and evaporation resistance by thermodynamic arguments has been previously considered by Blank (1964), who arrived at the result

$$\frac{A_{diff}}{A_{min}} = \frac{1}{2} exp[-(\gamma - \Pi)\sigma_o/kT] . \tag{5.6}$$

Blank's derivation is similar to the development of equation (5.4), with the major differences being that the energy associated with a fluctuation in area is $\sigma_o(\gamma - \Pi)$, that the ratio A_{diff}/A_{min} is equal to the absolute probability P, and that ζ is implicitly assumed to be unity. Dickinson (1978) commented that it would seem more appropriate to calculate the energy associated with a fluctuation in area as $\sigma_o \Pi$, which is a concept that has been used in deriving equation (5.4). Another major difference between the two derivations is that each open window is assigned an effective area for diffusion equal to the cross-sectional area of a single gas molecule, while Blank uses the entire area of the window. The net result of these three differences is that equation (5.6) predicts much larger values of A_{diff}/A_{min} than does equation (5.4).

In summary, the observed values of the five parameters do not provide enough information to identify uniquely the surface-active substances from which the nuclear skins are formed. Saturated lecithins and phosphatidylethanolamines do, however, have C_1 and A_γ/A_1 values and collapse pressures near that observed in gelatin nuclei, and their minimum compression areas lead to reasonable values of A_{diff}. The observed parameters are therefore within the range of those characteristic of commonly occurring natural surfactants.

5.2. The equilibrium size distribution and the growth of nuclei

One of the basic results of the gelatin experiments is that the nuclei have the initial size distribution given by equation (2.7). This size distribution has been observed to remain unchanged over intervals of several days, from which it is concluded that the distribution is stationary with regard to time, that is

$$\frac{dn}{dt} = 0 \ . \tag{5.7}$$

In this section the physical processes by which nuclei can grow or be created and destroyed are examined in view of the constraints imposed by the above experimental results.

The observation that the distribution of nuclear sizes is time independent does not necessarily imply that each individual nucleus is of constant size. Any particular nucleus is free to grow, and nuclei may be added to or deleted from the sample, in any manner that leaves the net size distribution unchanged. Beginning with an examination of the mechanisms by which pre-existing nuclei might grow, constraints will be placed on the creation and destruction of nuclei by requiring that these processes combine with the rate of individual nuclear growth to produce a stationary distribution of the observed exponential form.

The nuclei in a fluid sample are ordinarily in stable equilibrium. Their radii are related to the number of surfactant molecules in the skins by the equation

$$4\pi r^2 = A\gamma N_{mol} \ . \tag{5.8}$$

It is evident that a nucleus will grow larger or smaller as molecules are added to or lost from the surfactant monolayer. In equilibrium situations the net rate at which material is transferred from the skin into the surrounding fluid, or vice versa, is given by Fick's law of diffusion,

$$\frac{dN_{mol}}{dt} = 4\pi r^2 D \left.\frac{dC}{d\rho}\right|_r \ , \tag{5.9}$$

where $dC/d\rho$ is the gradient of the concentration of dissolved surfactant molecules. This derivative may be approximated by the equation

$$\frac{dC}{d\rho} \approx (C_o - C_f)/\ell \ , \tag{5.10}$$

where C_f is the molecular concentration just outside of the nuclear skin, C_o is the concentration in the fluid, and ℓ is a characteristic length. The value of C_f will depend on both the concentration of molecules at the liquid-gas interface and on how strongly they are bound to the interface.

At any instant most of the surfactant molecules will have energies less than the desorption energy E_{sol} and will therefore be bound into the skin and

not be available for diffusion. The fraction of molecules that are candidates for diffusion can be calculated using the Boltzmann energy distribution to be

$$F = \int_{E_{sol}}^{\infty} e^{-E/kT}\, dE \Big/ \int_{0}^{\infty} e^{-EkT}\, dE = e^{-E_{sol}/kT} \ . \tag{5.11}$$

The concentration C_f is therefore related to the molecular density by the equation

$$C_f = FS/A\gamma \ , \tag{5.12}$$

where S is a solubility constant having units of cm^{-1}. The molecular transfer rate is given by the equation

$$\frac{dN_{mol}}{dt} = -4\pi r^2 D(FS/A\gamma - C_o)/\ell \ . \tag{5.13}$$

The rate at which the nuclear radius changes in response to this molecular transport may be computed using the differential form of equation (5.8), remembering that the molecular area remains fixed at the equilibrium value throughout this process. Hence,

$$\frac{dr}{dt} = \frac{A\gamma}{8\pi r}\frac{dN_{mol}}{dt} = -\frac{1}{2} rA\gamma D(FS/A\gamma - C_o)/\ell \ . \tag{5.14}$$

Defining the parameter

$$\kappa = -\frac{1}{2} A\gamma D(FS/A\gamma - C_o)/\ell \ , \tag{5.15}$$

this last expression can be rewritten as

$$\frac{dr}{dt} = \kappa r \ . \tag{5.16}$$

This equation gives the rate at which the nuclear radius changes as a result of the accretion or loss of skin molecules. Note that if κ vanishes, then dr/dt is zero and all nuclei remain of fixed size.

If nuclei were neither created nor destroyed, then the size distribution would, if κ were non-zero, change in response to the growth of individual nuclei. This rate of change may be expressed using the integral size distribution defined by equation (2.5) and the ordering theorem introduced in section 2.4 as

$$N(r+dr, t+dt) = N(r,t) \ , \tag{5.17}$$

where the differentials dr and dt are related by equation (5.16). This last result may be written in the differential form

$$dN = \frac{\partial N}{\partial r}\, dr + \frac{\partial N}{\partial t}\, dt = 0 \ . \tag{5.18}$$

Substituting for dr in terms of dt yields

$$N(r+\kappa r dt, t+dt) = N(r,t) \ , \tag{5.19a}$$

or

$$\kappa r \frac{\partial N}{\partial r} + \frac{\partial N}{\partial t} = 0 \ . \tag{5.19b}$$

Note that if κ is zero, then the derivative $\partial N/\partial t$ vanishes and the distribution is stationary.

In order to include the possibility of the creation or destruction of nuclei in this formalism the two functions $f(r)$ and $g(r)$ are defined. The "destruction function" $f(r)$ is the probability per unit time that a nucleus of radius r will be deleted from a unit volume of the sample; the "creation function" $g(r)$ is the probability per unit time per unit volume for the spontaneous creation of a nucleus of radius r. By definition these functions are always positive valued, that is

$$f(r), g(r) \geq 0 \ . \tag{5.20}$$

Allowance can now be made for the discontinuous addition and removal of nuclei by modifying equation (5.17) to obtain

$$N(r+dr, t+dt) = N(r,t) - dt \int_r^\infty [f(\rho)n(\rho) - g(\rho)]d\rho \ . \tag{5.21}$$

Using the chain rule of integral calculus, this equation can be rewritten as

$$\frac{\partial N}{\partial r}\, dr + \frac{\partial N}{\partial t}\, dt = dt \int_r^\infty h(\rho)d\rho \ , \tag{5.22}$$

where the function $h(r)$ is defined to be the net rate at which nuclei of radius r are added to the sample,

$$h(r) \equiv g(r) - f(r)n(r) \ . \tag{5.23}$$

In order to find those forms of $h(r)$ which result in stationary distributions, the value of $\partial N/\partial t$ in equation (5.21) is set equal to zero, and this equation becomes

$$\frac{\partial N}{\partial r}\frac{dr}{dt} = \int_r^\infty h(\rho)d(\rho) \ , \tag{5.24}$$

or, using equation (2.6) and the fundamental theorem of integral calculus,

$$\frac{d}{dr}\left[n(r)\ \frac{dr}{dt}\right] = h(r)\ . \tag{5.25}$$

The value of dr/dt is given by equation (5.16); putting this in the last equation gives

$$\frac{d}{dr}\ [\kappa r n(r)] = h(r)\ . \tag{5.26}$$

This equation is the desired relationship between known values of κ and the distribution $n(r)$, and the unknown function $h(r)$. Substituting from equation (2.7) for $n(r)$ and performing the mathematical operations yields the final result

$$h(r) = \kappa n(r)(1 - 5.38r)\ . \tag{5.27}$$

This equation is the necessary and sufficient condition to insure that $\partial N/\partial t$ vanishes, given the distribution in equation (2.4) and the nuclear growth rate expressed by equation (5.15). It expresses the net rate at which nuclei must be added to the sample to offset the growth of individual nuclei and thus keep the size distribution constant.

It is of interest to speculate on the physical interpretation of equation (5.27). Because it has been assumed that the surfactant involved in the nuclear skin is nearly insoluble ($C_o \approx 0$) and because the ratio $F/A\gamma$ is calculated from the numerical results in subsection 4.3.2 to be 4.6×10^7, it follows from equation (5.15) that κ is most probably less than zero. The creation and destruction functions can then, in the simplest case, be found by identifying $g(r)$ with the positive term in equation (5.27) and $f(r)$ with the negative term, i.e.,

$$f(r) = \kappa \tag{5.28a}$$

and

$$g(r) = 5.38\ \kappa r n(r) = 5.38 r f(r) n(r)\ . \tag{5.28b}$$

The destruction of nuclei is seen to be indiscriminate in that it does not depend on nuclear size, while the creation function is seen to depend multiplicatively on the number of nuclei and the nuclear radius.

Although the rates of nuclear creation and destruction are given by equation (5.28), the mechanisms involved in these processes remain unknown. One possibility is that living organisms within the gelatin or the water with which it was mixed trap both nuclei and surfactant molecules which they encounter. The adsorbed material accumulates until a critical point is reached where new nuclei, formed from the components of the trapped nuclei and from gas liberated by the organism, are returned to the gelatin. This picture is, however, only speculative and further work is needed to establish the actual mechanisms of chemical reprocessing.

CHAPTER 6. DECOMPRESSION SICKNESS

Decompression sickness is caused by the formation of bubbles in the tissues and fluids of the body. It is most commonly associated with activities involving rapid pressure changes, such as deepsea diving, pressurized caisson work, flying in unpressurized aircraft, and excursions from spacecraft. The disease is not limited to man but also occurs in animals having widely differing physiology, such as brine shrimp, snakes, fish, and other mammals. The first indication of the etiology of this malady was the observation by Boyle (1670) of the formation of a bubble in the eye of a viper that had been decompressed using Boyle's newly invented vacuum pump. Decompression sickness in humans was initially reported among tunnel and caisson workers in the middle of the nineteenth century. Because its victims sometimes assumed contorted positions reminiscent of the steps from a then popular ladies walk known as the Grecian Bend, the disease acquired its nickname of "the bends."

In the first chapter of this report, it was noted that the minimum pressure reduction required to induce decompression sickness in humans is about 0.6 bar. This is more than three orders of magnitude below the theoretical value given in section 1.2 for bubble formation by homogeneous nucleation. Evidently, the bubbles that cause the bends originate from cavitation nuclei, and any detailed understanding of decompression sickness must therefore include in its foundation a knowledge of the nature of the cavitation nuclei present in living animals. The crucial importance of the nucleation process to decompression sickness has been previously pointed out, especially by Harvey (1951), Hills (1966), and Albano (1970), but little experimental effort has been directed toward elucidating the nature of the cavitation nuclei present in humans or other animals. This is, in part, because of the difficulty in relating the clinical signs and symptoms of decompression sickness to the underlying nucleation process. For this reason, the manner in which the number and volume of bubbles formed in various body structures may be related to the onset of decompression sickness is discussed briefly below.

6.1. Determining factors in the onset of decompression sickness

Bubbles induced by supersaturation form in many parts of the mammalian body. Upon post-mortem examination they have been found throughout the vascular system in both veins and arteries; in the lymph of the thoracic duct; in the aqueous and vitreous humor; in cerebro-spinal, synovial, amniotic, pericardial, and peritoneal fluids; in bile and urine; in liver, lungs, and spinal cord; in the spleen; in the adrenal cortex, the myelin sheath of nerve fibers, and hepatic cells; and in tendon sheath and bone. Evidently, the formation of bubbles is a general phenomenon not limited to a few body structures. Studies of humans by Rubissow and Mackay (1974) and Evans and Walder (1970) have shown that gas emboli can be present in blood and tissue without signs or symptoms of bends.

The pervasive but sometimes asymptomatic occurrence of bubbles suggests a general principle concerning the nature of decompression sickness first enunciated by Boycott et al. (1908): that the chance of being striken with decompression sickness depends on the total volume of gas evolved into bubbles. The assumption that the released gas volume is the determining factor in the onset of decompression sickness has also been discussed by Behnke (1951) and Hills (1970), and more recently by Hennessy and Hempleman (1977).

Based on the concept of critical released gas volume, the study of decompression sickness may be divided into three parts. The first part involves elucidating the mechanisms responsible for the initial formation of bubbles within the body; the second part concerns calculating the total volume of gas evolved into these bubbles; and the third part deals with estimating the probability and severity of decompression sickness associated with a given volume of evolved gas.

In the simplest case, the probability P of contracting decompression sickness depends on the volume of gas rapidly released into bubbles per unit volume of tissue. In mathematical terms, P is a function of V:

$$P = P(V) \ . \tag{6.1}$$

Because the body is composed of many different structures, each of which might be reasonably expected to behave differently than its neighbors, the simple function in equation (6.1) must be replaced by the more generalized summation

$$P = \sum_{j=1}^{n} P_j(V_j) \ , \tag{6.2}$$

where V_j is the volume released in the j^{th} structure, and the function $P_j(V_j)$ is the probability that this release of gas will result in the bends. But decompression sickness itself is not a single disease, but an array of conditions ranging from itching and tingling sensations through limb bends and vertigo to central nervous system damage, permanent paralysis, and death. The single probability in equation (6.2) is therefore to be replaced with the discrete probability of a given endpoint, i.e., the probability of a particular decompression malady. Equation (6.2) evidently must be supplanted by an expression of the form

$$P^{\ell} = \sum_{j=1}^{n} P_j{}^{\ell}(V_j) \ , \tag{6.3}$$

where $P_j{}^{\ell}(V_j)$ is the probability that a volume of gas V_j released into the j^{th} structure induces the ℓ^{th} type of condition. The cumulative probability of displaying any sign or symptom is given by the summation of the individual probabilities,

$$P = \sum_{\ell=1}^{m} P^{\ell} = \sum_{\ell=1}^{m} \sum_{j=1}^{n} P_j{}^{\ell}(V_j) \ , \tag{6.4}$$

where m is the number of recognized maladies.

The functional form of the probabilities $P_j{}^{\ell}(V_j)$ is not known. However, the limiting condition

$$\lim_{V_j \to 0} P_j{}^{\ell}(V_j) = 0 \tag{6.5}$$

can be assumed. This expresses the idea that if no bubbles are formed, then there is *ipso facto* no chance of decompression sickness. It is also logical to assume that the liberation of larger volumes of gas will never decrease the chance of becoming bent. This implies that the probabilities must be monotonically increasing functions; hence,

$$\frac{dP_j^{\ell}}{dV_j} \geq 0 \ . \tag{6.6}$$

The conditions under which the net probability of a given endpoint will be constant can be determined by setting the derivative of equation (6.3) to zero. This yields

$$\partial P^{\ell} = \sum_{j=1}^{n} \frac{dP_j^{\ell}}{dV_j} \partial V_j = 0 \ . \tag{6.7}$$

The evolved gas volumes V_j are related to the size and number of bubbles occurring in a structure by the integral equation

$$V_j = \frac{4}{3} \pi \int_0^{\infty} n_j(r) r^3 dr \ , \tag{6.8}$$

where $n_j(r)$ is the size distribution of bubbles in the j^{th} structure. The radius of a spherical bubble within a tissue is given by the equation

$$p = p_{amb} + \frac{2\gamma}{r} + \delta \ , \tag{6.9}$$

where δ is the "deformation pressure" of the tissue surrounding the bubble. If there is sufficient time and sufficient gas for the bubble to reach diffusive equilibrium with the environment, its final size r_e will be determined by the equation

$$r_e = 2\gamma_j/(p_{ss} - \delta_j) \ , \tag{6.10}$$

where p_{ss} is the supersaturation pressure. Therefore, in the case of complete bubble growth, equation (6.8) becomes

$$V_j = \frac{4}{3} \pi r_e^3 \int_0^{\infty} n_j(r) dr \equiv V_e N_j \ , \tag{6.11}$$

where r_e is the equilibrium radius determined by equation (6.10) and where N_j is the total number of bubbles per ml. A constraint on equation (6.11) is that sufficient gas must be available in the initial supersaturation to insure that each nucleated bubble can grow to the equilibrium size. In quantitative terms, this requires the validity of the inequality

$$N_j \leq S_j p_{ss} RT/pV_j \ , \tag{6.12}$$

where S_j is the gas solubility of the j^{th} structure. If the solubility is taken to be that of nitrogen in gelatin (see Table 4.2) and the equilibrium radius to be 50 μm, which is about the size of the bubbles commonly detected by ultrasonic Doppler techniques in venous blood, then the constraint on N_j becomes

$$N_j \leq 3{,}000 \frac{p_{ss}}{p_s} , \tag{6.13}$$

where p_s is the pre-decompression saturation pressure.

In the next section it will be shown that the limiting value of the ratio p_{ss}/p_s required for the onset of decompression sickness in humans has a numerical value between 0.3 and 0.7. Evidently, large numbers of bubbles must be evolved before equation (6.11) will fail. The concept of critical released gas volume is therefore at least sometimes synonymous with the assumption that the determining factor in the onset of decompression sickness is the number of bubbles formed per unit volume of tissue. In mathematical terms, the probabilities $P_j{}^{\ell}$ are in this case functions of N_j:

$$P_j{}^{\ell} = P_j{}^{\ell}(N_j) . \tag{6.14}$$

The concept that the number of bubbles is critical in determining the onset of decompression sickness has been previously suggested in Yount and Strauss (1976) and in Kunkle (1977), and its applicability to rats and humans has been quantitatively investigated in Yount (1979a).

6.2. Pressure-reduction limits

In this section the results of three studies designed to measure the maximum pressure decrease that can be tolerated before the onset of decompression sickness in rats and humans are considered. The pressure profile used in these programs is similar to that shown in Figure 2.3. It involves rapidly compressing a subject from one atmosphere to an exposure pressure p_s, letting the animal equilibrate for a time t_s, and then rapidly decompressing by an amount Δp to the final pressure p_f. The object is to determine Δp as a function of p_s for a fixed incidence of a specific type of decompression malady.

In Figure 6.1 the measurements of Berghage et al. (1976) of pressure-reduction limits in rats are plotted. This series of experiments involved helium-oxygen dives of subjects drawn from an initial population of 350 male albino rats. In each dive, five rats were placed in a rotating cage within a pressure vessel and then compressed to the exposure pressure p_s at the rate of *0.8 bar/min*. Following a 40-minute saturation exposure, the rats were decompressed to the final pressure at a rate of *0.5 bar/sec*. The animals were then observed for 15 minutes and rated on their ability to walk within the rotating cage; those who would or could not walk normally were considered to be bent. The pressure reduction which resulted in unwillingness or inability to walk in 50 percent of the rats was established using a least-squares linear fit to the data at each exposure.

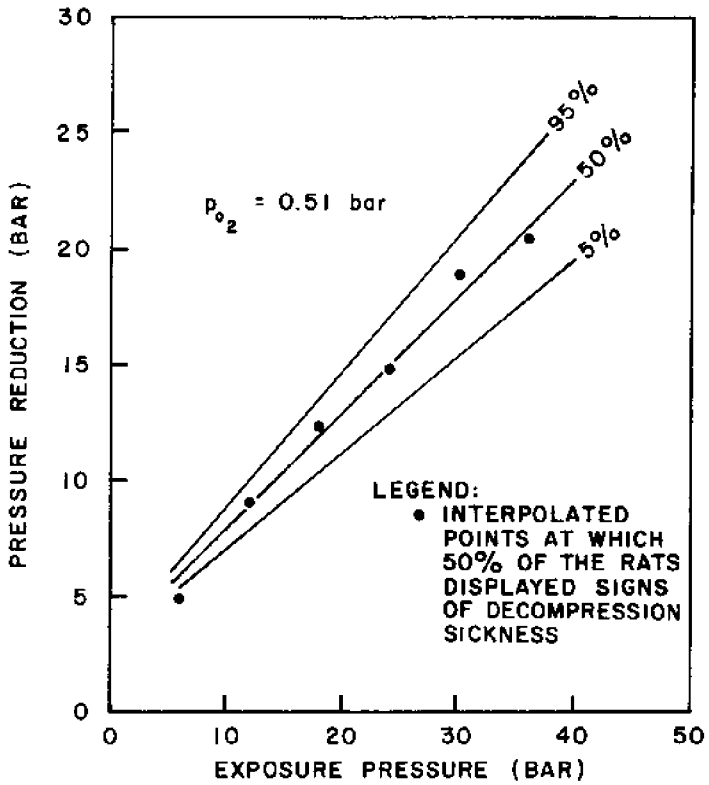

Figure 6.1. Reduction in pressure necessary to produce decompression sickness in rats following saturation helium-oxygen exposures. Solid lines are best linear regressions showing pressure reduction required for 5 percent, 50 percent, and 95 percent incidence of decompression sickness. (After Berghage et al., 1976)

The no-stop decompression thresholds for heliox breathing humans have been measured by Barnard (1976), who subjected volunteers, three at a time, to rapid decompressions following saturation exposures. The exact experimental protocol was, as might be expected, more complicated and had a different endpoint than did the rat experiments. In particular, the saturation exposures lasted for 24 hours, and the compressions and decompressions were done at rates between *0.1 bar/min* and *1.2 bar/min*. The endpoint was the onset of any decompression malady, usually the aches and pains of limbs. The results of this study are shown in Figure 6.2, where the decompression limits established by Gray (1944), Van der Aue (1946), and Belne and Bergeret (1951) for rapid decompression of humans breathing air have been included.

Examination of Figures 6.1 and 6.2 shows that the no-stop decompression limits depend almost linearly on the saturation pressure, and that higher incidences of decompression sickness are associated with larger pressure reductions. In quantitative terms, these results determine the conditions under which the

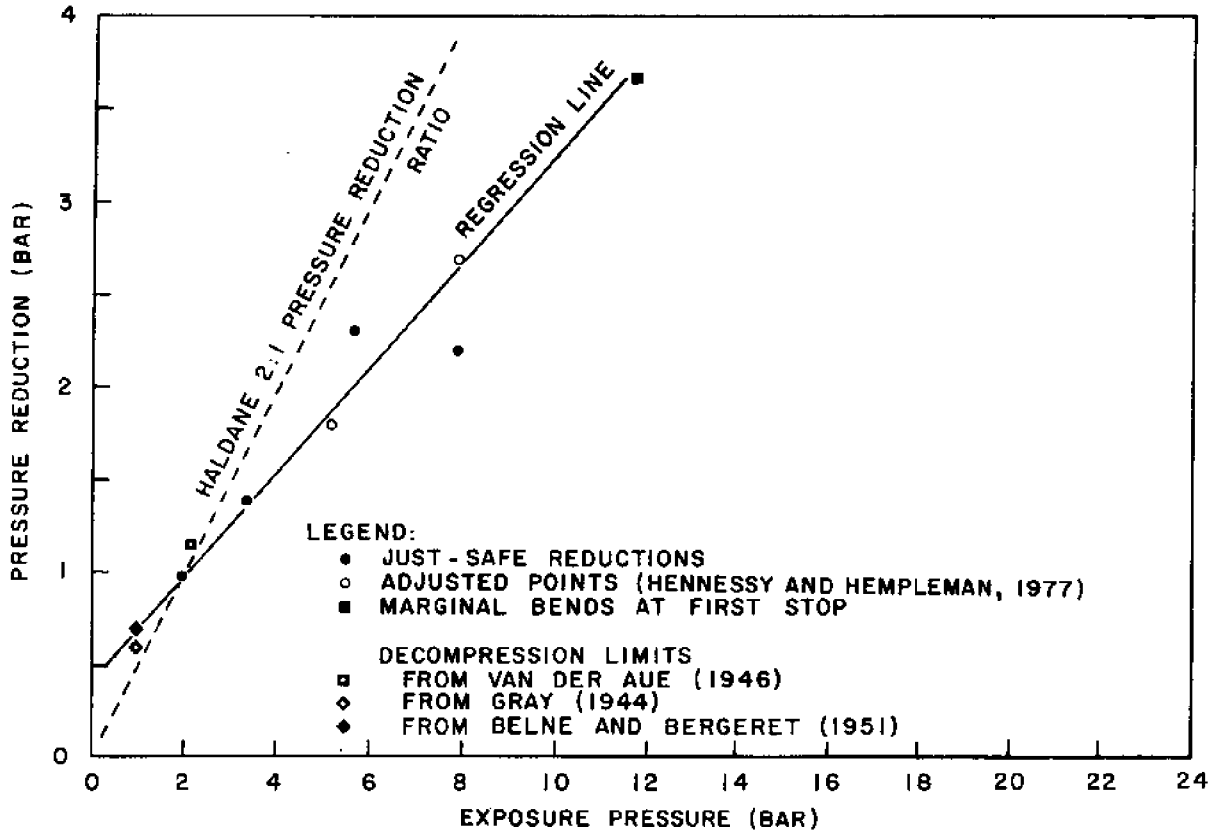

Figure 6.2. Reduction in pressure necessary to produce decompression sickness in humans following a saturation exposure. Data points are from Barnard (1976) for one-day exposures breathing heliox (PO_2 = 0.22 bar); regression line computed by Hennessy and Hempleman (1977).

probabilities P^{ℓ} will remain constant as the saturation and decompression pressure vary. If it is assumed that the volumes of released gas do not decrease along the isopleths of constant P^{ℓ}, then equations (6.6) and (6.7) indicate that the derivatives dV_j must vanish along these paths. Therefore, in terms of the critical volume hypothesis, the isopleths in Figures 6.1 and 6.2 can be associated with fixed values of V_j, and these experiments thus determine the pressures p_s and Δp required to liberate fixed, but unknown volumes of gas V_j. In terms of the critical bubble number hypothesis, the isopleths are associated with lines of constant bubble number.

An important question concerning the decompression limits observed in the above experiments is the degree of asymptomatic bubble formation that occurred before the onset of clinical manifestations. More precisely, what is the minimum pressure reduction required to induce any bubble formation? This question has been recently investigated by Watt and Lin (1979), who used ultrasound techniques to identify bubbles in venous return blood of rats decompressed after one-hour exposures breathing air. The results of their program are shown in Figure 6.3. As in the human and rat decompression data, the thresholds depend almost linearly on the exposure pressure, which indicates that bubble formation in rats--and by inference in humans--is a threshold phenomenon in the sense that

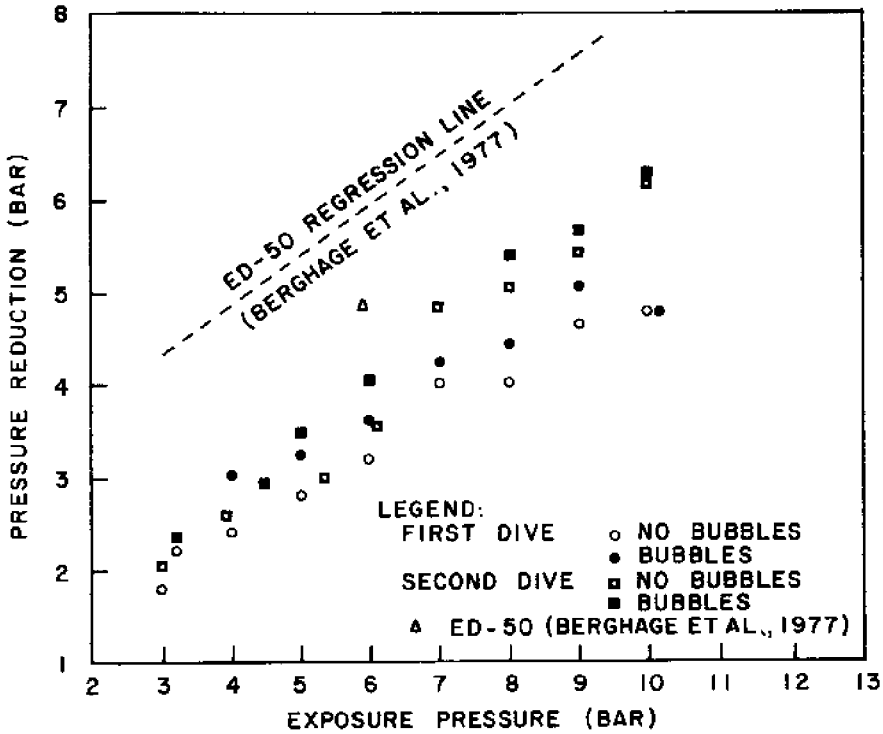

Figure 6.3. Decompression thresholds for venous gas emboli in rats (After Watt and Lin, 1979)

critical supersaturation pressures are required to induce the formation of bubbles. In the manner in which the threshold pressure increases with increasing crushing pressure, the initial formation of bubbles in rats is similar to that observed in gelatin (see Figure 2.10).

Hennessy and Hempleman (1977) analyzed the results of Barnard (1976) in terms of the critical released gas volume concept. Following the ideas of Hills (1966) and Boycott et al. (1908), they assumed that all of the excess gas present in supersaturation is liberated into bubbles, but that a critical pressure drop is required to initiate bubble formation. Hennessy and Hempleman found that a linear relationship between p_g and Δp follows from these assumptions, and that the ratio of relative released gas volume to solubility necessary for the onset of bends is 0.40. Using the solubility of nitrogen in gelatin given in Table 4.2, this implies a critical fractional volume of about one percent.

Kunkle (1977) and Yount (1979a) interpreted the results of Berghage et al. (1976) in terms of the critical bubble number concept. The loci of decompression limits are here associated with isopleths of constant bubble number, with larger numbers of bubbles producing higher incidences of decompression sickness. A comparison of Figure 6.1 with Figure 2.10 shows that the assumption of critical bubble number immediately enables the observed decompression limits in rats to be understood in terms of the gelatin experiments. The quantitative correspondence between bubble number and the incidence of decompression sickness is shown in Figure 6.4, where the number of bubbles produced by decompression

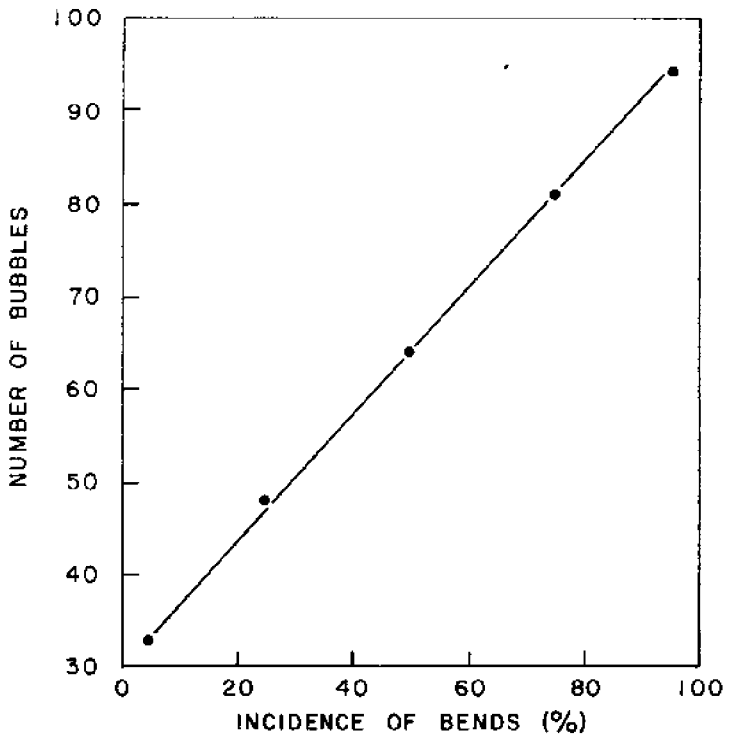

Figure 6.4. Relationship between the incidence of decompression sickness in rats and the number of bubbles produced in a similar gelatin experiment

gelatin batch D samples from a saturation pressure of 21.7 bar is plotted against the incidence of bends in rats exposed to similar pressure profiles. The probability of decompression sickness is seen to be strongly correlated with the number of bubbles produced in the gelatin samples. It should be noted that relatively large numbers of bubbles form a gelatin when using schedules that result in a zero incidence of bends in rats. This is consistent with the asymptomatic occurrence of bubbles in humans observed by Rubissow and Mackay (1974) and Evans and Walder (1970). Yount (1979a) has shown quantitatively that the decompression limits in both rats and humans can be associated with isopleths of constant bubble number, and that a somewhat better fit to the data is provided by his approach than by the critical volume model of Hennessy and Hempleman (1977).

6.3. The nature of cavitation nuclei in animals

As was noted earlier, an important part of the study of decompression sickness involves determining the mechanisms responsible for the initial formation of bubbles within the body; that is, it involves elucidating the nature of cavitation nuclei in animals. The experiments outlined in section 6.2 demonstrate two important characteristics of these nuclei: that a critical decompression is necessary to induce the growth of bubbles and that for saturation exposures this limit increases with increasing pressure. This behavior is similar to that observed in gelatin (see Figure 2.7 and 2.10), and suggests that the cavitation

nuclei present in living animals are similar to those observed in water and gelatin, i.e., they are surfactant-stabilized nuclei. This supposition is not surprising since animals are, from a microscopic point of view, composed mainly of water and gelatin.

Albano (1970) proposed that the nuclei in animals are of the crevice variety (see section 3.1) with the interstitial spaces between cells serving as crevices. The manner in which such a nucleus might grow into a bubble, or a chain of bubbles, is shown schematically in Figure 6.5. Albano developed an

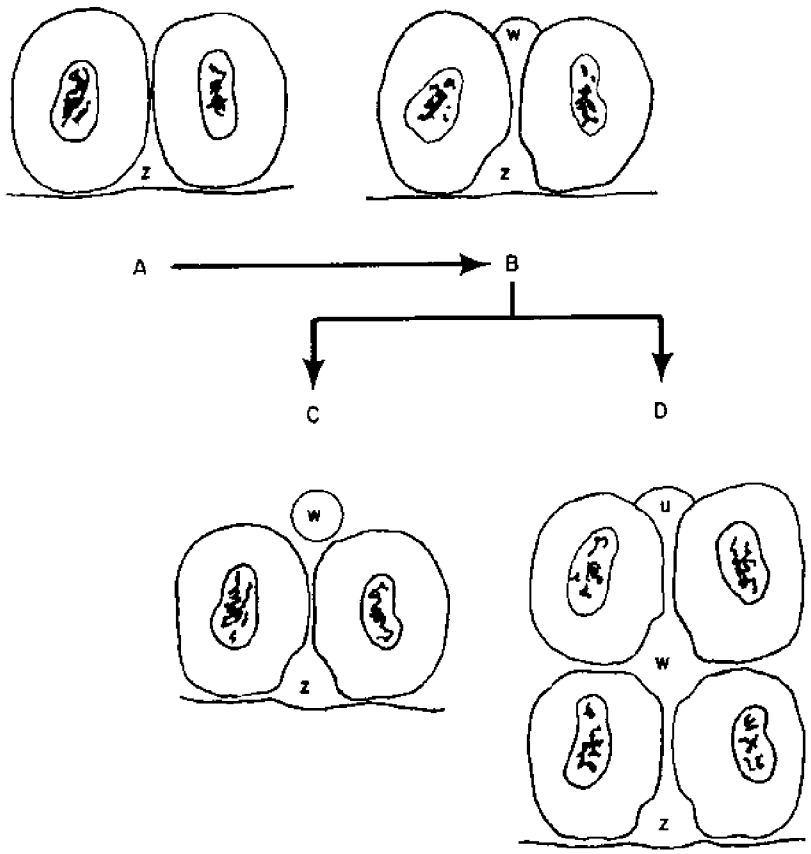

Figure 6.5. Growth of gas nuclei in the interstitial spaces (from Albano, 1970). (a) The nucleus (z) at rest within a cavity with negative surfaces. (b) By effect of decompression, the nucleus has increased in volume so that it pushes between the elements of the tissue and projects in the opposite direction together with the cap (w). This, because of a further increase, can free itself in liquids (blood), in the shape of a spherical nucleus [as in (c)], or give birth to a new duplication (d) or even a chain ("rosary") of bubbles.

elegant theory of such nuclei in which the geometry of an interstitial crevice is idealized by a cone having a convex lateral wall; the critical pressure difference required to induce nuclear growth is determined by the geometry of the cone and the liquid-solid-vapor contact angles. When such a nucleus is rapidly compressed, its volume is immediately reduced, but as the surrounding tissue equilibrates at the exposure pressure the entire gas volume of the nucleus is restored. Albano assumed that the restoration rate is exponential, with a half time in humans of about 6.3 minutes ($k \approx 0.011$, $C \approx 10$). For exposures longer than several half times, i.e., in excess of 30 minutes for humans, the decompression threshold for such a nucleus is independent of the exposure pressure, a prediction in disagreement with the experimental results. Evidently, cavitation nuclei in animals do not consist mainly of gas phases stabilized in the interstitial spaces between cells having exposed hydrophobic surfaces.

Hills (1966) argued that bubble nucleation in animals occurs at interfaces between aqueous and lipoidal fluids and is essentially a random process caused by thermodynamic fluctuations at the interface. This method is similar to that suggested by Plesset (1969) for nucleation around hydrophobic spheres, the major difference being the change from spherical to plane geometry. As discussed in section 3.1, nucleation around small hydrophobic spheres is found both through theory and observation not to be a viable process; the generalization of this concept to plane interfaces would therefore seem to be equally invalid. Hills (1966) conducted a series of experiments to investigate bubble nucleation at various liquid-liquid interfaces. He found the no-bubble pressure reduction limit from one atmosphere to be about 0.3 bar, and that beyond this point the bubble number increased exponentially with increasing supersaturation pressure. Evans and Walder (1969) repeated these experiments and found similar behavior. However, when the fluids were exposed to a crushing pressure of 816 bar before decompression, no bubble formation was observed. Evans and Walder concluded that "...although the interface in Hill's experiment appeared to have been free of gas nuclei it is apparent that they must have been present; they can be eliminated by a suitable high pressure treatment." Hills himself stated that "it was almost impossible to be certain that no micro-bubbles were present before decompression." Because nucleation at hydrophobic liquid-liquid interfaces is not expected theoretically and has not been clearly demonstrated experimentally, this process does not seem to be a viable mechanism for explaining nucleation in animals.

In the remainder of this chapter it is assumed that the cavitation nuclei occurring in animals are surfactant-stabilized nuclei similar to those observed in gelatin and that their behavior can be modeled by the SS model equations described in Chapter 4. This assumption is necessary because the only other nucleation process known to be viable--the crevice model--does not seem applicable to animals. A strong indication of the validity of the assumption of surfactant-stabilized nuclei is its ability to explain a number of decompression phenomena. It would, of course, be significant if the existence of surfactant-stabilized nuclei in animals could be demonstrated directly, perhaps by *in vivo* experiments with tissues and fluids; proposals for such studies have been made.

The assumption that surfactant-stabilized nuclei are the progenators of bubbles induced by decompression allows the observed pressure reduction limits to be interpreted in terms of nuclear sizes. The limiting pressure reduction for a human equilibrated at a pressure of 1 bar absolute has been estimated by

Gray (1944) to be 0.6 bar, by Belne and Bergeret (1951) to be 0.7 bar, and by Hennessy and Hempleman (1977) to be 0.70 bar. The radius of the smallest surfactant-stabilized nucleus that will be induced to grow by a supersaturation of 0.7 bar can be determined using equation (4.99). The result is

$$r = 77/(0.7 \times 10^6) = 1.1 \ \mu m \ . \tag{6.15}$$

The diameter of the largest nuclei normally present in humans is evidently about 2.2 μm.

The upper limit to nuclear sizes given by equation (6.15) may be controlled by one or more of the various filter systems in the human body. In particular, the spleen may be critical in determining the upper limit, since it is the smallest blood filter in the body. The spleen is a blood filter and reservoir placed in the pathway of a wide blood stream, the lienal or splenic artery. It removes dead and worn-out erythrocytes (red blood cells), bacteria, and other debris. Included among the debris filtered from the blood are, presumably, any nuclei larger than the effective filter size of the spleen. This filter diameter is not well known, but from measurements of photomicrographs reproduced by Bloom and Fawcett (1975), it appears to be between 2 and 3 μm. An independent estimate of the pore diameter can be arrived at by considering that one of the prime functions of the spleen is to remove non-elastic erythrocytes from the body. A normal erythrocyte is an extremely elastic torus, 7.7 μm in diameter, which is capable of deforming to pass through apertures much smaller than its normal diameter; the splenic filter removes those cells unable to deform adequately. The minimum diameter which an erythrocyte can assume may occur when the normally flat torus is rolled into an incomplete cylinder. The diameter of the resulting cylinder is related to its initial size by the equation

$$\pi d = 7.7 \ \mu m \ , \tag{6.16}$$

which indicates that the effective size of the splenic filter pores should be about 2.4 μm, in good agreement with the diameter measured in Bloom and Fawcett (1975). If this size is also assumed to be the diameter of the largest nuclei normally present in human blood, then equation (4.99) implies a decompression limit of 0.64 bar, a prediction in excellent agreement with the observed limits.

The effect of rapid compression on the equilibrium size of a surfactant-stabilized nucleus was discussed in subsection 4.3.2 and is shown graphically in Figure 4.19. Such a compression reduces the size of the nucleus by forcing surfactant molecules to desorb from the nuclear skin into the surrounding fluid. Because the equilibrium radius of a nucleus is inversely proportional to the supersaturation pressure required to induce bubble growth, a rapid compression results in an increase in the pressure reduction necessary to form a fixed number of bubbles. The observed increase in pressure reduction limits in both rats and humans with increasing exposure pressure can be understood in terms of a similar reduction in nuclear sizes.

The largest nuclei normally present in the human body apparently have a radius of about 1.2 μm. The rapid application of sufficiently large pressure will decrease the size of these nuclei and thus increase the pressure reduction limit. As an example, the data in Figure 6.2 indicate that rapid compression to 9.3 bar raises the decompression limit in humans from 0.70 to 3.03 bar; the size

of the largest nuclei prior to decompression is evidently reduced from 1.2 μm to 0.25 μm. A linear extrapolation of the data in Figure 4.19 yields a final size of 0.21 μm for a gelatin nucleus of similar initial size exposed to a crushing pressure of 8.3 bar. The increase in pressure reduction limits in humans with increasing exposure is therefore quantitatively similar to that observed in gelatin, and this strongly suggests that the cavitation nuclei occurring in humans are in fact surfactant-stabilized nuclei.

In general, the magnitude of the pressure reduction limit of a surfactant-stabilized nucleus will depend on the composition of the nuclear skin and on the surface tension of the surrounding medium. Because the chemical environment of living animals is expected to be different from that of gelatin and might differ from subject to subject, the quantitative results from the gelatin experiments are not expected to be immediately applicable to humans. The difference between humans and gelatin is shown in Figure 6.6, where the decompression thresholds for humans are compared with those calculated for gelatin nuclei having an initial size of 1.2 μm. The gelatin curve is seen to be somewhat steeper than the human curve, but it is in surprisingly good agreement considering the multiplicity of possibilities (see section 5.1). Yount (1979a) adjusted the parameters of his Varying Permeability model to fit the human data almost exactly. A similar procedure is possible using the SS model, but has not yet been done.

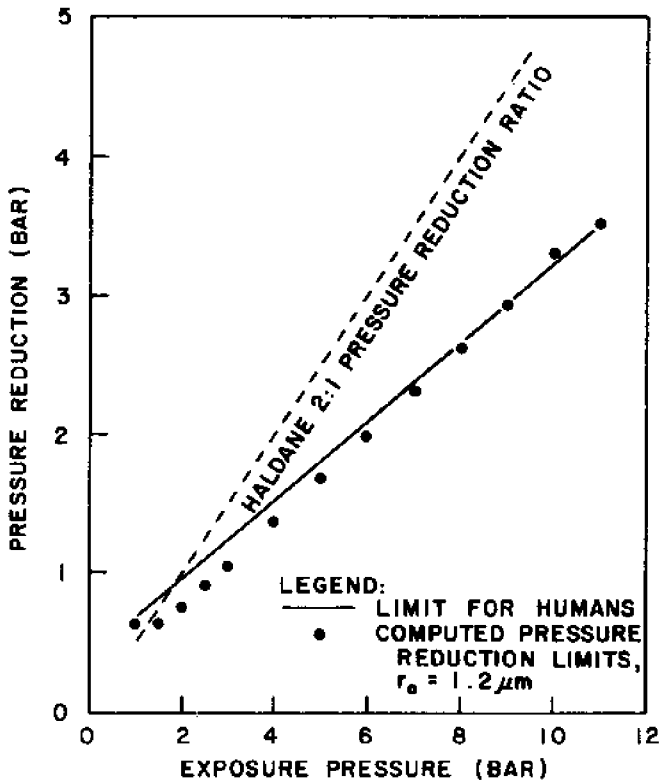

Figure 6.6. Comparison between the observed pressure-reduction limits for humans and those predicted by the SS model

The equilibrium size of a surfactant-stabilized nucleus depends on the type and number of surface-active molecules composing the nuclear size. In section 5.2 it was noted that the number of molecules will normally not remain constant, but will instead vary as they are gained or lost from the skin. The rate of change of the molecular number depends on the concentration of surface-active material in the surrounding fluid, and for concentrations near the critical micelle limit, it will involve an accretion of molecules. Because the mammalian body is rather heavily loaded with surfactant material, it is reasonable to assume that the nuclei will accrete material and thus steadily grow larger. This rate of growth is given by equation (5.15); according to this assumption, any given nucleus increases its radius exponentially with time.

If nuclei do grow larger with time, then the decompression limits shown in Figure 6.2 will depend on the duration of the exposures. It has previously been shown that a nucleus initially 1.2 μm in radius will be crushed to 0.25 μm when rapidly compressed by 8.3 bar. It will not remain at this reduced size indefinitely, however, but will instead immediately begin accreting surface-active molecules and grow larger. As the nucleus is restored, its decompression limit decreases. The process ends when the nucleus grows so large that it is trapped in the splenic filters and destroyed. If there is sufficient time for complete recovery to occur, the no-bends decompression limit should return to its initial value of 0.7 bar, regardless of the exposure pressure.

Experience with long duration exposures has shown that this predicted nuclear restoration does indeed happen. As an example, Beckman and Smith (1972) noted that the maximum allowable pressure reduction following very long--up to 60 days--exposures at 2.27 bar absolute is about 0.53 bar. The data in Figure 6.2 indicate that for a 12-hour exposure at this same pressure a decompression of 1.03 bar would be safe. Evidently, "short" saturation exposures must be handled differently from "long" saturation exposures. For exposures of intermediate length, the value of κ must be measured so that the size of the largest nucleus can be calculated by integrating equation (5.16).

The crushing and slow regrowth of nuclei provide an explanation of the common qualitative observation that greater pressure reductions can be tolerated on repeat dives than on first dives. This behavior is quantitatively shown by the data of Watt and Lin (1979) in Figure 6.3, where the no-bubble decompression limits are seen to be significantly larger for second exposures than for first exposures. Now consider a diver who works daily at a depth of 8.3 bar. On his first dive the largest nuclei are reduced in size from 1.2 μm to about 0.25 μm. The next day the nuclei have grown larger but have not yet been fully restored to their original size; the diver therefore begins the second day with nuclei of substantially reduced size, which are made even smaller by that day's dive. This process continues until an equilibrium condition is reached where during each day's diving the largest nuclei are crushed by an amount equal to that which they grew overnight. The decompression table is adjusted to reflect the corresponding increase in pressure reduction limits, and the work progresses. The diver then takes a week of vacation, during which time the largest nuclei are fully restored to their original 1.2 μm size, thereby decreasing the pressure reduction limit. The diver returns to work and dives using the same "safe" schedule used by his comrades, who have not been on vacation. The result may be a bent diver.

6.4. Calculation of decompression schedules

The problem of how to decompress a human without inducing bends was addressed just after the turn of the century by J.S. Haldane. Working at the behest of the Royal Navy, he developed the first set of practical, though empirical, decompression schedules. Haldane demonstrated that, at least at small depths, the body could withstand a two-to-one reduction in ambient pressure without symptoms, and he used this 2:1 ratio to compute the maximum allowable pressure reductions occurring in his tables.

If the onset of decompression sickness is associated with the initial formation of bubbles, then it may be seen from the gelatin results (see Figure 2.10) and from the data on rats and humans (see Figures 6.1 to 6.3) that the Haldane ratio principle is a reasonable first approximation for some exposures. However, as may be inferred from Figure 2.15 (Yount and Strauss, 1976), there are, at least in gelatin, many instances in which the ratio principle fails. This failure emphasizes the fact that the ratio principle was derived from empirical results on humans and makes no attempt to accommodate the nucleation process per se. In this section, methods by which non-Haldanian decompression schedules may be computed using a nucleation model to determine the onset of bubble formation are investigated.

6.4.1. Calculation of tissue gas tension

Before beginning with the calculation of decompression schedules it is necessary to consider briefly the manner in which tissue gas tensions may be determined. This is because models for bubble nucleation and growth require the supersaturation pressure be known. Continuing the development in section 6.1, it is assumed that the body can be viewed as being composed of a number of distinct structures. The gas tension in the j^{th} such structure τ_j is related to the gas concentration U_j by Henry's law, which states that

$$U_j = \tau_j S_j \ , \tag{6.17}$$

where S_j is the gas solubility. In general, four or more gases will be present: oxygen and carbon dioxide for tissue metabolism, water vapor, and the inert carrier gas, usually nitrogen or helium.

The nominal partial pressures of these four gases in arterial and venous blood are shown in Figure 6.7, which is reproduced from Strauss (1976). The arterial blood, with the exception of CO_2 and H_2O, is seen to be nearly equilibrated with the ambient atmosphere, while the venous blood is inherently unsaturated. This unsaturation is caused mainly by the metabolism of the less soluble oxygen into the more soluble carbon dioxide.

The amount of inert gas in a structure will depend on the ambient pressure history. It is usually assumed that the rate of inert gas flow into a structure is limited by blood perfusion and hence is determined by the equation

$$\frac{dU_j{}^I}{dt} = \left(\tau^I_{blood} - \tau_j{}^I \right) C_j{}^I \ , \tag{6.18}$$

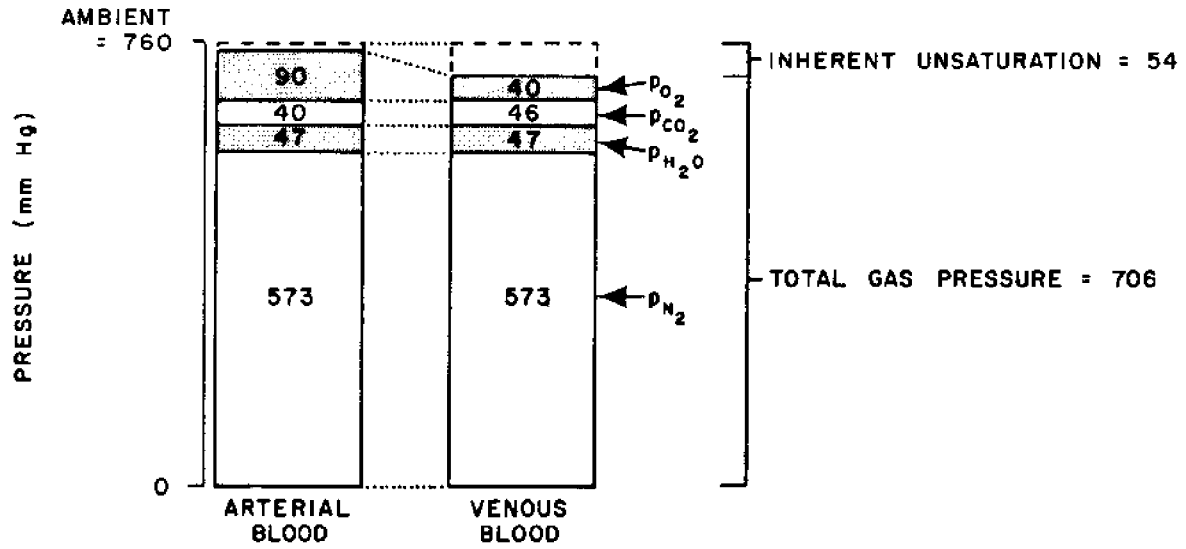

Figure 6.7. Normal gas tensions in venous and arterial blood (After Strauss, 1976)

where τ^I_{blood} is the inert gas tension of the arterial blood in the capillaries supplying the structure, and where $C_j{}^I$ is an inert gas uptake parameter. The arterial blood is often assumed to be in diffusive equilibrium, through the lungs, with the ambient atmosphere. In this case, the arterial inert gas tension is equal to the ambient partial pressure p^I_{amb}, and equation (6.18) becomes

$$\frac{d\tau_j{}^I}{dt} = \left[p^I_{amb}(t) - \tau_j{}^I\right] C_j{}^I / S_j{}^I \ , \tag{6.19}$$

where equation (6.17) has been used to convert concentrations into tensions.

Equation (6.19) allows the inert gas tension $\tau_j{}^I$ to be computed, given the ambient pressure history and the initial tension. As an example, if at time zero the ambient pressure is rapidly changed from an equilibrium value of P_1 to a final value of P_2, then equation (6.19) can be integrated to yield

$$\tau_j{}^I(t) = P_1 + \left(1 - e^{-tC_j{}^I S_j{}^I}\right)\left(P_2 - P_1\right). \tag{6.20}$$

The rate at which a tissue equilibrates is seen to depend on the ratio $C_j{}^I/S_j{}^I$, with tissues having large gas solubility taking longer to equilibrate. It should be noted that the uptake parameter $C_j{}^I$ is not ordinarily constant since it depends on the density of capillaries and on the rate of blood flow, the latter of which can change by an order of magnitude in response to physiological stress.

6.4.2. Decompression following saturation exposures

In this subsection the optimum decompression schedule for the case of initial diffusion-equilibrium with the ambient atmosphere is computed. The basic idea is to prevent the formation of bubbles by requiring that the supersaturation pressure never rises above some critical value throughout decompression. Quantitatively, this means that at all times the inequality

$$\tau_j - p_{amb} \leq p_j^* \tag{6.21}$$

must be satisfied, where p_j^* is the minimum supersaturation pressure required for bubble nucleation in the j^{th} structure. As discussed in section 6.3, the value of p_j^* is related to the size of the largest nuclei, which will in turn be determined either by the ambient pressure history or by the filtering mechanism of the body.

If it is assumed that the breathing mixture is regulated so that the partial pressure of oxygen is held constant at $160\ mm\ Hg = 0.21\ bar$, then the tissue partial pressures of oxygen and carbon dioxide will remain constant, and equation (6.19) can be used to compute the rate of change in total tissue gas tension. The result is

$$\frac{d\tau_j}{dt} = [p_{amb}(t) - \tau_j - 0.07]C_j^I/S_j^I \ , \tag{6.22}$$

where the $0.07\ bar$ term is the normal inherent tissue unsaturation. Substitution of equation (6.21) into equation (6.22) yields the maximum allowable rate at which the tissue gas tension can change without the formation of bubbles:

$$\frac{d\tau_j}{dt} = -(p_j^* + 0.07)C_j^I/S_j^I \ . \tag{6.23a}$$

Equation (6.23a) may be immediately integrated to give an equation for the tissue gas tension as a function of time:

$$\tau_j(t) = \tau_j(0) - \frac{C_j^I}{S_j^I}(p_j^* + 0.07)t \ . \tag{6.23b}$$

The decompression schedule is then:

$$p_{amb}(t) = (p_s - p_j^*) - \frac{C_j^I}{S_j^I}(p_j^* + 0.07)t \ . \tag{6.23c}$$

Evidently, the decompression consists of a first pull during which the pressure is decreased by an amount $(p_s - p_j^*)$, followed by a linear pressure reduction at a rate of

$$\left[C_j^I/S_j^I(p_j^* + 0.07)\right] bar/sec \ .$$

The validity of this type of decompression schedule has been checked in gelatin by Yount and Strauss (1976). In experiments with gelatin samples in which the ratio (S^I/C^I) was 15 minutes, they found that the optimum decompression was obtained using a short "first-pull" followed by a linear pressure reduction. The resulting schedule was shorter than the proper US Navy diving table for this type of dive, taking 12 minutes as opposed to 17 minutes, and it yielded many fewer bubbles, producing 0.42 ± 0.19 *bubbles* per sample as compared with 12.9 ± 1.0 *bubbles* per sample for the Navy decompressions.

The value of p_j^* to be used in equation (6.23c) will depend on the depth and the duration of the exposure. As described in section 6.3, this is because a rapid compression initially reduces the size of the largest nuclei and because the nuclei subsequently regrow by the accretion of surfactant molecules until they are removed from the body by the various filter systems. For "long" diffusion-equilibrium exposures of more than a week, the value of p_j^* is set by the splenic filter at about 0.6 bar, while "short" exposures of around 24 hours, the value of p_j^* will depend on the exposure pressure, as shown in Figure 6.2. Hennessy and Hempleman (1977) have empirically determined the relationship between p_s and p_j^* for short diffusion-equilibrium exposures to be

$$p_j^* = 0.285\ p_s + 0.41\ bar \tag{6.24}$$

Substitution of this result into equation (6.23c) yields the optimum decompression schedule for a short diffusion-equilibrium exposure:

$$p_{amb}(t) = (0.72\ p_s - 0.41) - \frac{C_j^I}{S_j^I}(0.29\ p_s + 0.41)t \tag{6.25}$$

For "long" exposures the nuclei are fully restored in size so that the value of p_j^* returns to its original value of 0.6 bar. The optimum decompression schedule is in this case given by the equation

$$p_{amb}(t) = (p_s - 0.7) - \frac{C_j^I}{S_j^I}\,0.77\ t \tag{6.26}$$

The usefulness of equation (6.25) or equation (6.26) in computing decompression tables is limited by the fact that these equations refer to specific body structures and not the organism as a whole. To prevent the occurrence of any bubbles, the maximum value of the ratio (C_j^I/S_j^I) must be known. An estimate of this critical value in humans is provided by experience with long equilibrium exposure dives, such as the TEKTITE project, which indicate the maximum permissible ascent rate to be about 2 fsw/hr or 1×10^{-3} bar/min (Beckman and Smith, 1972). Putting this result in equation (6.26) yields a critical value for the ratio (C_j/S_j) of 770 inverse minutes, which corresponds to a tissue half-time of 530 minutes. Because the tissue solubility and uptake rates entering into this ratio are not expected to depend on the ambient pressure, it is reasonable to assume that this value of (C_j^I/S_j^I) is constant for all exposure pressures. Substituting this ratio into equations (6.25) and (6.26) yields a

decompression schedule for short equilibrium exposures of

$$p_{amb}(t) = (0.72\ p_s - 0.41) - (3.7\ p_s + 5.3) \times 10^{-4}\ t \qquad (6.27a)$$

and a schedule for long equilibrium exposures of

$$p_{amb}(t) = (p_s - 0.7) - 1.0 \times 10^{-3}\ t\ , \qquad (6.27b)$$

where time is measured in minutes.

As an example of these schedules, consider a rapid compression normox dive to a depth of 30 msw. The exposure pressure is 4 bar absolute. For bottom times of around a day, the dive is classified as a "short" diffusion-equilibrium exposure, and the decompression schedule is given by equation (6.27b). The decompression consists of a first pull to a pressure of *2.45 bar = 14.5 msw* followed by a linear ascent at a rate of *1.2 msw/hour*; the total decompression time is 12.0 hours. For exposures lasting over a week, equation (6.27b) for "long" diffusion-equilibrium exposures must be used. The resulting pressure schedule consists of a first pull to *3.30 bar = 23.0 msw*, followed by a linear ascent at a rate of *0.60 msw/hour*, the total decompression time being 38.4 hours.

6.4.3. Decompression following non-saturation exposures

The optimum decompression schedule for a non-saturation dive may be defined as the fastest ascent profile that produces no bubbles. The condition for zero bubble incidence is given by equation (6.21),

$$\tau_j - p_{amb} \leq p_j^*\ ,$$

which states that at no time can the supersaturation pressure exceed the critical limit p_j^*. The calculation of the gas tensions τ_j during arbitrary pressure schedules can, in principle, be accomplished by integrating equation (6.19). This calculation is in reality much more complex than a simple integration, since it depends strongly on the physiological state of the subject. Because such considerations are outside the scope of this report, it is assumed that a reliable method is available for computing gas tensions and that the values of $\tau_j(t)$ are known at all times.

The magnitude of p_j^* depends on the size of the largest nucleus present in the structure. As has been discussed in section 4.3 and 6.3, this maximum radius will depend on the pressure history, the gas tension, and the nuclear growth rate. In general, the only way to determine p_j^* is by use of a nucleation model such as the SS model or the VP model of Yount (1979a). The calculation of optimum decompression schedules is therefore predicated on the existence of accurate mathematical models of cavitation nuclei and upon detailed knowledge of the chemical nature of the nuclei occurring in animals.

REFERENCES CITED

Adam, N.K. 1928. "The structure of thin films. Part XI. Oxygenated derivatives of benzene." *Proc. Roy. Soc. Lond.* A119:628-644.

Adam, N.K., and G. Jessop. 1926. "The structure of thin films. Part VII. Evaporation phenomena at low compressions." *Proc. Roy. Soc. Lond.* A110: 423-441.

Akulichev, V.A. 1966. "Hydration of ions and the cavitation resistance of water." *Akust. Zh.* 12(2):160-166. (English translation: *Sov. Phys.-Acoust.* 12(2):144-149.)

Albano, G. 1970. *Principles and Observation on the Physiology of the Scuba Diver.* English translation: ONR Report DR-150. Office of Naval Research, Department of the Navy, Arlington, Virginia.

Apfel, R.E. 1970. "The role of impurities in cavitation-threshold determination." *J. Acoust. Soc. Am.* 48(5):1179-1186.

Apfel, R.E. 1971. "A novel technique for measuring the strength of liquids." *J. Acoust. Soc. Am.* 49(1):145-155.

Barnard, E.E.P. 1976. "Fundamental studies in decompression from steady-state exposures." In *Proceedings of the Fifth Symposium on Underwater Physiology*, ed. C.J. Lambertsen. Bethesda: Federation of American Societies for Experimental Biology.

Barnes, G.T., T.I. Quickenden, and J.E. Saylor. 1970. "A statistical calculation of monolayer permeation by water." *J. Colloid and Interface Sci.* 33:236-243.

Bartels, H. 1971. "Diffusion coefficients of gases in water." In *Respiration and Circulation*, eds. P.L. Altman and D.S. Dittmer, pp. 23-24. Bethesda: Federation of American Societies for Experimental Biology.

Bateman, J.B., and J. Lang. 1944. "Formation and growth of bubbles in aqueous solutions." *Canadian J. of Research* 23(E):22-31.

Becker, R., and W. Döring. 1935. "Kinetische behandlung der keimbildung in iibersättigten dampfen." *Ann. d. Phys.* 24(5):719-752.

Beckman, E.L., and E.M. Smith. 1972. "TEKTITE II medical supervision of the scientists in the sea." *Texas Reports on Biology and Medicine* 30(3): (special issue).

Behnke, A.R. 1951. "Decompression sickness following expsoure to high pressures." In *Decompression Sickness*, ed. J.F. Fulton. Washington, D.C.: National Research Council.

Belne and Bergeret. 1951. Cited by Albano (1970), p. 266.

Berghage, T.E., J.A. Gomez, C.E. Roa, and T.R. Everson. 1976. "Pressure-reduction limits for rats following steady-state exposures between 6 and 60 ATA." *Undersea Biomed. Res.* 3(3):261-271.

Bernd, L.H. 1963. "Study of the surface films of gas nuclei." Report TIS 64GL143. Advanced Technology Lab, General Electric Company, Schenectady, New York.

Blank, M. 1962. "Monolayers: permeability to several gases." In *Retardation of Evaporation by Monolayers*, ed. V.K. LaMer, pp. 75-95. New York: Academic Press.

Blank, M. 1964. "An approach to a theory of monolayer permeation by gases." *J. Phys. Chem.* 68:2793-2800.

Bloom, W., and D.W. Fawcett. 1975. *A Textbook of Histology*, 10th edition. Philadelphia: Saunders.

Boycott, A.E., G.C.C. Damant, and J.S. Haldane. 1908. "The prevention of compressed-air illness." *J. of Hygiene* 8:342-443.

Boyle, R. 1670. "New pneumatic experiments about respiration." *Philos. Trans.* 5:2011-2031.

Dickinson, E. 1978. "A hard disk fluid model of monolayer permeation and evaporation resistance." *J. Colloid and Interface Sci.* 63(3):461-471.

Epstein, P.S., and M.S. Plesset. 1950. "On the stability of gas bubbles in liquid-gas solutions." *J. of Chem. Phys.* 18:1505-1509.

Evans, A., and D.N. Walder. 1969. "Significance of gas micronuclei in the aetiology of decompression sickness." *Nature* 222:251-252.

Evans, A., and D.N. Walder. 1970. "Detection of circulating bubbles in the intact animal." *Ultrasonics* 8(4):216-217.

Frenkel, J. 1946. *The Kinetic Theory of Liquids*. Oxford: Clarendon Press. pp. 366-413.

Fox, F.E., and K.F. Herzfeld. 1954. "Gas bubbles with organic skin as cavitation nuclei." *J. Acoust. Soc. Am.* 26:984-989.

Gaines, G.L. 1966. *Insoluble Monolayers at Liquid-Gas Interfaces*. New York: Interscience Publishers, John Wiley & Sons, Inc.

Gent, A.N., and D.A. Tompkins. 1969. "Nucleation and growth of gas bubbles in elastomers." *J. Appl. Phys.* 40(6):2520-2525.

Gerrard, W. 1976. *Solubility of Gases and Liquids*. New York: Plenum Press.

Gray, D.E., coordinating ed. 1963. *American Institute of Physics Handbook*, 2nd edition. New York: McGraw-Hill. pp. 4-167.

Gray, J.S. 1944. *Aeroembolism Induced by Exercise in Cadets at 23,000 Feet.* US NRC. Comm. Aviat. Med. Report 260, Washington, D.C.

Harkins, W.D. 1952. *The Physical Chemistry of Surface Films.* New York: Reinhold Publishing Corp.

Harvey, E.N. 1951. "Physical factors in bubble formation." In *Decompression Sickness*, ed. J.F. Fulton. Washington, D.C.: National Research Council.

Harvey, E.N., D.K. Barnes, W.D. McElroy, A.H. Whiteley, D.C. Pease, and K.W. Cooper. 1944. "Bubble formation in animals. I. Physical factors." *J. Cell. Comp. Physiol.* 24(1):1-22.

Hawke, J.G., and A.E. Alexander. 1962. "The influence of surface-active compounds upon the diffusion of gases across the air-water interface." In *Retardation of Evaporation by Monolayers*, ed. V.K. LaMer, pp. 67-73. New York: Academic Press.

Hemmingsen, E.A. 1970. "Supersaturation of gases in water: absence of cavitation on decompression." *Science* 167:1493-1494.

Hennessy, T.R., and H.V. Hempleman. 1977. "An examination of the critical released gas volume concept in decompression sickness." *Proc. Roy. Soc. Lond.* B197:299-313.

Herzfeld, K.F. 1957. Comment in *Proc. First Sympos. Naval Hydrodynamics*, ed. F.S. Sherman, pp. 319-320. Washington, D.C.: Nat. Acad. Sci.

Hills, B.A. 1966. "A thermodynamic and kinetic approach to decompression sickness." Doctoral thesis, The University of Adelaide, Australia.

Hills, B.A. 1970. "Limited supersaturation versus phase equilibrium in predicting the occurrence of decompression sickness." *Clinical Sci.* 38:251-267.

Kunkle, T.D. 1977. "Physics of surfactant stabilized gas nuclei." *Undersea Biomed. Res.* 4(1):A33.

Kunkle, T.D., and D.E. Yount. 1975. "Gas nucleation in gelatin." In *Proc. of the Sixth Symposium on Underwater Physiology*, ed. M.B. Kent, pp. 459-467. Bethesda: Federation of American Societies for Experimental Biology.

Landau, L.D., and E.M. Lifshitz. 1938. *Statistical Physics.* Oxford: University Press.

Le Messurier, D.H. 1972. "Supersaturation and preformed nuclei in the etiology of decompression sickness." Paper presented at the Second International Meeting on Aerospace Medicine, Melbourne.

Le Messurier, D.H., T.N. Smith, and W.R. Wood. 1979. "Diffusion and nucleation of gas in gel and some implications for the development of decompression procedures." *Undersea Biomed. Res.* 6(2):175-188.

Liebermann, L. 1951. Personal communication with F.E. Fox and K.F. Herzfeld. Cited in Fox and Herzfeld (1954), p. 985.

Love, A.E. 1944. *The Mathematical Theory of Elasticity*, 4th edition. New York: Dover Publ.

Moore, E.M. 1953. "Sea foam stabilized by an organic skin." *Nature* 171:913.

Munden, J.W., and J. Swarbrick. 1973. "Effect of spreading solvent on monolayer characteristics of dipalmitoyl lecithin." *J. Colloid and Interface Sci.* 42:657-659.

Phillips, M.C., and D. Chapman. 1968. "Monolayer characteristics of saturated 1, 2-diacyl phosphatidylcholines (lecithins) and phosphatidylethanolamines at the air-water interface." *Biochim. Biophys. Acta* 163:301-313.

Plesset, M.S. 1969. "The tensile strength of liquids." In *Cavitation State of Knowledge*. ASME Fluids Engineering and Applied Mechanics Conference, Evanston, Illinois, pp. 15-25.

Pockels, A. 1891. "Surface tension." *Nature* 43:437-439.

Rabinovitch, W., R.F. Robertson, and S.G. Mason. 1960. "Relaxation of surface pressure and collapse of unimolecular films of stearic acid." *Can. J. Chem.* 38(1):1881-1890.

Rubissow, G.J., and R.S. Mackay. 1974. "Decompression study and control using ultrasonics." *Aerosp. Med.* 45:473-478.

Sirotyuk, M.G. 1970. "Stabilization of gas bubbles in water." *Akust. Zh.* 16:237-240. (English translation: *Sov. Phys.-Acoust.* 16:286-290.)

Strasberg, M. 1956. "The onset of ultrasonic cavitation in tap water." Ph.D. dissertation, Catholic University of America, Washington, D.C.

Strasberg, M. 1959. "Onset of ultrasonic cavitation in tap water." *J. Acoust. Soc. Amer.* 31(2):163-176.

Strauss, R.H. 1974. "Bubble formation in gelatin: implications for prevention of decompression sickness." *Undersea Biomed. Res.* 1:169-174.

Strauss, R.H. 1976. "Decompression sickness." In *Diving Medicine*, ed. R.H. Strauss, p. 75. New York: Grune & Stratton.

Strauss. R.H., and T.D. Kunkle. 1974. "Isobaric bubble growth: a consequence of altering atmospheric gas." *Science* 186:443-444.

Tolman, R.C. 1949. "The effect of droplet size on surface tension." *J. Chem. Phys.* 17(3):333-337.

Van der Aue. 1946. Cited by Albano (1970), p. 267.

Watt, D.G., and Y.C. Lin. 1979. "Doppler detection of thresholds for decompression-induced venous gas emboli in the awake rat." *Aviation, Space, and Environmental Medicine* 50(6):571-574.

Yang, W., and C.Y. Liang. 1972. "Dynamics of dissolution of gas bubbles or pockets in tissues." *J. Biomechanics* 5:321-332.

Yount, D.E. 1979a. "Application of a bubble formation model to decompression sickness in rats and humans." *Aviation, Space, and Environmental Medicine* 50(1):44-50.

Yount, D.E. 1979b. "Skins of varying permeability: a stabilization mechanism for gas cavitation nuclei." *J. Acoust. Soc. Am.* 65(6):1429-1439.

Yount, D.E., and R.H. Strauss. 1976. "Bubble formation in gelatin: a model for decompression sickness." *J. Appl. Phys.* 47(11):5081-5089.

Yount, D.E., and T. D. Kunkle. 1975. "Gas nucleation in the vicinity of solid hydrophobic spheres." *J. Appl. Phys.* 46(10):4484-4486.

Yount, D.E., C.M. Yeung, and F.W. Ingle. 1977a. "Gelatin filtration: a new technique for determining the radii of gas cavitation nuclei." *Undersea Biomed. Res.* 4(1):A33.

Yount, D.E., T.D. Kunkle, J.S. D'Arrigo, F.W. Ingle, C.M. Yeung, and E.L. Beckman. 1977b. "Stabilization of gas cavitation nuclei by surface-active compounds." *Aviation, Space, and Environmental Medicine* 48(3):185-191.